Proceedings of International Conference
Applications of Structural Fire Engineering
Prague, 19-20 February 2009

Session 6

Composite Structures

ASSESSMENT OF STEEL – CONCRETE – STEEL SHEAR WALL

David Dunne [a], Dr. Nutan Subedi [b]

[a] University of Dundee, School of Engineering, Physics & Mathematics, Civil Engineering, Dundee, Scotland.
[b] Reader Structural Engineering (Retired), University of Dundee, Dundee, Scotland.

1 INTRODUCTION

Fire safety is an important consideration in design. Concrete as a construction material is extensively used in structures. Its inherent fire resistance property provides protection for life, property and the environment we live in [1]. Moreover, concrete is a material possessing low thermal conductivity and high specific heat capacities. These properties render its heat transfer rate very slow and fire resistance very good [2]. Steel-Concrete-Steel, S-C-S, construction has the capacity to contribute and enhance this function as in the case with steel deck composite floors. The steel plates on both sides of the concrete core can provide good insulation to concrete retarding the heat flow and early spalling of concrete [3,4].

S-C-S is a robust form of construction in which the composite action can be achieved in a number of ways, such as: the use of shear studs, overlapping shear studs, overlapping J-hooks, bi-steel welded stud system and epoxy resin plate bonding. The applications include beams in common structures, wall panels, tunnels and aircraft hangars to name but a few [5]. In S-C-S composite construction the conventional reinforcement is replaced by external steel plates; its main advantage being its robustness, derived from the composite action between these steel plates on the outside and the concrete core on the inside. The current research programme was to extend the application of S-C-S system to shear walls in tall buildings. The main aim was to investigate the behaviour of two different structural forms of shear walls, a conventionally reinforced shear wall and a S-C-S composite construction. It was considered that the S-C-S system would fully utilise the properties of both the steel and concrete making it a more efficient, robust and durable form of structural system and performing better under variable loading conditions. An experimental study was carried out using one of each of the two systems of wall and subjected to static and impact loadings. The main conclusion from this preliminary study was that the S-C-S composite system possesses significantly greater stiffness and thus significantly reduced degree of deflection compared to that of a conventionally reinforced shear wall system. Other significant design parameters such as strain development, crack patterns and their effects are also discussed.

2 EXPERIMENTAL MODEL

The model depicted in Figures 1 and 2 and in more detail elsewhere [5], consists principally of two shear walls of the same size 900mm x 40mm x 300mm, one conventionally reinforced with the second containing a S-C-S form of construction which consists of two external plates as reinforcement. The walls were cast into a specially designed concrete block providing a rigid foundation for testing. For testing purpose the walls were laid horizontal while still being restrained at the base.

The conventional reinforcement consisted of 6mm diameter and 1180mm length mild steel, placed longitudinally and spaced at 23mm centres. Additionally, two horizontal reinforcement bars were placed at the top and bottom of the wall increasing both tensile and compressive zones of the wall respectively. Furthermore, 6mm diameter link bars at 50mm centres and at lengths of 260mm were placed at staggered centres either side of the main horizontal steel vertically tying the reinforcement together. The second form of reinforcement to be employed was that of steel plates, which were placed on both sides of the externally reinforced wall, 1180mm x 0.7mm x 300mm in size. There was also reinforcement required for the concrete block which was to consist of a steel cage of eight links of 10mm diameter steel bar. The final element in the steel reinforcement was the addition of four reinforcing plates along the top of each wall, 50mm x 40mm x 10mm in size with each plate having two number 100mm lengths of 6mm

diameter steel bar welded to its base. These plates which can be seen in Figure 1 and in greater detail elsewhere [5], were placed at loading locations on the top of both walls, their purpose being to distribute the applied loads to reduce the local damage under the bearing plate.

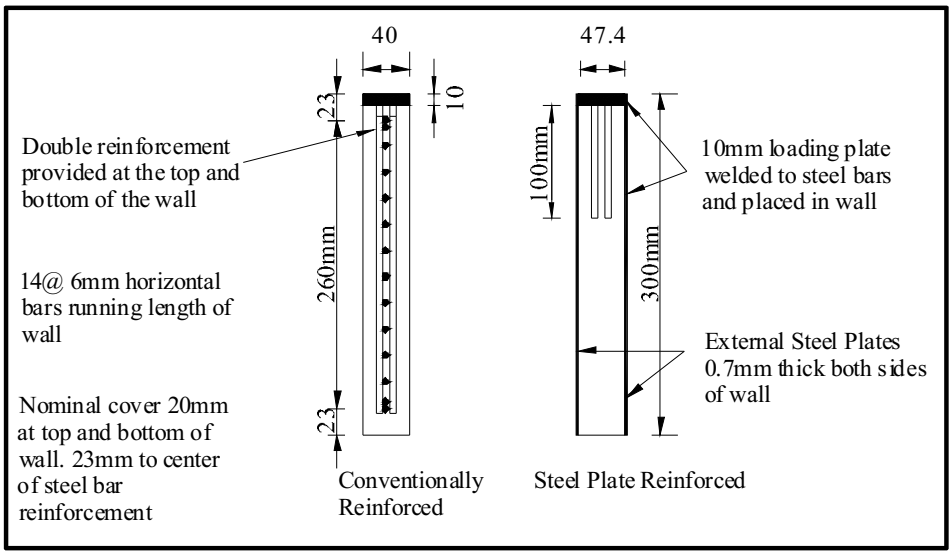

Figure 1 Shear Walls cross sections

3 MATERIAL PROPERTIES AND TEST PROCEDURES

The material properties were chosen to be representative of full size structures.

3.1 Concrete & Steel

Two different grades of concrete were used, with the first, used in the restraint block being a standard RMC Ready-Mix design C50 grade concrete. Secondly, the concrete in the shear walls was a specially designed micro-concrete mix with a w/c ratio of 0.4. Two cubes and two cylinders, one from each wall, were tested for strength development at designated periods up to day of testing as in Table 1, where the average of the two results are presented. For reinforcement two standard 0.7mm grade S275 mild steel plate sections and two 6mm (for the shear wall) diameter bars were tested. Tensile test properties for the steel are also given in Table 1.

Table 1 Concrete and Steel properties

Day Strength	Concrete			Steel		
	f_{cu}	f_{ct}	E_c	Materials	f_y	E_s
	(N/mm^2)		(kN/mm^2)		(N/mm^2)	(kN/mm^2)
7	48.0	----	31.1	6.0 mm	490.0	----
28	52.0	----	32.4	0.7 mm plate	373.5	225.0
44	----	3.9	----	----	----	----
Test Day	54.0	4.0	33.1	----	----	----

3.2 Epoxy Resin

A two part cold cure epoxy resin, manufactured and supplied by Sika and commonly used for structural bonding purposes in the UK was employed to attach the steel plates to the concrete surface.

3.3 Instrumentation

Common LVDT transducers were used to measure the wall deflections under static loading. A SPECTRA data logger system was used for data recording. Additionally a dial indicator gauge was employed to record readings of end deflection of both walls during the static testing experiment, to an accuracy of 0.01mm.

3.4 Static & Impact Testing

The static testing apparatus shown in Figure 2(A), consisted of a number of weights 1, 2, 5 and 10 kilograms applied manually to the walls. The measurements consisted of deflection from the transducers, strain readings from the strain gauges and the dial gauge positioned beneath the front of each wall. The main piece of equipment required in the impact test was the use of an impactor. This consisted of a cylindrical steel section of 2.5kg weight which could be manually placed onto a threaded bar allowing incremental increase in weights to be applied. The first steel section has a domed end as this impacted the wall with the remaining sections being cylindrical in shape, 100mm long and 63.5mm in diameter as can be seen in Figure 2(C). A hook located on the top of the bar allowed a rope to be threaded and for a pulley mechanism to be employed. Finally, a guidance tube was used, its function being to guide the impactor over the loading location, with the testing mechanism layouts impact loading detailed in Figure 2(B).

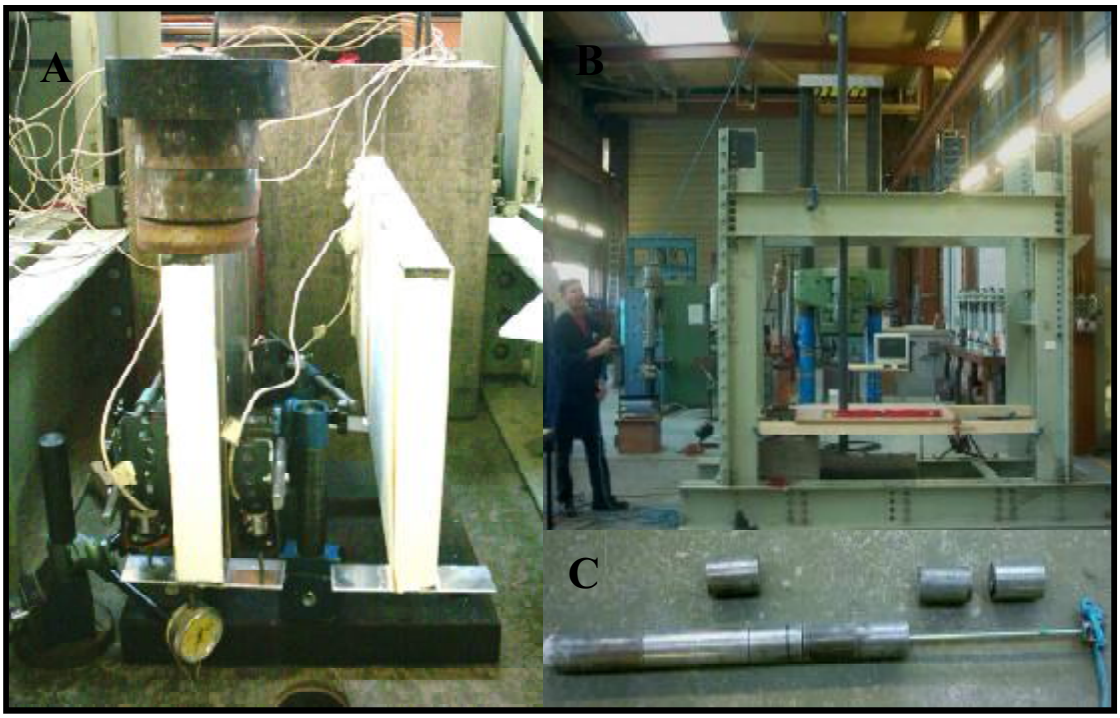

Figure 2 (A) Static test setup (B) Impact test setup (C) Impactor

4 RESULTS AND DISCUSSION

4.1 Deflection: Static testing

The plots of the deflection readings for both systems of the wall are shown in Figure 3. The load cycles represent the load values from 1kg up to 40kg. It is clear from the figure that the deflections of the S-C-S wall are considerably lower as well as linear over the span of the wall. The conventionally reinforced wall demonstrated a greater mid span deflection and greater end span deflection. The main finding from the presented graph is that under static loading the stiffness of the S-C-S wall is much greater compared to the conventionally reinforced wall and over the range of the applied load its behaviour is more or less described as linear.

4.2 Strain: Static testing

Strain readings for the cantilever S-C-S shear wall showed that the top of the wall was in tension and the bottom of the wall in compression under loading, as expected and can be seen in Figures 4. These Figures also illustrate that the action of elastic deformation is taking place, with the strains increasing gradually under increased loading in a linear fashion. Furthermore, the strains in both plates were also similar which infers that the epoxy resin bonding gave an even distribution of strain built up in the steel plates under static loading as also supported by the findings of Barnes et al [6]. It is noted that the obtained values were of a very small magnitude signifying that the plates were grossly under stressed.

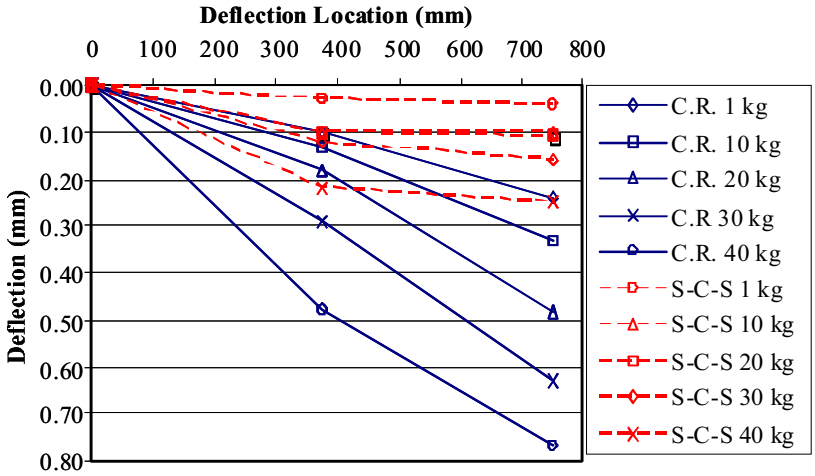

Figure 3 Deflection of both systems under 1kg - 40kg static loading

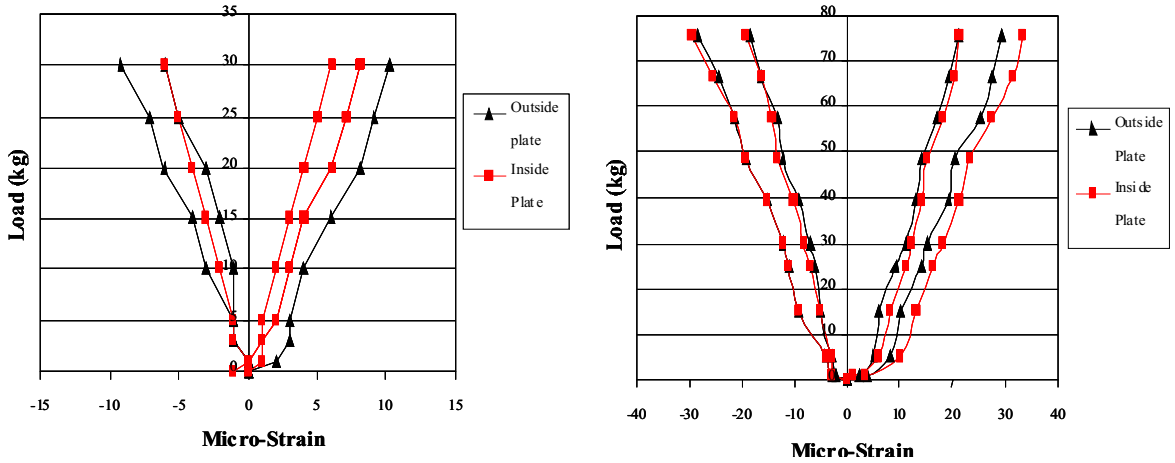

Figure 4 Strain in steel plates under static loading cycles 1 and 3 (left – right)

4.3 Crack Inspection: Impact Testing

The behaviour of the walls under impact loading was recorded as observed. This being a preliminary study no instrumentation was incorporated. All reinforced concrete structures possess cracks in order for reinforcement to function properly, however it is important to limit the developments of these cracks in order to achieve serviceability requirements. Throughout the experimental procedure it was visible that although extensive cracks had formed in the S-C-S wall it was still structurally sound and the widths of the cracks remained visually small until ultimate failure mechanism developed. At failure the behaviour was somewhat brittle. This can be attributed to the early peeling and onset of separation of the plates near the base from the concrete surface. In the conventional wall however, as the load increased large deflections were taking place accompanied by wider main cracks.

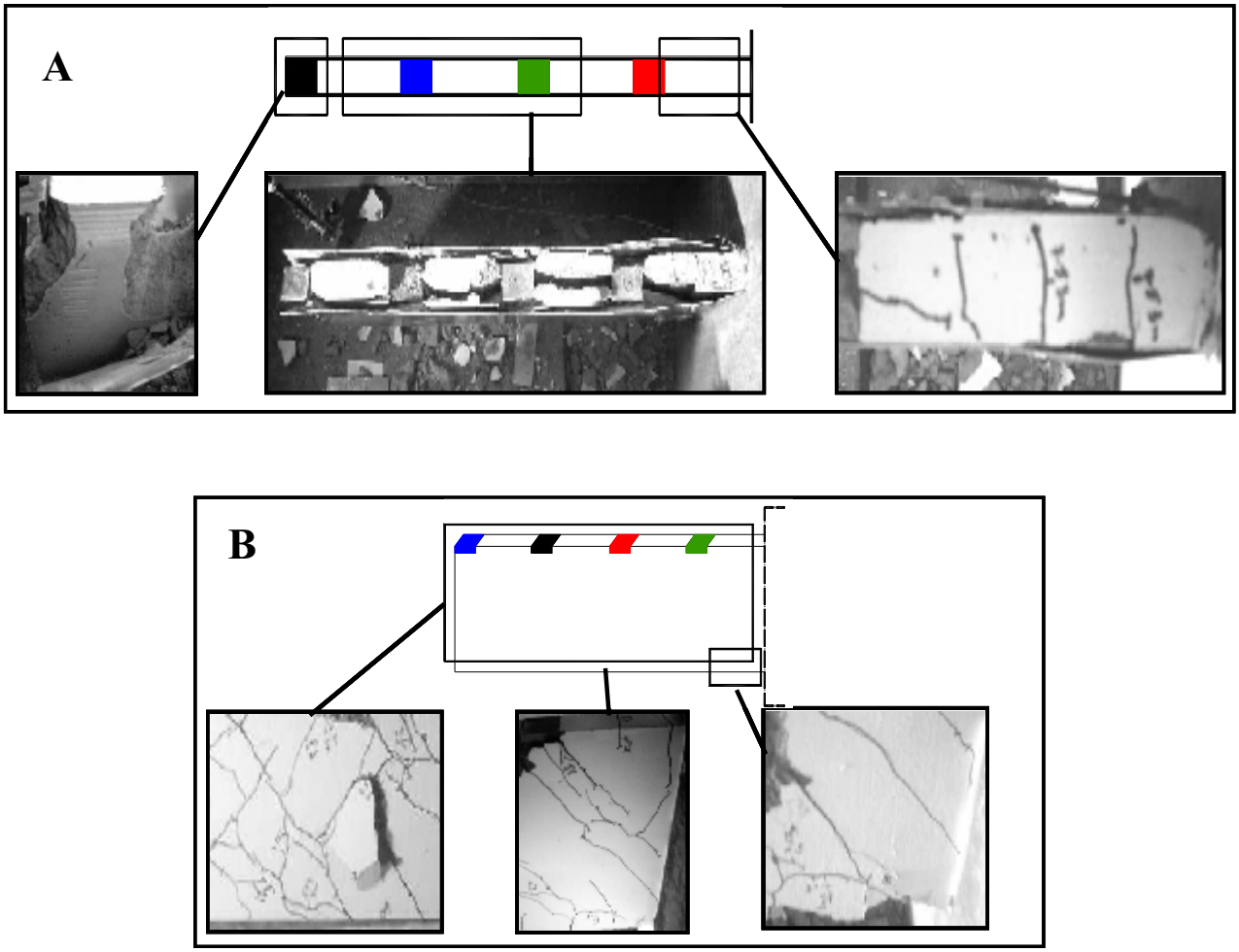

Figure 5 (A) Failure of S-C-S shear wall, (B) Failure of conventionally reinforced shear wall on impact loading

Throughout the experiment the S-C-S system possessed a visible resistance to the effects of impact loading with little disturbance to the wall. Plate separation, reduction in shearing, small deflections and increased ultimate strength were the characteristics at failure as observed by Oh et al [7] in their study. All of the above mechanisms were also observed here during the test. In particular at a fairly early stage the onset of plate peeling initiated by local buckling of the plates near the base where high compressive stress was present was noted. It was evident from the experiment that extensive cracking of the tensile zone of the wall took place which can be seen in Figure 5(A), which was attributed to a high tensile stress build-up at the top of the wall caused due to a confinement of stresses. Plate buckling was also visible from an early stage, which would imply an unsatisfactory transfer mechanism of shear flow from the concrete to the epoxy. The ultimate failure was attributed to the plate peeling accompanied by concrete rip-off as the contact area of concrete with the steel plate was reduced, Figure 5(A). The main observations from the study were (a) Early peeling of plates initiated by the local buckling of the plate on the compression side is a real possibility. (b) As the peeling progresses, the plate-concrete composite action is reduced and appears to be controlled by brittle behaviour of the concrete. It is clear that adequate means of preventing early buckling of plates near the base is a very important consideration in the design of S-C-S walls.

With respect to the conventional reinforced system severe cracking was evident from an early stage as expected in a normal R.C. construction, Figure 5(B). The impact effect caused the initiation of diagonal cracking as well as some cracks forming in the web at the rebound effect of the impact force. The ultimate failure mechanism was as a result of diagonal shear failure, which occurred as a continuation of shear cracking towards the restraint position leading to local crushing in the bottom corner of the wall

attached to the concrete block. The shear crack formed as a diagonal splitting crack inclined at 45° from the loading plate to the compressive zone of the wall where final compression failure took place through the break-off of concrete as can be seen in Figure 5(B).

5 CONCLUSION

The following conclusions are drawn from the preliminary study of conventionally reinforced and steel-concrete-steel shear walls subject to static and impact loading:

(a) S-C-S offers enhanced overall economical structural system with a reduction in construction time, due in the main to reduced, less complicated cross-sections, a direct consequence of conventional reinforcement omission.

(b) S-C-S reinforcement was found to be an inherently stronger and more robust system than the conventional reinforcement.

(c) Plated elements can resist large degrees of static and impact loading through composite action.

(d) Failure of the S-C-S system was due to the initiation of local buckling of the plates in the lower highly compressed area of the wall. The progress of peeling reduced the composite action causing concrete to fail in a brittle manner.

(e) To take full advantage of the S-C-S system early buckling of the plates should be delayed. This can be done by taking extra precaution in detailing near the base.

(f) S-C-S is a system highly suitable for tall buildings and other structures where robustness against impact, fire and terrorist activities are the main design considerations.

ACKNOWLEDGEMENTS

The first author would like to sincerely thank and acknowledge the support and help of Dr. Nutan Subedi, both in the undertaking of this study which formed part of the said authors Bachelors Degree study and in the preparation of this paper.

REFERENCES

[1] Chana, P., Fire safety with Concrete, Proceedings, *International conference held at the University of Dundee, Scotland, UK, 2008*, Concrete for Fire Engineering, pp. 13-26.
[2] Khoury, G. A., Passive fire protection of concrete structures, Proceedings, *Institution of Civil Engineers Structures & Buildings*, Vol. 161, June 2008, pp. 135–145.
[3] Corus, Fire resistance of steel-framed buildings, *Corus Construction & Industrial*, 2006 edition.
[4] Bostrom, L., Concrete exposed to fire, Proceedings, *International conference held at the University of Dundee, Scotland, UK, 2008*, Concrete for Fire Engineering, pp. 319-328.
[5] Dunne, D., Assessment of steel – concrete - steel shear wall, *B.Eng. Dissertation,* University of Dundee, 2005.
[6] Barnes, R.A., Baglin, P.S., Mayes, G.C. and Subedi, N.K., External steel plate systems for the shear strengthening of reinforced concrete beams, *Journal of Engineering Structures*, Vol. 23, No. 9, 2001, pp.1162-1176.
[7] Oh, B.Y., Cho, J.Y. and Park, D.G., Failure behaviour and separation criterion for strengthened concrete members with steel plates, *Journal of Structural Engineering,* Vol. 129, No. 9, 2003, pp. 1991-1198.

LONG SPAN COMPOSITE BEAMS SUBJECTED TO FIRE
Effects of Fire on Lateral Stability

Graeme Flint[a], Barbara Lane[a]

[a] Arup, 13 Fitzroy Street, London UK, W1T 4BQ

INTRODUCTION

With the recent increase in fundamental knowledge of structures coupled with the ease of use of modern design tools, building designers are able to create ever more efficient structures in the modern urban landscape. Structural design is typically governed by the well understood static load cases in the normal range of ambient temperatures, i.e. gravity, wind and snow.

By creating highly efficient and optimised structures for very specific ambient load conditions, the inherent strength reserve of a structure can be reduced. It is this strength reserve that a composite steel structure relies on when subjected to abnormal loading conditions such as severe fire. Therefore, it becomes necessary to explicitly consider fire loading during the design process to ensure that an acceptable level of safety is maintained in the structure.

This paper reports on the case study of a failure mechanism which was observed during a structural fire assessment of a new office building design. The structure includes long span, composite floor systems supported by a unique connections and a highly optimised structure. When subjected to fire, failure of the floor system occurred due to a mechanism which involved lateral stability failure of the bottom flange of the highly optimised long span beams. This resulted in a loss of load carrying capacity and failure of the structure.

The building presented as part of this study was a proposed design for a high-rise office building in the City of London. This paper concentrates on a local study of the response of long span cellular beams. The investigation was conducted using the ABAQUS Finite Element Analysis software.

A detailed investigation of the structure indicated a potential failure mechanism in the beams at the fire limit state. The failure mechanism was further investigated using a parametric study in order to better understand the causes of the failure mechanism. The paper shows the value of advanced structural fire analysis for the structural design and assessment of the robustness of this highly optimised structure with its unique beam connections.

1. STRUCTURAL DETAILS

The structural system of the proposed building is a perimeter braced frame. Vertical support around the perimeter of the building was provided through the use of a robust diagrid megaframe. The diagrid members were typically single- and double-web fabricated I sections.

One important structural detail is that the load bearing megaframe is located outside the main floor plate perimeter, as indicated in Figure 1 which shows part of a typical floor plant. Therefore the primary beam connecting into the perimeter column has an extension of approximately 1m beyond the normal floor-plate and thus is unrestrained by the floor slab. Additionally the support of the primary beam includes a substantial movement joint, comparable to a bridge movement joint. This joint acts to de-couple displacements between the floor structure and the megaframe. This movement joint allows movement in the direction indicated in Figure 1.

Internal columns were generally single- and double-web fabricated I sections.

The composite floor slabs were supported by fabricated beams that work compositely with the concrete floor plates. The floor I-beams spanned up to 16m and were generally 700mm deep with 200mm wide flanges. They have cellular web openings and gained additional strength by acting compositely with the concrete slab. The single spanning composite slab consisted of 150mm thick lightweight concrete cast onto a Ribdeck 80 trapezoidal profiled metal deck that acted as permanent formwork. The slab span ranges from 3m to approximately 4.85m.

2. STRUCTURAL FIRE PROTECTION

The structural fire analysis of the model was primarily intended to assess the robustness of the floor system assuming a reduced level of structural fire protection compared to code requirements. In this case, primary and secondary beams attached to columns were provided with 90 minute protection while intermediate secondary beams were left unprotected.
It has been shown in a number of recent analyses of tall office buildings (e.g. [1]) that this type of fire protection layout is a safe and efficient alternative to "code compliant" generic solutions. The analysis presented here was conducted in order to gain an understanding of the response of the building to fire under this engineered structural fire protection scheme. Such detailed knowledge of the building would not be gained from merely applying standard fire protection. The analysis utilized cutting edge modelling techniques and the latest analysis software.

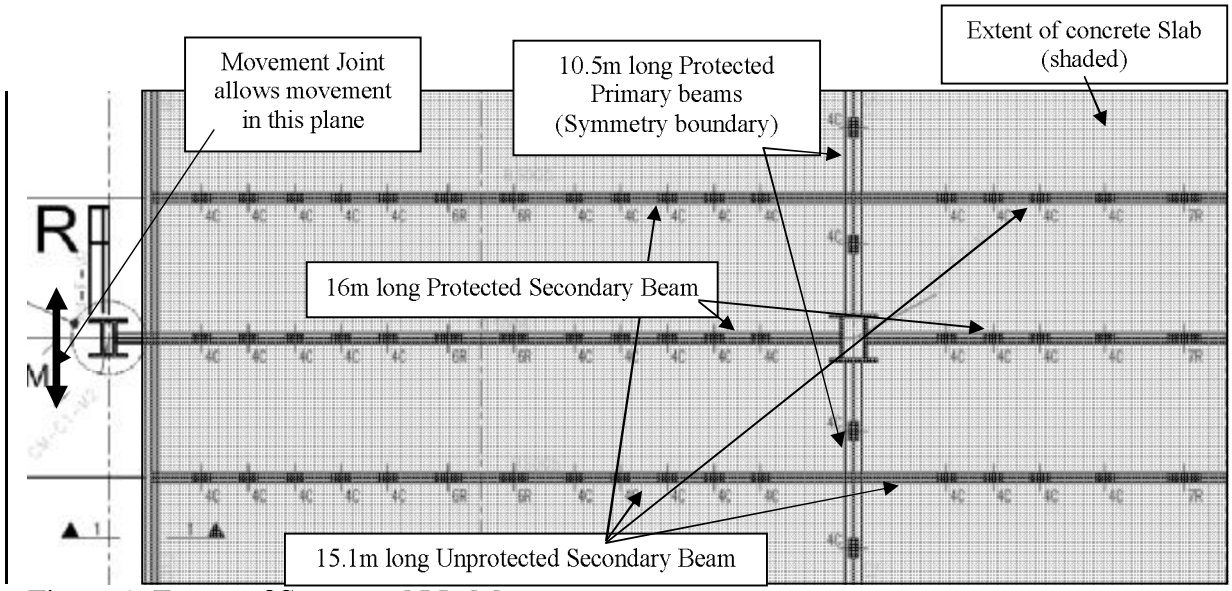

Figure 1: Extent of Structural Model

3. DESIGN FIRE

Our experience as consultants investigating the response of structures to Fire Limit State loading is closely linked to the use of the Eurocode Parametric Fire equation [2]. The Authorities Having Jurisdiction require the Eurocode Parametric Fire (PD6688.1-2)[3] to be used as the design fire. This method often leads to an extensive design fire including a substantial heating phase and an extended cooling phase to be applied simultaneously throughout the entire office floor plate. This type of temperature-time curve is considered onerous and may be unrealistic for the large compartments common in modern, open plan office buildings.
This conservatism is evident in the significant increase in temperature of protected steel members during the cooling phase until gas phase and solid phase temperatures are equal. Combined with the other conservatism included as part of the Eurocode calculation process, it is deemed to bring the design basis beyond that considered a reasonable worst case.
Therefore, the decay phase of the design fire of this case study was based on the results of the Cardington Office Fire Demonstration test. As the Cardington test was also conducted in a compartment that is considerably smaller than the office floors that are studied here, some modification to the Cardington test results were included to ensure the cooling phase was more representative.
As can be seen in Figure 2, the heating phase of the design fire was follows the standard fire curve up to 90 minutes. Previous experience has shown that the most conservative results of the Eurocode parametric equations for this type of building gives very similar results to the standard fire curve. To implement an appropriate cooling phase, the Cardington fire curve for the "office demonstration test" was conservatively translated until the start of the cooling phase coincides at 90 minutes. A

simple bi-linear curve was then fitted to the resulting test profile. As may be seen in Figure 2, the bi-linear curve is on the conservative side of the Cardington results throughout the duration of the cooling phase, until temperatures drop below 200°C.
The proposed design fire was compared with a number of full scale, natural fire tests (3 of the Cardington Tests and 1 test from the 140 William Street series performed in Australia) to ensure the cooling phase proposed captures the worst case of currently available test data from real compartment fires in the cooling phase. The proposed bi-linear cooling phase was observed to be consistent with the cooling phases of each of these tests. The design fire was applied to a single fire floor only.

4. HEAT TRANSFER

The heat transfer calculations for the steelwork were conducted using the Eurocode heat transfer equations in Eurocode 3 Part 1.2 [4] for the protected and unprotected steel members. Thermal gradients over the depth of the beams were included to introduce additional thermal curvature effects. Additionally, it was assumed that the voids between the beams and the underside of the trapezoidal deck would be left unfilled, thereby increasing the temperature in the top flange of the beams. The code [5] requires that the voids be filled with fire rated infill.
Columns were modelled assuming a uniform temperature throughout their cross section effectively assuming that all columns will be simultaneously heated from 4 sides. These are considered to be conservative assumptions. The temperature gradient through the depth of the slab varying with time was modelled using a 1D heat transfer model in ABAQUS.

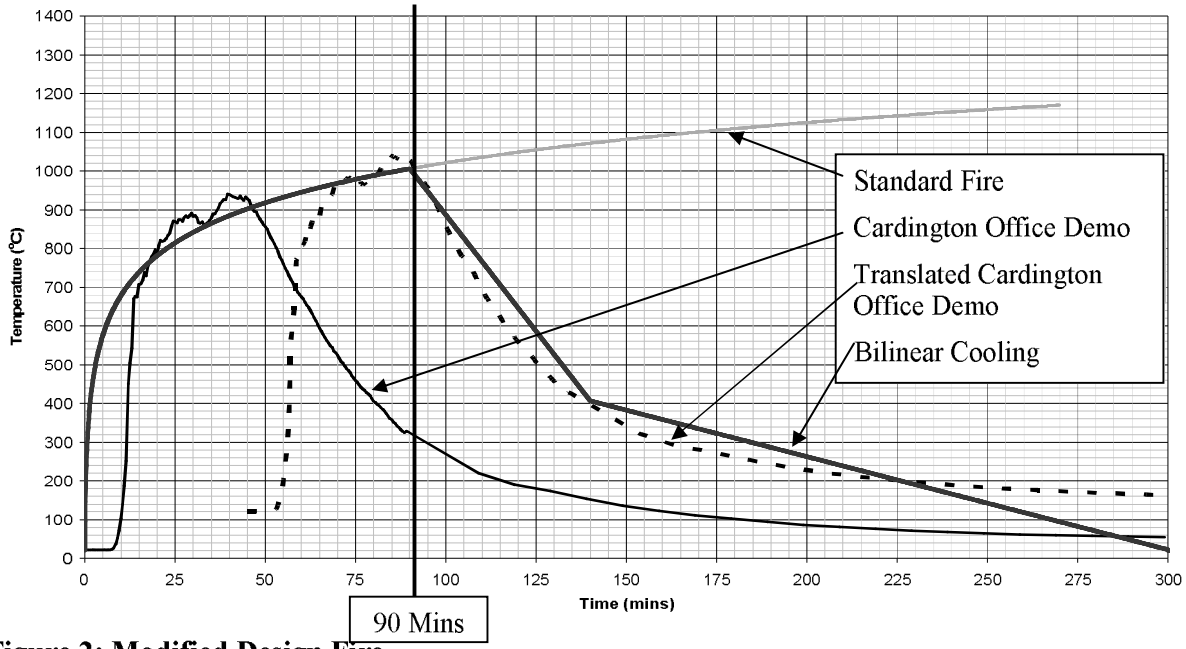

Figure 2: Modified Design Fire

5. MODEL CONSTRUCTION

The model investigated for the case study is presented in Figure 3. The model is shown both with and without the concrete slab for clarity.

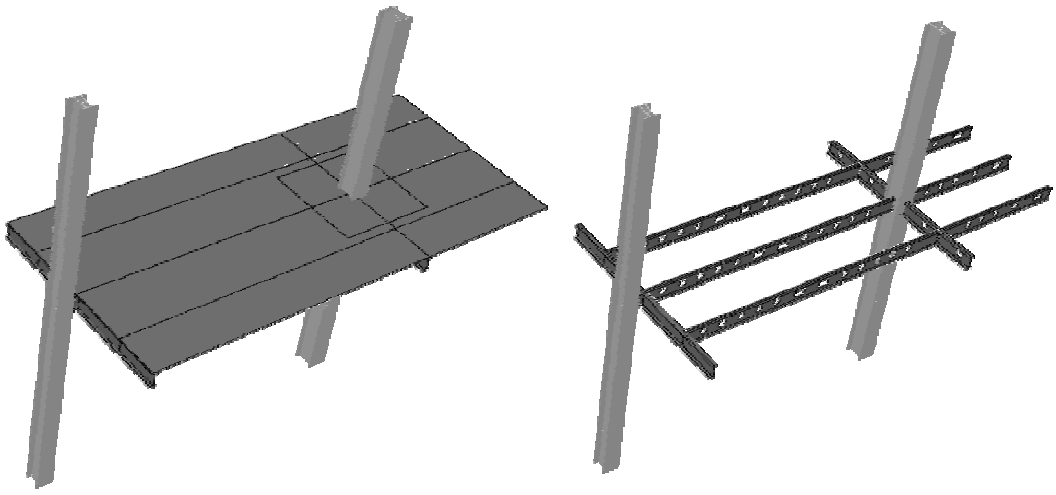

Figure 3: Structural Model (shown with and without slab)

In the model, the beams and slab were represented using 4-noded reduced integration shell elements. Columns were represented by 2-noded linear beam elements. Shell elements were used for the beams in order to capture local buckling behaviour, which would not be detected by beam structural elements. All material models for the analyses were based on Eurocode recommended values [4,6&7].

6. STRUCTURAL FIRE RESPONSE

The primary response identified by the analysis is the significant lateral deformation of the protected primary beam, as indicated in Figure 4 and also Figure 5 which shows the deformed shape of the beam at the onset of failure. Figure 5 shows the local buckling of the top flange and upper web. This behaviour occurred towards the end of the heating phase, starting at approximately 45 mins into the design fire. At this point, the temperature of the bottom flange was approximately 375°C while the web was at 400°C. This temperature is significantly lower than the temperature that a beam would normally be expected to fail (Usually 620°C). The resulted in twisting of the entire protected beam which led to failure of the connections between the beams and the megaframe (external perimeter) column, and subsequently collapse of the floor system.

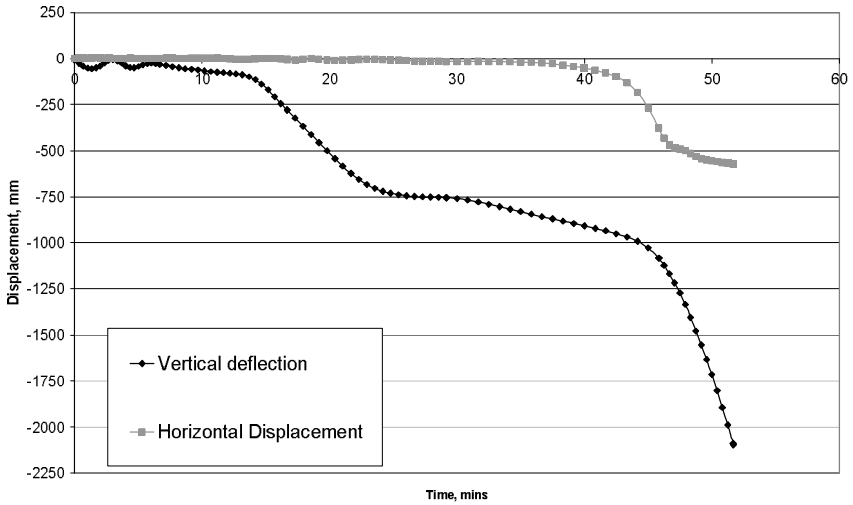

Figure 4: Protected Primary Beam Deflections at Mid-span

This type of lateral failure mechanism has been observed in real testing, for example the live fire test at Mokrsko testing facility conducted on the 18th September 2008, indicated in Figure 6.

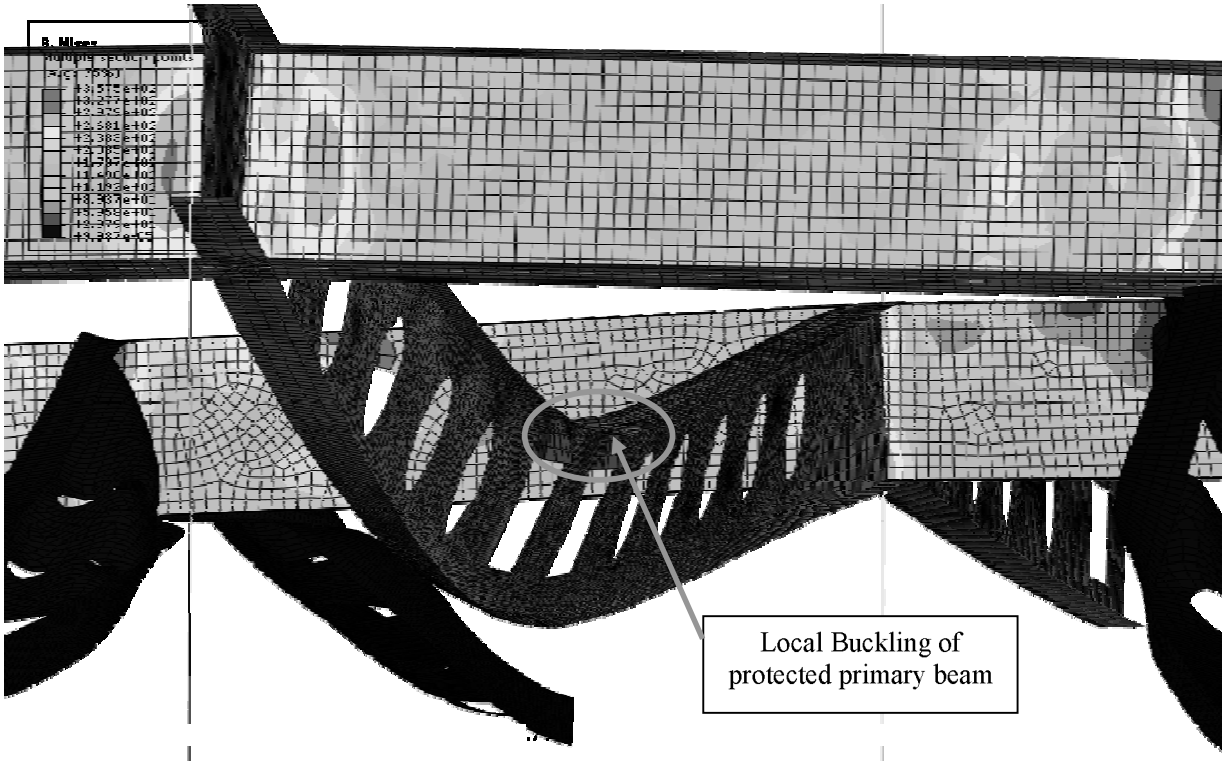

Figure 5: Protected Secondary Beam Failure (Slab not shown)

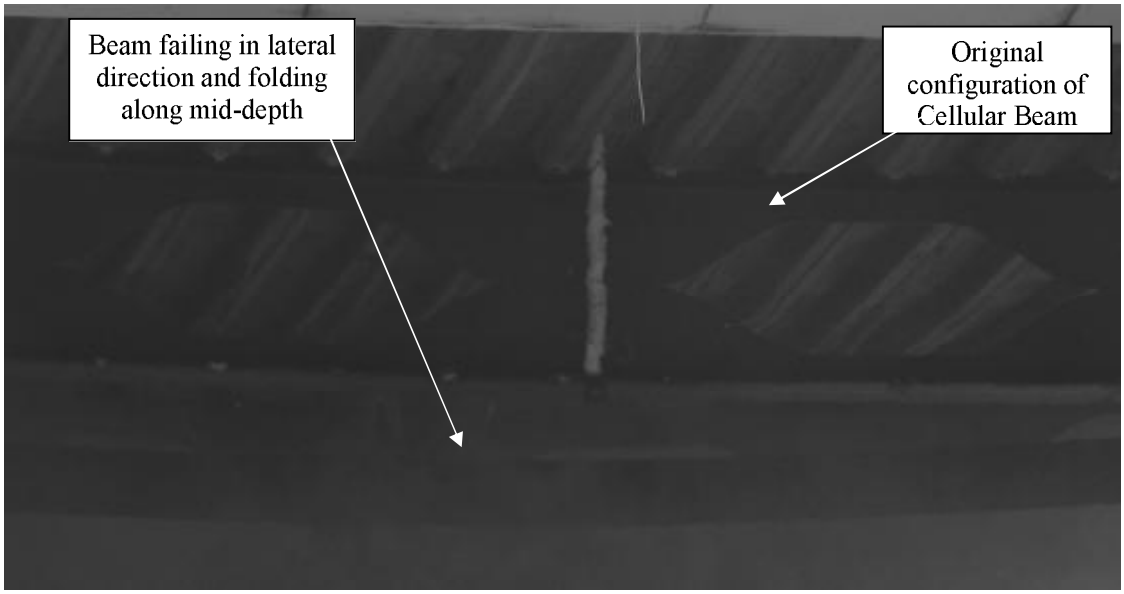

Figure 6: Lateral failure of comparable beam in Mokrsko live fire test

A parametric study was undertaken to determine the cause of the instability of the protected beam. The parameters investigated are indicated in Table 1. It should be noted that the increase in web thickness and structural fire protection to steel were also incorporated in models 3-8. The parametric study showed that failure was linked to the use of a deep beam (700mm deep) in combination with a relatively narrow bottom flange (200mm wide). This particular section geometry leads to a lateral instability of the beam at the fire limit state reducing the overall robustness of the floor system.
This kind of instability has not been observed in previous projects due to the unique nature of the building design.

Table 1: Parametric Study

Model	Parameter	Detail Changed	Result
1*	Web thickness	Protected secondary beam web thickness increased from 12 to 14mm	Fails
2*	Increased protection to steel	Thickness of fire protection on protected secondary beams increased by 10%	Fails
3	Holes in web	Central rectangular holed filled	Fails
4	Top flange temperature	Trapezoidal Deck voids assumed filled	Fails
5	Rebar location	Rebar moved to slab mid-depth to reduce temperatures	Fails
6	Secondary beam location	Unprotected secondary beams moved to equalize slab spans to 3.5m each.	Fails
7	Mid-span stiffener	Stiffener included at the mid-span of the protected secondary beam.	Fails
8	**Bottom flange width**	**Width increased from 200mm to 300mm (flange thickness reduced to 16mm to maintain original overall section area)**	**Stability maintained**

Note: * - The detail altered was incorporated in all following models.

7. CONCLUSIONS

This investigation was designed to assess the structural robustness of the of a proposed office building design. The structure designed for use under the standard ambient limit states (i.e. gravity, wind, etc) was subjected to a severe compartment fire.

The key response of the structure was a lateral failure mechanism in the protected long span primary beams during the heating phase of the design fire. This mechanism has also been observed in a recent large scale tests and is considered to be a realistic failure mechanism for beams with tall, relatively narrow sections.

A parametric study was conducted and the analysis indicated that in order to maintain stability throughout the design fire, the following alterations would need to be applied to the protected beams spanning onto the perimeter columns:

- Web thickness increased from 12mm to 14mm
- Fire protection thickness increased by approximately 10% above the typical 90 minute rating
- Width of the bottom flange of the beam would have to be increased from 200mm to 300mm (flange thickness may be reduced to 16mm to maintain original overall section area)

This paper has shown that detailed structural fire analyses can provide significant value in the design for robustness of highly unconventional and unique buildings. By analysing the structure in detail a failure mechanism was observed that would not have been detected if the structure had been protected to the usual code provisions without such an analysis.

REFERENCES

[1] A. Heise, G. Flint & B. Lane, Effect of fire on tall buildings: Case study, *Proceedings of the 3rd International Conference on Steel and Composite Structures (ICSCS07)*, 2007

[2] BSI, Eurocode 1: Actions on structures. General actions - Actions on structures exposed to fire, BS EN 1991-1.2:2002, 2002

[3] BSI, Background paper to the UK National Annex to BS EN 1991-1.2, PD 6688-1.2:2007, 2007

[4] BSI, Eurocode 3: Design of steel structures. General rules - Structural fire design, BS EN 1993-1.2:2005, 2005

[5] ASFP, Fire protection for structural steel in buildings 4th edition, ASFP Publications, Revised April 2008

[6] BSI, Eurocode 2: Design of concrete structures. General rules - Structural fire design, BS EN 1992-1.2:2004 2004

[7] BSI, Eurocode 4: Design of composite steel and concrete structures. General rules - Structural fire design, BS EN 1994-1.2:2005, 2005

Application of Structural Fire Engineering, 19-20 February 2009, Prague, Czech Republic

PERFORMANCE OF SHEAR STUDS IN FIRE

Sengkwan Choi[a], Sanghoon Han[a], Sungbae Kim[b], Ali Nadjai[a], Faris Ali[a] & Joungyoon Choi[c]

[a] FireSERT, School the Built Environment, University of Ulster, Newtownabbey, BT37 0QB, UK
[b] R & D Division, Sen Structural Engineering, Seoul, Republic of Korea
[c] Centre of Reliability Research, Korea Institute of Construction Materials, Gunpo, Republic of Korea

INTRODUCTION

There have been significant improvements in the structural design of multi-storey buildings in recent years, many of which have been the result of developments in composite construction. The wide variety of automatically fabricated long-span composite structures not only has economic benefits due to fast, light-weight and accurate construction, but also maximizes the potential for flexibility in internal layout, which is a greatly desired feature in modern buildings. In particular, understanding and technology surrounding fire safety design for steel and concrete composite structures has been noticeably advanced due to the introduction of new insulation materials, the improvement of computational modelling technology and advanced design methodologies obtained through extensive full scale experiments in fire.

Structural fire safety calculations have been traditionally based upon prescriptive methods – according to hourly ratings, on code requirements with respect to standard fires such as ASTM E119 [1], BS 476 Part 20 [2] or ISO 834 [3]. Now, however, both domestic (UK) and international regulations permit design for structural fire safety to be carried out according to performance based concepts. This approach can be particularly beneficial when considering various types of composite structures, such as composite truss, slim floor, cellular beams, as these can be shown to obtain potentially significant structural performance benefits by adopting an optimal configuration of structural sections and relevant insulation requirements.

A wide-ranging investigation of the in-fire performance of such composite structures has highlighted various local instabilities that are deemed to likely govern the overall flexural performance of the structures. The research presented here aims to act as a pilot study to examine the in-fire performance of headed shear studs. These are commonly used in composite structures over the world and appear to be a key element in maintaining the global structural integrity of composite structures.

CONTEXT OF RESEARCH

The flexural performance of composite structures depends on the effective transfer of longitudinal shear stress and control of uplift force at the interface between the steel and concrete constituents. The mode of collapse initiated by failure of the bond at this interface is brittle and often catastrophic and the appropriate use of mechanical shear connectors is therefore essential when trying to achieve composite action of the two materials at the ultimate limit state. Similarly, there is a requirement for the capacity of shear connectors to be maintained in fire to prevent premature brittle failure. It is furthermore preferable for the structure be resistant to local buckling and load carrying mechanism transition.

Although various configurations of shear connectors have been proposed and used over the last half century, a headed stud (commonly 19 mm diameter and 100 to 125 mm pre-welded length) is now the most widely used type of flexible shear stud in composite construction in buildings due to the speed, convenience and reliability of the welding process involved in their placement

The strength and ductility performance of headed stud shear connectors are typically investigated by push-out tests using a solid slab and by using the load – slip relationship obtained from the test, composite action can be reliably designed into a flexural member. The capacities of stud shear connectors embedded in a solid slab were first evaluated by Ollgaard, Slutter and Fisher [4]. Through the use of empirical methods, the authors developed a formula to assess the strength of a

stud as a function of the stud area and concrete properties, with an upper limit equal to the tensile strength of the stud:

$$Q_u = 0.5 A_{sc} \sqrt{f_{ck} E_c} \leq A_{sc} f_u \quad (1)$$

where A_{sc} is the cross-sectional area of the stud shear connector

f_{ck} is the cylinder compressive strength of the concrete ($= 4730\sqrt{f_{ck}}$)

E_c is the modulus of elasticity of concrete

f_u is the ultimate tensile strength of the stud material

Eq. 1 is included in both the AISC [5] and CSA [6] codes of practice as a fundamental formula to assess the strength of studs. In Eurocode 4 Part 1.1 [7], however, the strength of headed studs in solid slabs is based on the simplified engineering assumption that a stud fails either in the concrete alone (height / diameter of stud > 4) or in the steel alone as follows.

$$Q_u = 0.37 A_{sc} \sqrt{f_{ck} E_c} \leq 0.8 A_{sc} f_u \quad (2)$$

Stark et al [8] determined the coefficient of 0.37 used in Eq. 2 by means of a statistical study, and the upper limit is taken as 80% of the tensile strength of the stud. The design capacity of the shear connector is introduced with a partial safety factor of 80% of the nominal strength to ensure that the material ductility requirements and discrete nature of resistance are met [7].

In the UK, Menzies' regression analysis of standard push-out experiments [9] is used to determine the design strength of headed studs embedded in solid concrete slabs (provided in tabulated form in BS5950 Pt 3 [10]). A large number of additional tests have been conducted in Europe and North America with the aim of identifying the strength reduction effects of studs embedded in various shapes of profiled deck slabs. However, as this work is beyond the scope of current publication, the detail is not included. It is noted that, as the force developed in composite beams is not identical to that developed in push-out tests, caution needs to be taken if applying the test results to beams. It is nevertheless known that the performance of shear connectors in beams is much better than in push-out tests.

Zhao and Kruppa [11] conducted experiments to determine the shear capacity of headed studs and angled connectors, subject to the standard ISO fire, in conjunction with solid slabs and composite slabs with profiled sheets. The results of this study suggest that the strength of headed studs at elevated temperatures must be assessed using an absolute 20% strength reduction and that the strength retention of steel material in relation to the ultimate tensile strength is:

$$Q_{u\theta} = 0.8(0.8 A_{sc} f_u) SRF_{u\theta} \quad (3)$$

Where $SRF_{u\theta}$ is the strength retention of steel at θ°C with respect to the ultimate tensile strength

Eq. 3 is used in Eurocode 4 Part 1.2 [12] as verification of the shear resistance of studs in fire and, whilst concrete crushing failure at elevated temperatures is also considered in the code, it is generally considered that the stud failure governs the performance in fire.

The plastic resistance of composite beams (found using rectangular stress blocks) is determined with the provision that the shear connectors have sufficient capacity to deform - hence they must maintain resistance to shear at slips. A design application rule to accept the ductility of the connector is implemented in a form of 5 mm available slip. Since the deflection of composite beam in fire is often significantly larger (commonly up to span/20), care is also considered in the subsequent levels of the stud slip.

EXPERIMENTAL PROGRMAMS

In order to investigate the performance of the stud connectors in fire, the standard push-out test was

modified to use half of the standard set-up [13]. In the modified experiment (Figs. 1a and 1b), one side of the solid concrete block in the standard push-out specimen was replaced with an electric furnace to expose the steel member to fire from 3 sides. Vertical loading was applied downward from the top of the steel section and the relative displacements were measured between the top of the steel section and the top of concrete slab. To provide appropriate stability to the test assembly under loading, lateral movements of the slab base and top of the steel section were restrained. Under these boundary conditions, the development of uplift forces in the connectors could be limited to acceptably low levels.

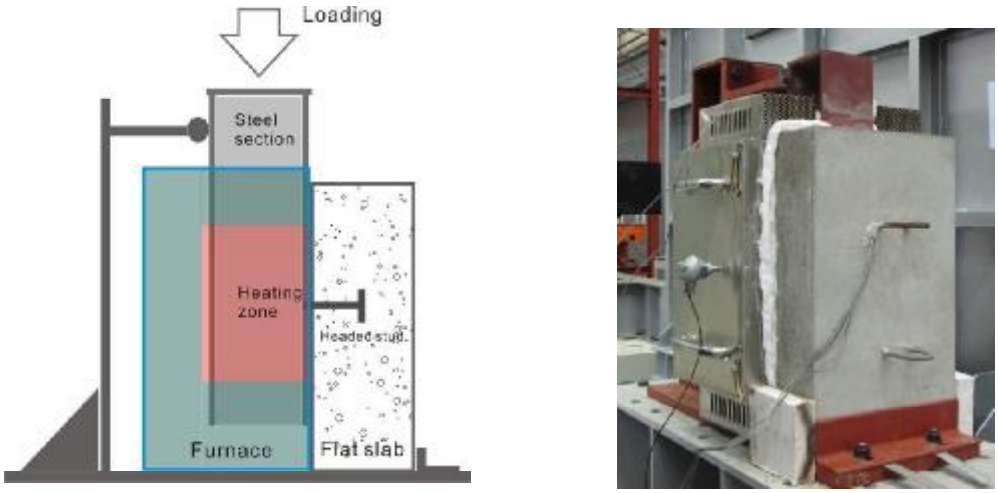

(a) Schematic drawing of the modified push-out test (b) Instrumentation arrangements

Fig. 1. Modified push-out tests in fire

The specimen (Fig. 2a) consisted of a 650 mm length of S355 steel section (150×150×30 UC) connected to a C30 flat concrete slab (400 mm width × 150 mm depth × 500 mm height), using two headed studs of 19 mm diameter × 100 mm depth. A natural bond at the interface was prevented by greasing the steel flanges before casting the slab. K-type thermocouples were installed to measure temperature developments of the flanges and web in the steel section and locations at 10 mm, 30 mm and 50 mm depths of the headed studs from the fire exposed surface (Fig. 2b). Tension testing of the studs reported that the average characteristic properties of the steel were yield strength of 349 N/mm^2, an ultimate tensile strength of 427 N/mm^2 and an elongation of 25 %. Two specimens were loaded until collapse for cases of room temperatures (20^{o}C), 30 minutes and 60 minutes of the standard ISO fire.

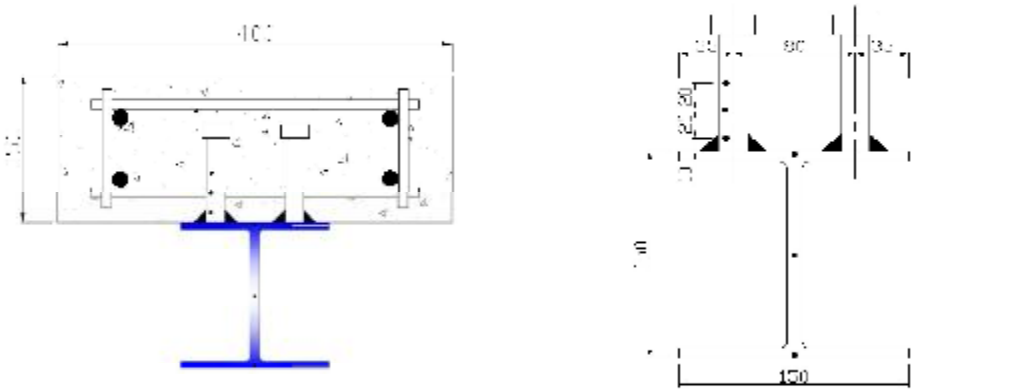

(a) Cross-section of specimen (b) Locations of thermocouples (marked by •)

Fig. 2. Specimen for modified push-out test

ANALYSIS OF RESULTS

In order to establish the shear capacity of the headed stud when subjected to the standard ISO fire the temperature developments of the specimen were obtained for the duration of the tests, as shown in Figure 3. It was found that the temperature difference between the 10 mm and mid-depth (50 mm) reference points was in excess of 200 °C within 30 minutes of the standard fire and approximately 300 °C at 60 minutes. As the temperature rise at 10 mm was over 400 °C at 30 minutes, a corresponding and significant reduction of strength was seen in this area. Further, as the temperature rise of concrete slabs is generally much lower that that of steel elements in fire, it could be expected that the collar area of the shank will experience the highest levels of strength reduction due to the temperature increase.

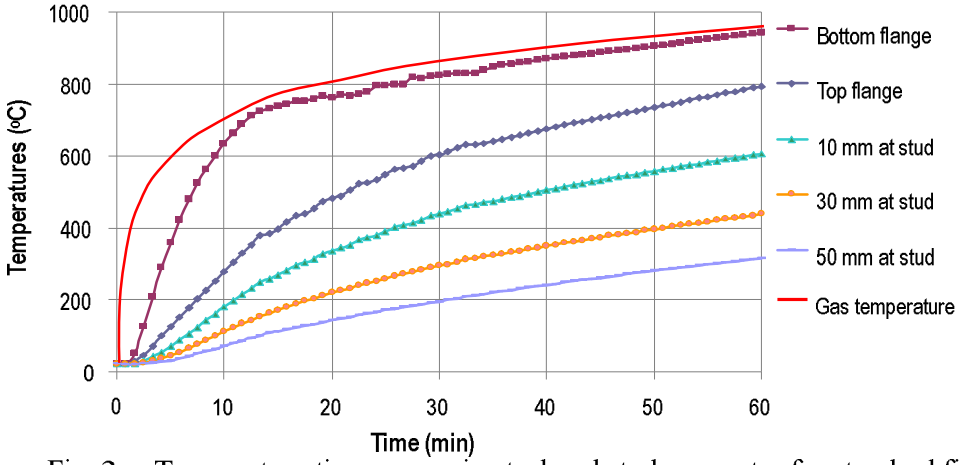

Fig. 3. Temperature-time curves in steel and stud connector for standard fire

The load-slip relationship for stud shear connectors was monitored at ultimate limit state, 30 and 60 minutes of the standard ISO fire; the relationship per stud is plotted in Figure 4. At a slip of 5 mm, the ultimate capacity of the stud was measured to be 120 kN at 0 minutes, 85.0 kN at 30 minutes and 38.0 kN at 60 minutes respectively. By modifying Eq. 1 an equation can be proposed to evaluate the stud strength at elevated temperatures:

$$Q_{u\theta} = A_{sc} f_u SRF_{u\theta} \tag{4}$$

The strength of the stud at ULS when estimated using Eq. 1 (121 kN), shows very good agreement with the test result of 120 kN at ULS. Using Eq. 4, the residual strength of the studs at 30 and 60 minutes in fire is calculated as 88.7 kN and 38.0 kN respectively, which also demonstrates excellent agreement with the experimental results of 85.0 kN and 38.0 kN respectively.

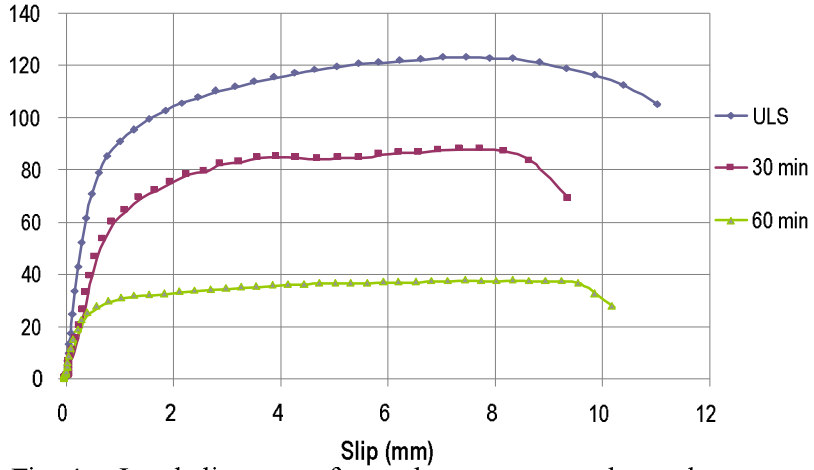

Fig. 4. Load-slip curves for stud connectors at elevated temperatures

Examination of the failure mechanism exhibited by the studs, as the resistances estimated using Eq. 1 for crushing of the concrete surrounding the connector and connectors shearing off at the base are similar, interaction of the failure modes occurred at ultimate limit state. At elevated temperatures, shear failure consistently occurred at the weld-collar/shank interface, as shown in Figure 5. The reasons for this behaviour are that at the weld-collar/shank interface (1) a concentration of high stress occurs in the push-out tests and (2) a higher temperature rise develops in the area due to the heat flux through the top flange of steel section in fire. When compared to the research of Zhao and Kruppa [11], the observed failure mode of headed studs in fire is generally alike, but in the tests reported here a higher strength was recorded due to the presence of lateral restraint at the bottom of the slab.

(a) Surface of concrete section (b) Surface of steel section (c) Failure of headed stud (601-2)

Fig. 5. Failure of stud shear connector after push-out test at 60 minutes of the standard fire

CONCLUSIONS

This pilot project was designed to investigate the capacity of headed shear studs at elevated temperatures through the use of a modified push-out test with a solid concrete slab. An electric furnace attached to the test assembly provided three-sided fire exposure to the specimen. At room temperature, 30 and 60 minutes of the standard ISO fire, tests were conducted to identify the strength retention properties of the studs. Temperature developments were measured across the steel section and along the stud shank. The headed studs failed at elevated temperatures due to shear of the weld-collar/shank interface. An equation was proposed to allow assessment of the residual strength of the stud in fire and this demonstrated a very good agreement with the test results.

REFERENCES

[1] American Society for Testing and Materials , ASTM E119-95a Standard Test Methods for Fire Tests of Building Construction and Materials, West Conshohocken, PA, 1995

[2] British Standards Institution, BS476: Fire Tests on Building Materials and Structures: Part20: Method for Determination of the Fire Resistance of Elements of Construction (General Principles), UK, 1987

[3] International Organization for Standardization, ISO834: Fire resistance tests - Elements of building construction, Geneva, 1975

[4] Ollgaard, J.G., Slutter, R.G. and Fisher, J.W., Shear strength of stud connectors in lightweight and normal weight concrete, engineering Journal, AISC, 8(2), 1971, pp. 55-64

[5] American Institute of Steel Construction, Load and Resistance Factor Design Specification for Structural Steel Buildings, Chicago, IL., 1993

[6] Canadian Standards Association, Steel Structures for Buildings – Limit State Design, CAN3-S16.1-M84, Rexdale, Ontario, 1994

[7] European Committee for Standardisation, ENV 1994-1-1: Eurocode 4: Design of Composite Steel and Concrete Structures. Part 1.1: General Rules and Rules for Buildings, BE, 1994

[8] Stark, J.W. and von Hove, B.W.E.M., Statistical Analysis of Pushout Tests on Stud Connectors in Composite Steel and Concrete Structures, TNO Buildings and Construction Research, Delft, Report BI-91-163, 1991
[9] Menzies, J.B., CP117 and shear connectors in steel-concrete composite beams made with normal-density or lightweight concrete, Structural Engineers, 49(3), pp. 137-153
[10] British Standards Institution, BS 5950: Structural use of steelwork in building Part 3: Design in composite construction Section 3.1: Code of Practice for design of simple and continuous composite beams, UK, 1990
[11] Zhao, B. and Kruppa, J. EUR 16822-Properties and Service Performance: Fire resistance of composite slabs with profiled steel sheet and of composite steel concrete beams Part2: composite beams, Luxembourg, 1997
[12] European Committee for Standardisation, ENV 1994-1-2: Eurocode 4: Design of Composite Steel and Concrete Structures. Part 1.2: General Rules: Structural Fire Design, Brussels, BE, 1994
[13] British Standards Institution, BS 5400: Steel, concrete and composite bridges Part 5: Code of practice for design of composite bridges, UK, 1979

FIRE COMPOSITE FLOOR CELLULAR STEEL BEAMS FOR BUILDINGS

Nathan Goodfellow[a], Ali Nadjai[a], Kong Fah Tee[a] , Faris Ali[a], Sengkwan Choi[a],

[a] Ulster University, School Built Environment, FireSERT Block 27, Shore Road, Jordanstown, Belfast BT37 0QB, United Kingdom

INTRODUCTION

Cellular beams (CBs) are currently being widely used in multi-storey buildings where, as well as reducing the total weight of the steelwork, they help decrease the depth of floors by accommodating pipes, conduits and ducting. They are also used in commercial and industrial buildings, warehouses and portal frames. CBs produced by modern automated fabrication processes can be competitive for the construction of both floor and roof systems.

Fig. 1. Use of cellular beams in buildings

A composite concrete floor-slab has the effect of significantly increasing the flexural resistance of a steel section; however its effect on shear resistance is more complex. Investigation of the behaviour of composite beams with isolated web openings in otherwise solid webs has shown that the slab significantly increases the shear-carrying capacity beyond that of the steel beam alone. This is due to the enhanced flexural and shear capacity of the upper part of the beam across an opening, although an unsupported web-post is more susceptible to buckling. In fire, the temperature distribution across a composite member is non-uniform, since the web and bottom flange have thin cross-sections and a greater exposed perimeter than the top flange. The deterioration of the material properties of the web will therefore become an important effect on the overall performance of the member in the event of fire (Figure 1). The structural behaviour of beams with opening is relatively complex and involves the main failure modes which are included in the design model for ULS design at ambient temperature and in fire conditions described in the literature review [1-9]

This paper describes an experimental study at elevated temperatures on the behaviour of full scale composite floor cellular steel beams. A total of four specimens, comprising two different steel geometries, applied load ratios and different temperature time curves. The beams were designed to fail by web buckling, which was observed in all the tests. Failure temperature observed in the fire tests indicated that failure by web post buckling of cellular beams in fire cannot simply be estimated by applying temperature dependent reduction factors on stiffness, as given in codes. Simple model was developed to calculate the deflections and ultimate loads for cellular beams in fire situations. Also, a finite element model using DIANA was then established with both material and geometrical non-linearity using shell elements to compare the experimental results and the simple model. The comparison between the finite element prediction, actual tests results and simple model are quite good in terms of failure modes, load deflection behaviour and ultimate loads.

1 EXPERIMENTAL RESULTS TESTS AT ELEVATED TEMPERATURES

Initially two composite cellular steel beams were tested under the same fire slow curve [7]. This fire curve was set up in order to produce lower peak temperatures but of longer duration sufficient to permit significant heat conduction, which may produce a large build up of vapour pressure and the creation of significant thermal expansion producing a restraint force coming from the concrete slab. Whereas, the last two composite beams were tested under the ISO 834 temperature – time curve subjected to 0.3 x failure load obtained from the cold tests given respectively as 108 kN and 126 kN [7]. The positions of the thermocouples (Figure 2) were located at each web post along its depth of the section and also around the openings.

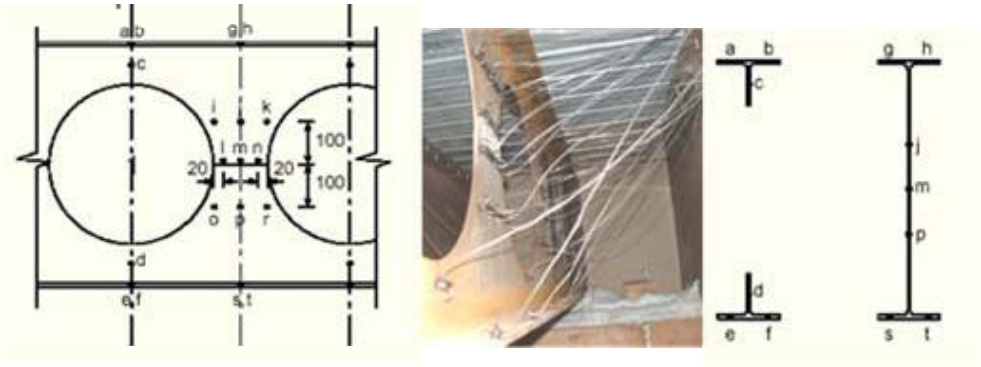

Fig. 2. Typical Thermocouples locations

The stiffness in beam (Fig 3) is linear elastic up to 13 minutes (T_{fur}= 717 ^{o}C) with a reading deflection of 23 mm, whereas Figure 4 stayed linear up to 16 minutes (T_{fur}= 748 ^{o}C) with a deflection equal to 26 mm. At 30 minutes of time (T_{fur}=842 ^{o}C) both beams A and B failed with a recording different respectively 179 mm and 235 mm. The instability of the beams and the rapid loss of stiffness of web post capacity occur faster than the beams tested during the slow fire curve [7] and this is due to the severity of the ISO834 temperature time curve.

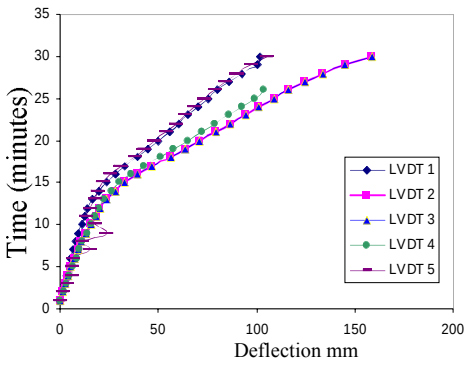

Fig. 3. Time versus deflection of test A

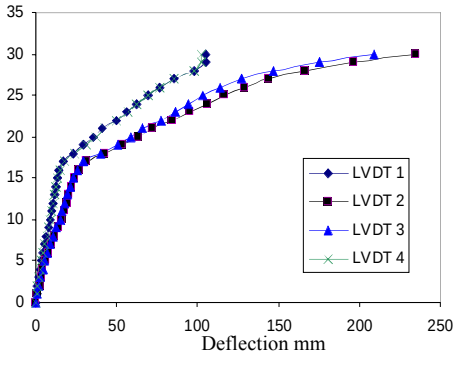

Fig. 4. Time versus deflection of test B

2 FINITE ELEMENT MODEL AND COMPARISONS

The composite cellular steel beams in ambient and fire tests were modelled using the commercial finite element software DIANA [10] at the University of Ulster. Shell elements with the ability to handle large strains, large deformations, and plasticity were used to model the cellular steel beam. Composite brick elements were used, incorporating a smeared crack approach for the concrete, to model the composite slab. Both the steel deck, as a bottom layer, and the reinforcing mesh as a layer within the concrete was included within the composite shell element. Due to the high density of the shear connectors used in the test, full interaction between the beam and supporting composite slab was assumed. This assumption is also justified from test observations [7] which confirmed that no stud failure occurred before web-post buckling of the beam.

Imperfections were introduced, based on an Eigen value buckling analysis, with the amplitude of the imperfections being governed by the thickness of the steel plate for local bucking and the overall length of the section for global buckling [13]. An implicit analysis was conducted in two steps, where the load was applied in the first step and the temperature was applied in the second step.

Figure 5 shows the output deformed shape of the Diana program compared with the actual failure mode of the symmetric test specimen. It is obvious when comparing the two that the same failure mode has occurred as the web post buckles under the applied load forming and S shape caused by the formation of hinges around the openings.

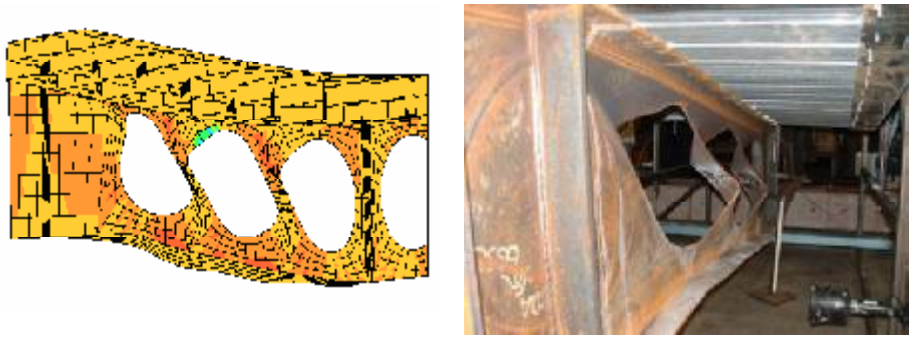

(a) Diana output (b) Test failure mode

Fig. 5. Asymmetric section at point of failure

The measured yield and ultimate tensile strength of the steel was used in the simulation. The beam geometry was based on measured dimensions. The stress-strain curve at elevated temperatures for steel given by EN1994-1-2 [11] was adopted. For the stress-strain of the concrete in compression, at elevated temperatures, the relationship given in EN1994-1-2 [11] was adopted. For concrete in tension, at both ambient and elevated temperatures, the fracture energy concept [12] is used to estimate the ultimate tensile strain of the concrete.
Thermocouples positioned in the top, middle and bottom of the concrete composite slab recorded the relevant values. These were applied to the model directly by defining temperature points through the shell thickness. The temperature variation along the beam section was modelled. In the last 10 minutes of the tests a decrease in temperature was recorded due to heat loss through a window.

Figure 6 shows the time-deflection comparison between the test and FEA at elevated temperatures. A very good correlation was obtained between the predictions and test results. In both cases (Figure 7) web post buckling is clearly observed in the modelling corresponding to the failure mode witnessed in the tests.

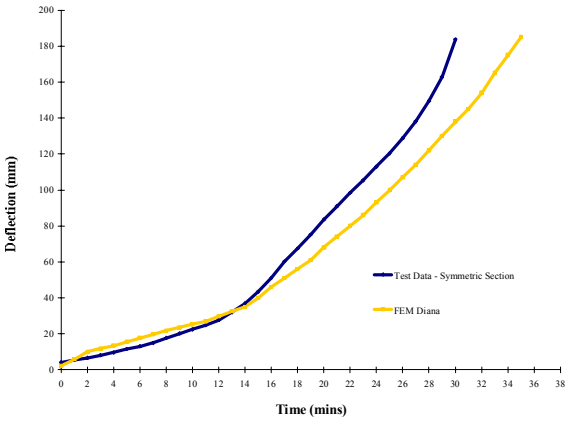

Fig. 6. Graph for symmetric section – ISO fire

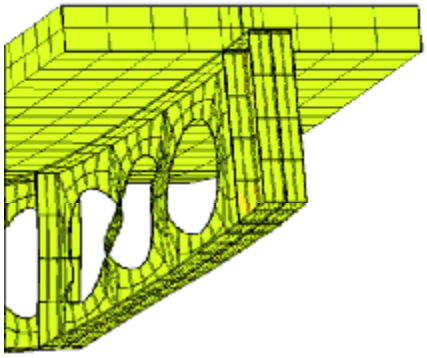

Fig. 7. Mesh Deformation

3 DEFLECTION

A method to estimate the beam mid-span (maximum) deflection is presented based on the ratio of applied moment to moment capacity as well as a new reduction factor for the second moment of area. The maximum deflections obtained from the experimental tests and different equations for the symmetric and asymmetric cellular composite beams are shown in Figures 8 and 9, respectively. The maximum deflections at the centre for simply supported beams at both ends with one centre load and two equal loads symmetrically placed are

$$\delta = \frac{Pa}{24EI}(3L^2 - 4a^2) \tag{1}$$

$$\delta = \frac{PL^3}{48EI} \tag{2}$$

Where P is the applied load, L the beam length, a the distance between the load and the support, E the Young's Modulus and I the second moment of area. The reduction factor for E at elevated temperatures is based on the Eurocode EN1993-1-2 [14]. The maximum thermal bowing deflection at the beam centre can be calculated as

$$\delta_t = \frac{\alpha \Delta T L^2}{8d} \tag{3}$$

Where α is the coefficient of thermal expansion, ΔT the temperature difference between the top and bottom of the beam cross-section and d the height of the cross-section. The ratio of the applied moment to the moment capacity [8] can be expressed as

$$MR = \frac{M_A}{M_\theta} \qquad (4)$$

If this moment ratio is less than 1 (before the web post buckles), the moment capacity is greater than the applied moment. Thus the deflections of the beams can be reasonably determined from the summation of Eqs. (1) and (3) or Eqs. (2) and (3). However, when the moment ratio is greater than 1 (after the web post buckles), the beam deflections can not be accurately determined from the above equations. Beyond these points the applied moment is resisted by the concrete slab. Therefore, the moment ratio has to be taken into account in the calculation of beam deflections.

Another important issue in the calculation of beam deflections is the reduction factor for *I* at elevated temperatures. For simplicity, only one-thirds of *I* are reduced when the moment ratio is greater than 1 (when the temperatures at the bottom flange and bottom web are greater than 550^{o}C). It is shown that *I* reduction factor is even larger (approximately three-fifths of *I*) for the asymmetric section as shown in Figure 9. Before comprehensive conclusions can be drawn, further research studies regarding the accurate *I* reduction factor at elevated temperatures will be necessary.

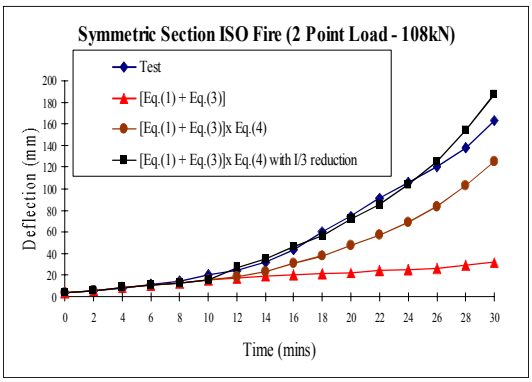

Fig. 8. Maximum deflections for the symmetric cellular composite beam

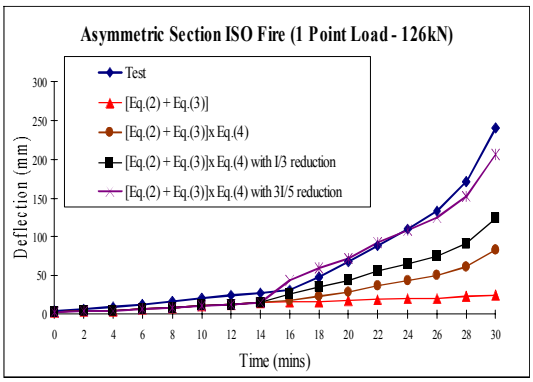

Fig. 9. Maximum deflections for the asymmetric cellular composite beam

4 CONCLUSION

This paper describes an analytical study of the behaviour of composite floor cellular steel beams in fire conditions conducted at the FireSERT, University of Ulster. The study suggests the following:

- The beams failed due to web post buckling and the instability resulted in sudden loss of stiffness and strength in the beams
- The experimental data has compared well with the results from the Finite Element Modelling, giving confidence that it can be used for further parametric studies.
- The numerical model is capable to simulate the mechanical behaviour of composite Cellular beam sections in both cold and at elevated temperature conditions with a relatively high accuracy.
- The deflection hand calculation approach compared very well with the experimental tests but needs to be improved to include the concrete cracking at elevated temperatures and the effects of the shear connectors. It is still necessary to validate the proposed approach with more numerical and experimental data.

REFERENCES

[1] Liu, TCH, Liew, KH, Behaviour of Cellular Steel Beams in Fire, Interflam 2004, pp157-168, 2004.

[2] SCI, 2004. RT1006 Version 02 - Fire Design of Cellular beams with Slender Web Posts, SCI, Ascot, 2004.

[3] Bitar, D.; Demarco, T.; Martin, P.O. 2005. Steel and non composite cellular beams – Novel approach for design based on experimental studies and numerical investigations, Proc. 4th Eurosteel Conference, Maastricht, June 2005.

[4] Lawson et al, Design of composite asymmetric cellular beams and beams with large web openings, Journal of Constructional Steel Research, V62, N6, June 2006

[5] BS5950-8:2003 Structural use of steelwork in building - Part 8: Code of practice for fire resistant design

[6] BS5950-1:2000 Structural use of steelwork in building - Part 1: Code of practice for design - Rolled and welded sections

[7] Nadjai, A.; Vassart, O.; Faris, A.; Talamona, D.; Allam, A. & Hawes, M. 2006. Performance of cellular composite floor beams at elevated temperatures, Proc. SIF 2006, pp. 813-823.

[8] Nadjai, A, Goodfellow, N, Vassart, O, Ali, F and Choi, S, Simple calculation method of composite cellular beams at elevated temperatures, Proc. SIF 2008, pp. 551-559.

[9] Vassart, O. , Bouchair, A.,, Muzeau, J.-P. and Nadjai, A, Analytical model for the web post buckling in cellular beams under fire, Proc. SIF 2008, pp. 3-11.

[10] TNO Building and Construction Research. DIANA finite element analysis. User's Manual release 9, Delft, 2005.

[11] ENV 1993-1-2:200, Design of steel and composite structures, Part 1-2: Structural fire design, 2003

[12] Ceb-Fip Model Code 1990: Design Code, Comit E Euro-International Du Beton, 1993.

[13] Schafar BW, Pekoz T. Computational modelling of cold-formed steel: characterizing geometric imperfections and residual stresses. Journal of Constructional Steel Research, 1998.

[14] Eurocode EN1993-1-2 Eurocode 3: Design of steel structures – Part 1-2: General rules – Structural fire design, 2005.

EXPERIMENTAL STUDY ON FULL SCALE COMPOSITE FLOOR SLABS UNDER FIRE CONDITION

Na-Si Zhang [a], Guo-Qiang Li [a], Guo-Biao Lou [a], Shou-Chao Jiang [a], Kun-Chao Hao [b]
[a] College of Civil Engineering, Tongji University, Shanghai, China
[b] China Jingye Engineering corporation Limited, Beijing, China

1 INTRODUCTION

Cardington test and real fire disaster show that, the performance of concrete floor slabs composited with unprotected steel decks and beams in fire condition was much better than the prediction without considering membrane action. The observation and analyses show that, during a fire, with the strength and stiffness decrease of the steel decks, the reinforcement and the concrete, the load capacity of the slab offered by traditional bending mechanism will not be enough to bear the applied load. Instead of bending mechanism, membrane action will contribute to keep the stability of the slab by forming an elliptical tensile reinforcement mesh in the center of the slab and a concrete compressive ring at the boundary of the slab. The development of the membrane action is shown in Fig.1. [1]

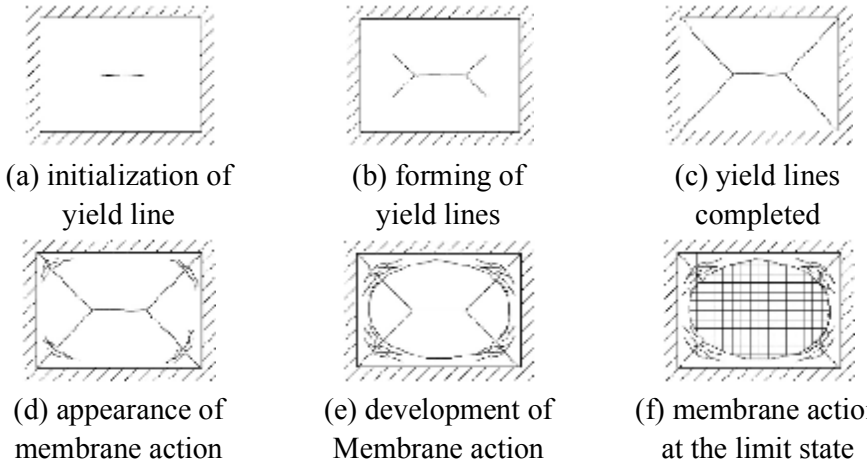

Fig.1. The development of membrane action in a floor slab

In the past decades years, many theoretical and experimental researches were performed to analyze membrane action.

From 1995 to 1996, six localized fire tests were conducted in a full-scale, eight-storey, steel frame building at Building Research Establishment Laboratory at Cardington. The test results showed that although the temperature of unprotected beam was higher than 1000℃, the slabs maintained their load bearing capacity during all the tests owing to membrane action. [2-3]

In 1999, to prove the existence of membrane action, Bailey performed a destructive test on a 9.5m*6.5m composite floor slab at ambient temperature based on the data of Cardington test. [4] After that, in order to validate the theoretical analysis, he performed some small scaled tests on 15 reinforced concrete floor slabs. However, all of Bailey's tests were under ambient temperature, which might not be appropriate to verify the validity of membrane theory. [5]

In 2008, ArcelorMittal and CTICM launched a project FRACOF in which an 8.735m*6.660m composite floor slab was tested under ISO standard fire. The test lasted for more than 120 minutes. Finally, the slab failed because of the fracture of the reinforcement bar. But, the fracture of the reinforcement was due to the failure of welding line at the joint of reinforced bars, which can be avoid by construction measures. Therefore, it caused a limitation to analyze the limit state and failure of the slab. [3]

In 2008, Guo-Qiang Li and Na-Si Zhang developed a new method to estimate the load capacity of composite floor slab under fire condition with considering membrane action. In order to observe the development of membrane action, analyze the membrane mechanism and verify the new method, 4 full-scaled slab tests were performed at Tongji University in China under the sponsoring from National Natural Science Foundation of China. [6]

2 GENERAL SITUATION OF THE TESTS

The test specimens were 4 pieces of 5.232m*3.72m composite floor slabs with steel decks unprotected. The specimens were numbered from S-1 to S-4. The slabs were contributed with the profiled steel sheet YX76-344-688 which is commonly used in China. The thickness of the deck was 1mm, and its strength was larger than 270N/mm^2 (270 N/mm^2 was considered in the calculation [7]). The decks were fixed on the primary beams and secondary beams (if existed) by shear connector with a diameter of 16mm and a height of 125mm.Total depth of the slabs was 146mm and the thickness of the concrete on the top of the decks was 70mm. The reinforcing mesh of the slabs was made by smooth reinforcement bar with the gird size of 150mm*150mm. The diameter of the reinforcement bar was 8mm, and the steel grade was Q235. The thickness of the protective layer of reinforcement was 21mm for S-1 and 30mm for S-2 to S-4. S-1 and S-2 had an unprotected secondary beam supporting the slabs in the middle, while S-3 and S-4 did not have. The cross section of the secondary beam was I25b, and the steel grade was Q235. The slabs, the primary beams and secondary beams were designed in according with the Chinese Code GB50017-2003[8] and YB 9238-92[9]. The general situations of the specimens were shown in *Table 1*. The arrangement of the specimens and the cross section of the composite slab are shown in the *Fig.2* and *Fig.3* respectively. The grade of the reinforcement was Q235 and the grade of the concrete was C25. The result of material property test for reinforcement and concrete are shown in *Table 2* and *Table 3* respectively (Where f_y, f_u and δ are the yield strength, ultimate strength and the ultimate elongation of the reinforcement respectively. f_{cu} is the cubic compressive strength of concrete).

In Cardington test, it was found that the reinforcement at the boundary of the slabs was fractured. In order to simulate this phenomenon, the reinforcement in these tests was not anchored at the boundary of the slabs, but exceeded the edge of the slab with a length of 150mm. The anchorage of the reinforcement is shown in *Fig.4*.

Table 1. Constructional information of test slabs [mm]

No.	Specim-ens size	Total depth	Thickness on the top of decks	Arrangement of the reinforcement	Thickness of the protective layer of reinforcement	Direction of the rib	Secondary beam
S-1	5232*3720	146	70	φ8@150	21	Along the **long** edge	In the middle of the long edge, unprotected
S-2	5232*3720	146	70	φ8@150	30	Along the **long** edge	In the middle of the long edge, unprotected
S-3	5232*3720	146	70	φ8@150	30	Along the **short** edge	No secondary beam

S-4	5232* 3720	146	70	φ8@150	30	Along the **long** edge	No secondary beam

Table 2. Properties of reinforcement bar at ambient temperature

No.	S-1	S-2	S-3、S-4
f_y(N/mm^2)	579.06	531.84	557.04
f_u(N/mm^2)	632.05	604.85	661.35
δ(%)	33.3	36	31.33
f_y/f_u	0.92	0.88	0.84

Table 3. Cubic compressive strength of concrete

No.	S-1	S-2	S-3	S-4
f_{cu}(N/mm^2)	26.1	21.0	22.37	22.87

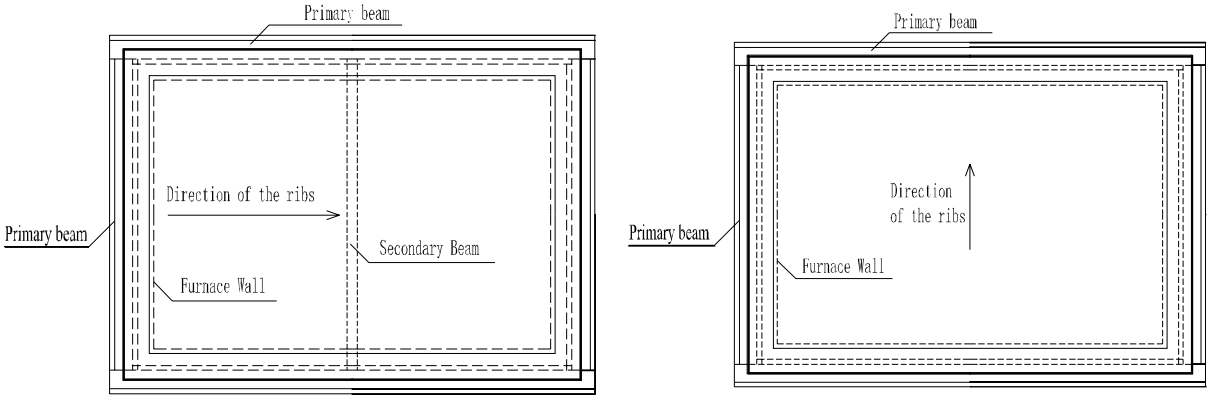

(a) specimens S-1 and S-2 (b) specimens S-3 and S-4

Fig.2. Arrangement of the specimens

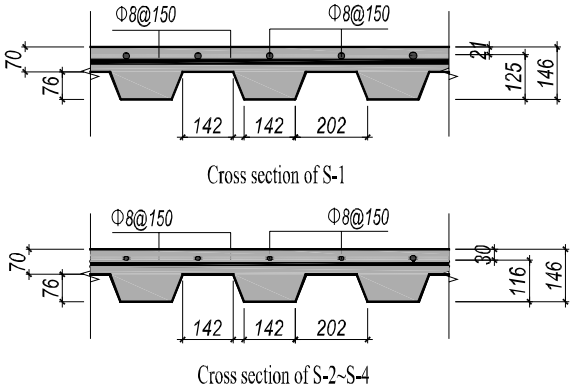

Fig.3. Cross section of the slabs

Fig.4. Anchorage of the reinforcement at the boundary of the slabs

The slabs were loaded at 24 points to stimulate uniform load (as shown in *Fig.5* and *Fig.6*) with the load ratio of 0.60~0.65 over the load-bearing capacity of the slabs at the room temperature. The temperature-time curve of the furnace used for the tests followed ISO834 standard fire. The displacement of slabs, the temperature at the surface and bottom of the slabs, the temperature and strain of the reinforcements in the slabs, as well as the strain of concrete were measured in the tests. The arrangements of the measuring points are shown in *Fig.7* to *Fig.10*.

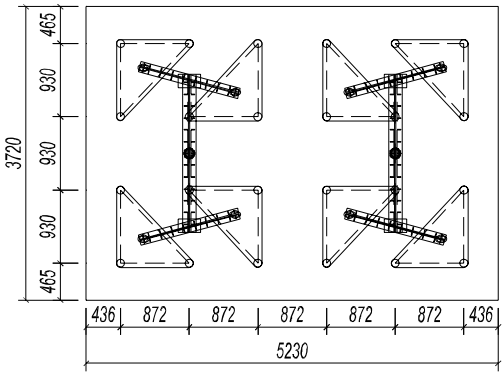

Fig.5. The planform of loading system

Fig.6. Loading system

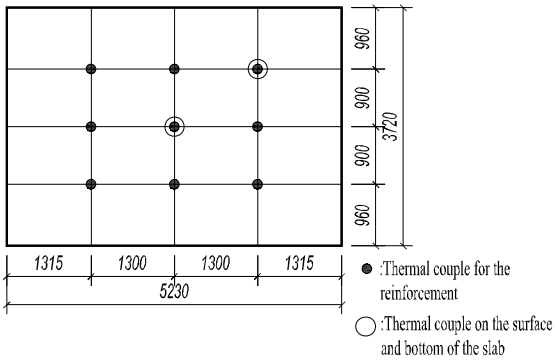

Fig.7. Arrangement of thermal couples

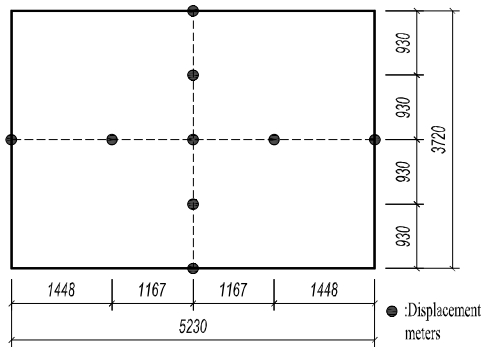

Fig.8. Arrangement of displacement meters

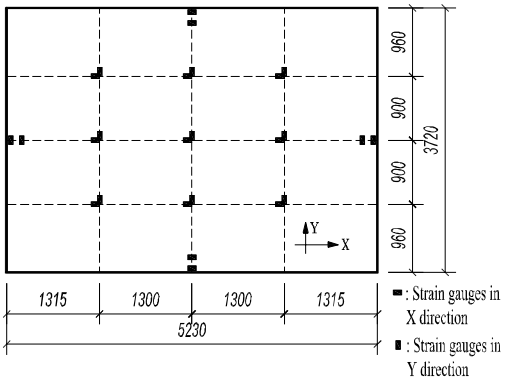

Fig.9. Arrangement of strain gauges for the reinforcement

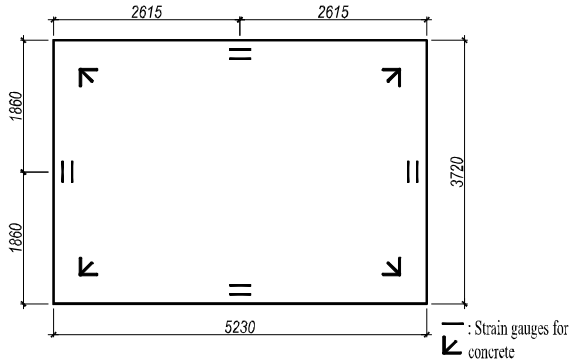

Fig.10. Arrangement of strain gauges for the concrete

3 TEST PHENOMENA

The tests were performed under ISO834 standard fire with uniform load which was applied on the slabs in 10 steps. After all the load was applied at ambient temperature, there was only slight deflection found in the middle of the slabs. No crack and other failure phenomena were found on the slabs. Tests began until load and deflection were stable at room temperature. The test load and duration for the 4 tests were shown in *Table 4*.

Table 4. Test load and duration for 4 tests

No.	Ultimate bearing capacity of design value (kN/m^2)	Test load (kN/m^2)	Load ratio (%)	Duration (min)
S-1	30.64	18.38	60	75
S-2	29.51	17.71	60	90
S-3	14.57	8.75	60	100
S-4	14.57	9.47	65	100

* Terminated without fail.

In test S-1 and S-2, cracks appeared beside secondary beam firstly due to the negative moment which was caused by the decrease of the strength and stiffness of the slabs. Then, significant cracks were found along the long edge of the slabs because of negative moment which was induced by the large deflection in the center of the slabs. These cracks located at the weakest cross section of the slabs (shown in *Fig.11*). Meanwhile, some cracks occurred along the short edge of the slabs. These cracks developed not only on the surface of the slabs, but also extended to the side face of the slabs (shown in *Fig.12*). After the test, significant yield lines were founded at the corner of the slabs. The concrete along the yield line was crushed (shown in *Fig.13*).

The deflection of the slabs was very large. The deformation of the slabs presented as an elliptic parabolic after the tests which validate that during the test membrane action was developed to bear the applied load (shown in *Fig.14*).

Fig.15 shows the distribution of the cracks on S-2 after the test, where cracks caused by the membrane action can be found both at the center and at corner of the slabs. *Fig.16* shows the deflection of S-2. Although the deflection of the unprotected secondary beam was huge, no failure was found on the secondary beam. *Fig.17* shows the condition at the bottom of S-2. It is found that the profiled steel decks did not melt down, which help the decks to keep the stability of the slabs after 90 min under standard fire.

Water vapor sweated seriously during the test. Even after the test was finished, some water vapor continued to sweat for a long time.

The test's phenomena of test S-3 and S-4 were similar to that of S-1 and S-2. Since there was no secondary beam in the center of the slabs, the concrete began to crack at the boundaries of the slabs in test S-3 and S-4 instead of beside secondary beam in test S-1 and S-2. The distributions of the cracks on S-3 and S-4 were shown in *Fig.18* and *Fig.19* respectively. The cracks in the center of S-3 and S-4 were not caused by the negative moment but by membrane action.

No collapse was found in these 4 tests, which shows that membrane action occurred to carry applied load on the slabs and to keep the stability of the floor system.

Fig.11. Cracks along the long edge

Fig.12. Cracks along the short side face

Fig.13. The yield line at the corner

Fig.14. The deformation of the slab after the test

Fig.15. The cracks on the S-2 after the test

Fig.16. The deformation at the bottom of S-2 after the test

Fig.17. The steel deck after the test

Fig.18. The cracks on S-3 after the test

Fig.19. The cracks on S-4 after the test

4 TEST RESULTS AND ANALYSES

4.1 Temperature

Fig.20 is the furnace temperature curve, which shows that the furnace temperature coincided well with the ISO834 fire curve.

Fig.21 is bottom temperature curve in the middle of the slabs. It shows that at the beginning of the test, the temperature of the slab at the bottom was low, and then it increased along with time. At the time of 75 minutes, the temperature can reach to 700 or 800℃. At the time of 90 minutes to 100 minutes, the bottom of the slab can be heated up to around 800℃ or 900℃.

Fig.22 is surface temperature curve in the middle of the slabs. It shows that during the whole test, surface temperature of the slab is very low. At the time of 90 minutes, the temperature was only around 100℃.

Fig.23 is the average temperature curves of the reinforcement. It can be found that the distance between the reinforcement and the bottom of the slab has a great impact to the temperature of the reinforcement.

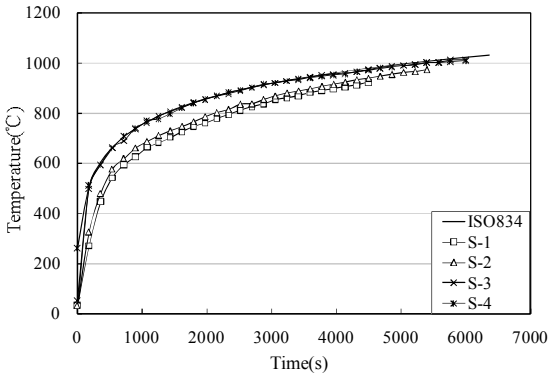

Fig.20. Furnace temperature curve

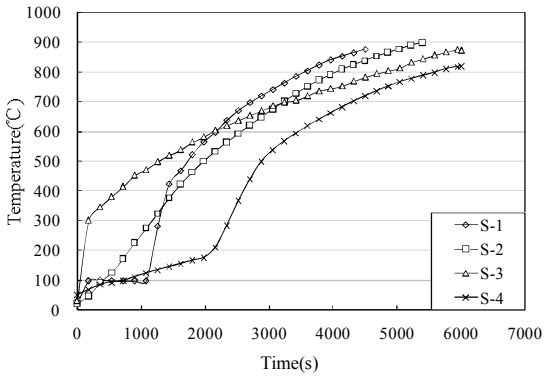

Fig.21. Bottom temperature in the middle of the slabs

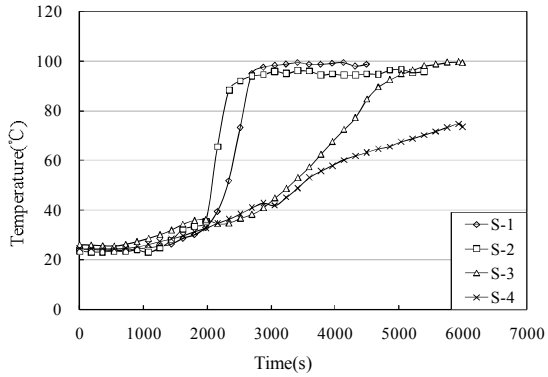

Fig.22. Surface temperature in the middle of the slabs

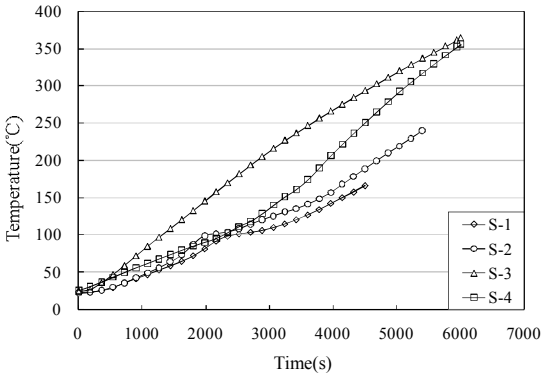

Fig.23. Average temperature of the reinforcement of S-1 to S-4

4.2 The strains of reinforcement and concrete

Fig.24 and *Fig.25* show the strains of the reinforcement along the short edge and long edge respectively. Since the effective working temperature of the strain gauges is less than 60℃, the data when the temperature was higher than 60℃ are taken out in the figures. According to the yield line theory, the reinforcement of these tests was located at the compression zone in the cross section of

the slabs, therefore the reinforcement should be under compression. However, the data show that the reinforcement was under tension during most of the test except for the beginning. This phenomenon proves the occurrence of tensile membrane action in the test.

Fig.26 is the strains curve of the concrete at the boundary of S-4. It can be found that the concrete in the middle of the boundary was under compression. It validates the existence of the concrete compressive ring which can provide the anchorage for the reinforcement.

According to analysis of the data taken by the strain gauges at the corner of the slab (see *Fig.10*), compressive strains were found at the corner at the angle between 30° and 60°, which coincides with the failure phenomenon shown in *Fig.13*.

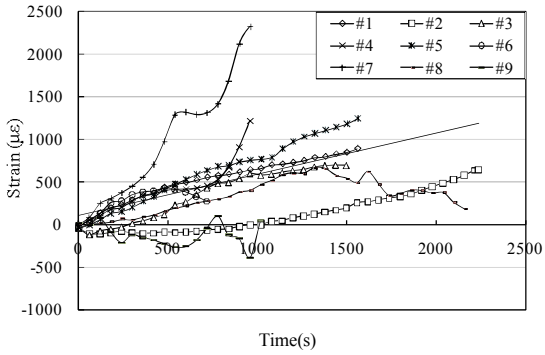

Fig.24. The strains of the reinforcement along short edge in S-1

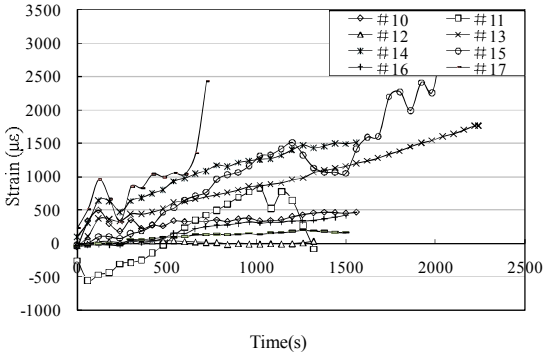

Fig.25. The strains of the reinforcement along long edge in S-1

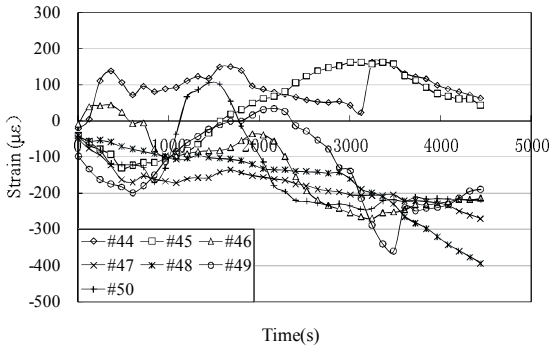

Fig.26. The strains of the concrete at the boundary of S-4

4.3 Deflection in the middle of the slabs

Fig.27 and *Fig.28* show the deflections in the middle of the slabs. It is found that the deflection can arrive at 1/25 of the short edge of the slabs. Therefore, it is reasonable to deduce that the load-bearing mechanism of the slabs has been changed from bending mechanism to membrane action one under such large deflection in the tests.

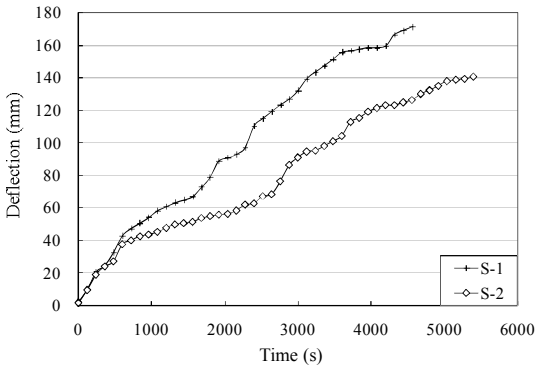

Fig.27. The deflection of S-1 and S-2

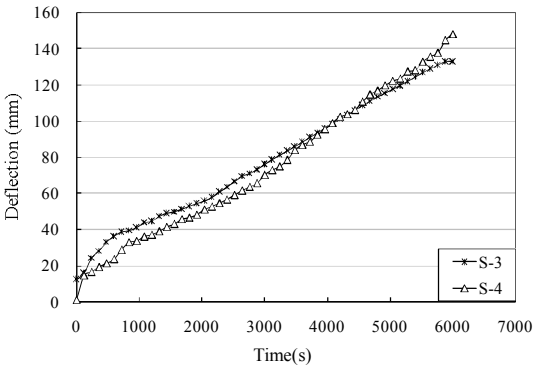

Fig.28. The deflection of S-3 and S-4

5 CONCLUSION

In this paper, full-scale tests were performed on 4 steel-concrete composite floor slabs. In the tests, the temperature of the furnace, slabs, and reinforcement, the strains of the reinforcement and concrete, and the deflection of the slabs were measured. Important conclusions can be presented as follow:

1. Membrane action will occur to carry the applied load instead of bending mechanism due to large deflection, when the composite floor slabs are subjected to fire. This membrane action can help to keep the load capacity of the slabs and maintain the stability of the floor system under fire condition.
2. Based on the data measured in the tests, the reinforcement in the slabs will be under tensile force and form an elliptical paraboloid tensile mesh which can bear the load on the slabs. A concrete compressive ring will be formed at the boundary of the slabs to provide anchorage for the reinforcement.
3. Due to the membrane action, the existence of secondary beams to support the slab is not necessary in fire condition, which can save the fire protection for secondary beams.

REFERENCES

[1] Guo-Qiang Li, Shi-Xiong Guo, Hao-Sheng Zhou, Modeling of membrane action in floor slabs subjected to fire, Engineering Structure, 2007

[2] Huang Zhaohui, Modeling Membrane Action of Concrete Slabs in Composite Buildings in Fire II: Validations, Journal of Structural Engineering, Vol.129, No.8, 2003

[3] Zhao Bin, Roosefid Mohsen, Vassart Olivier, Full scale test of a steel and concrete composite floor exposed to ISO fire, Proceeding of the Fifth International Conference on Structures in Fire (SiF'08), 2008

[4] Bailey Colin G, White D. S., Moore D. B., The tensile membrane action of unrestrained composite slabs simulated under fire condition, Engineering Structures, 2000

[5] Foster S. J., Bailey C. G., Burgess I. W., Plank R. J., Experimental behavior of concrete floor slabs at large displacement, Engineering Structures, 2004

[6] Na-Si Zhang, Guo-Qiang Li, A new method to analyze the membrane action of composite floor slabs in fire condition, Proceeding of the Fifth International Conference on Structures in Fire (SiF'08), 2008

[7] Continuously Hot-Dip Zinc-Coated Steel Sheet and Strip. GB/T 2518-2004, China

[8] Code for design of steel structures. GB50017-2003, China

[9] Specification for design and construction of steel-concrete composite floor system, YB 9238-92, China

ACKNOWLEDGEMENT

The work reported in this paper was financially supported by the National Natural Science Foundation of China under contract 50621062, 50738005 and 50728805. The support is gratefully acknowledged.

THERMAL RESTRAINT EFFECTS ON THE FIRE RESISTANCE OF STEEL AND COMPOSITE STEEL AND CONCRETE COLUMNS

Manfred Korzen [a], João Paulo C. Rodrigues [b] & António Moura Correia [b]

[a] Federal Institute for Materials Research and Testing, Berlin, Germany.
[b] Faculty of Sciences and Technology, University of Coimbra, Portugal

INTRODUCTION

The recently approved parts of Eurocodes concerning structural fire design, opens to the designer the possibility of using analytical and numerical methods as a way of guaranteeing the adequate fire resistance of the structures, apart from the expensive experimental tests. Although those documents foresee the possibility of making the use of advanced calculation methods for the analysis of the global behaviour of the structures subjected to fire, they also allow an analysis of single elements or parts of the structures, which is easier and more attractive for the common designer. In an analysis of single elements, the mechanical action of the surrounding structure, where the elements are inserted, is taken into account by the so-called "indirect fire actions". However, the Eurocodes allow that these actions are not taken into account in the case of an analysis of single elements subjected to the normalized fire. Tests and numerical studies carried out previously concerning steel columns with restrained thermal elongation indicate that the fire resistance of these elements can be significantly reduced with respect to the situation of free elongation [1].

This paper presents a comparison of results of fire resistance tests on steel and composite steel and concrete columns with restrained thermal elongation carried out at the Laboratory of Testing Materials and Structures of the Faculty of Sciences and Technology of University of Coimbra (FCTUC), Portugal and other ones carried out at the Federal Institute for Materials Research and Testing (BAM), in Berlin, Germany.

New three-dimensional experimental set-ups are under development in both Institutions to test building columns in conditions similar to the ones in real buildings. In the system of FCTUC, the stiffness of the surrounding structure to the column in fire is realized by a three-dimensional restraining frame while in the system of BAM it is done by the so-called substructuring method. Due to this concept the entire building is divided into two parts, which are connected through a special hardware-software interface. One part is represented by the column under testing in a special furnace, whereas the remaining building environment is simulated online by a model on a computer [2].

1. EXPERIMENTAL SET UP OF FCTUC

A new test set-up was used at FCTUC to measure the fire resistance of columns with restrained thermal elongation that are under development at this Institution (fig. 1).

The system comprised a restraining frame of variable stiffness (1) that had the function of simulating the stiffness of the surrounding structure to the column in fire.

The columns were subjected to a constant compressive load of 70% of the design value of buckling resistance of the column at room temperature. This load was controlled by a load

cell of 1MN located on the head of the hydraulic jack (6). This load simulated the serviceability load of the column when part of a real structure. The load was applied by the hydraulic jack (2) controlled by a servo hydraulic system.

The thermal action was applied by a modular electric furnace (3) that could closely follow the ISO 834 fire curve.

The restraining forces generated in the column due to heating were measured by a load cell of 3 MN located on a steel piston (4). This piston was placed between the testing column and the restraining frame.

The axial displacements and rotations on the top and base of the column were also measured by displacement transducers (5) orthogonally arranged in three different points, forming a deformation plane.

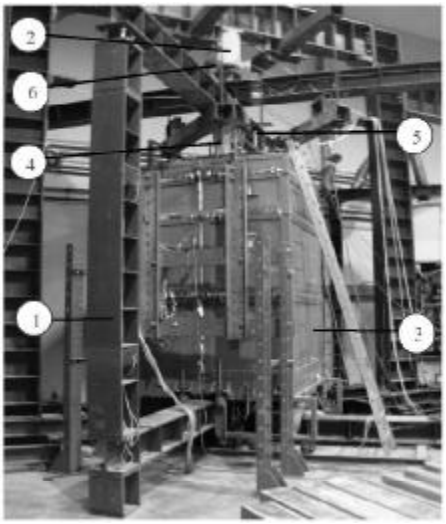

Figure 1. Test set-up of FCTUC

In the experimental programme, tests were carried out on steel and composite steel and concrete columns, with cross-sections of HEA160 and HEA200 and with stiffness ratios of 3, 13, 39, 68 kN/mm.

2. EXPERIMENTAL SET UP OF BAM

A central role of the substructuring method plays the *BAM* column furnace (Fig. 2 (a) – (b)). Mechanical and thermal actions are applied through this device to the specimen under test. Whereas the thermal set point is a known function of time for the mean gas temperature before starting the test, the mechanical set point has to be calculated online during a fire test in substructuring mode. Six electro-hydraulic control channels equipped with displacement and force sensors are available to influence the mechanical boundary conditions, i.e. two bending rotations each at top and bottom, one axial displacement at the bottom and one horizontal displacement at the top. During a substructuring test, forces and moments at the boundaries of the specimen, i.e. at the upper and lower bearings of the column, are measured and utilized for the computation of the corresponding displacements and angles, which are sent to the specimen in order to keep the entire building in mechanical equilibrium with its prescribed overall boundary conditions [2].

This closed loop for only one channel in substructuring mode is displayed in Fig. 2 (b) – (c). According to the free body diagram in Fig. 2 (c), the experiment is *driven* by the thermal displacement, which is diminished by the mechanical displacement u^{mech} due to the stiffness c^{mod} of the surrounding environment resulting in a compressive force on the column under test. The function of the control loop is to change the (total) displacement u by moving the position of the electro-hydraulic axial cylinder in such a way that the model force f^{mod} is equal to the measured force f.

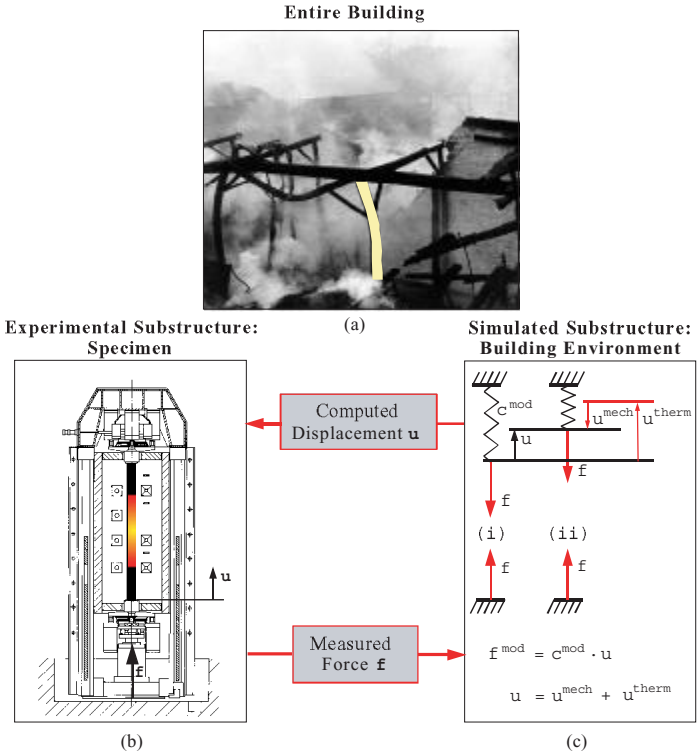

Figure 2 – BAM system - substructuring method

3. SPECIMENS

In order to compare the performance of both experimental systems several fire resistance tests on steel and composite steel and concrete columns were carried out.

In FCTUC fire resistance tests, the specimens were steel and composite steel and concrete columns HEA160 and HEA200, 3m high. The steel had the class S355 and the concrete C25/30. In BAM fire resistance tests the specimens were HEA140 and HEB180 for the steel columns and HEA200 for the composite columns, 3.60m in height. The steel of the steel columns had the class S235 and the composite S355 and the concrete C25/30 (fig. 3).

The specimens were fitted with thermocouples type k (chromo-alumel) to measure the temperatures in different points of the cross-section. All the specimens were subjected to an initial load, constant all over the test, of 70% of the design value of the buckling load at room temperature.

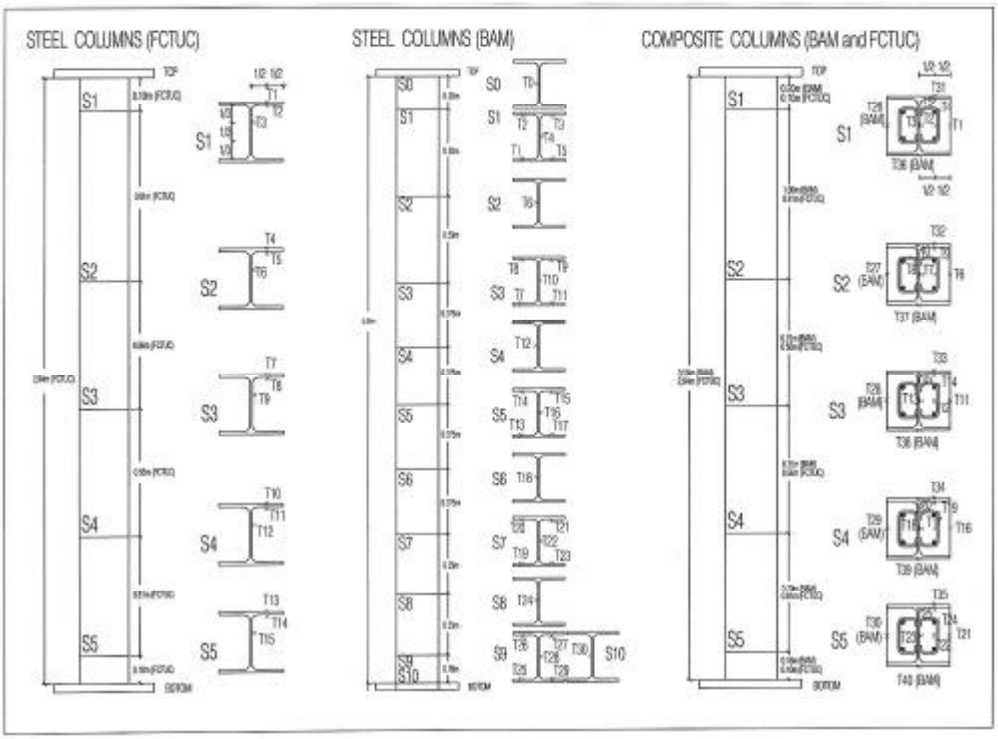

Figure 3 – Specimens in FCTUC and BAM tests

4. COMPARISON OF RESULTS

A lot of data was gathered from the tests carried out with both systems however, only some of these results will be compared and presented in this paper (table 1). The stiffness in BAM tests has to be corrected due to the difference of geometry between BAM and FCTUC specimens.

Table 1 – Tests

Reference	FCTUC1	FCTUC2	FCTUC3	FCTUC4	BAM1	BAM2	BAM3	BAM4
Type	steel		composite		steel		composite	
Section	HEA160	HEA200	HEA160	HEA200	HEA140	HEB180	HEA200	HEA200
Stiffness kN/mm	68.07	68.07	68.07	68.07	46.98	69.54	11.08	58.97
Initial load kN	606.69	885.58	591.36	1022.84	492.38	1052.00	1202.78	1199.71

4.1. Evolutions of Temperatures

The evolution of temperatures in the cross-sections of the steel columns was more uniform in BAM tests (fig. 5) than in FCTUC tests (figs. 4). This difference is maybe explained by the different heating curves followed in both furnaces. The heating in the BAM tests were very close to the ISO 834 curve and in the FCTUC tests a small delay in the heating was registered.

For the composite columns the expected thermal gradients in depth in the cross-section was observed (thermocouples 11, 12 and 13) (figs. 6 and 7). However, the heating was quite uniform around the cross-section (thermocouples 33 and 38, 11 and 28 of BAM tests).

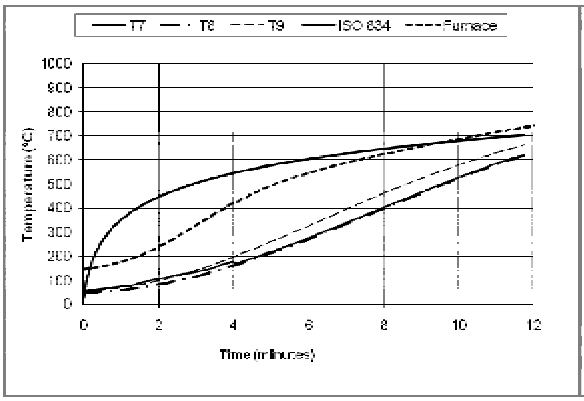

Figure 4 – Temperatures – FCTUC2 - Section S3

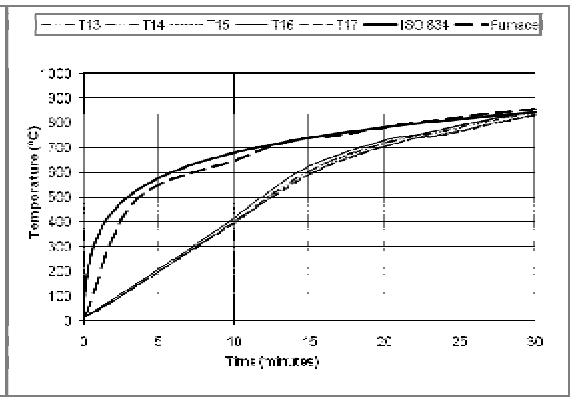

Figure 5 – Temperatures – BAM2 - Section S5

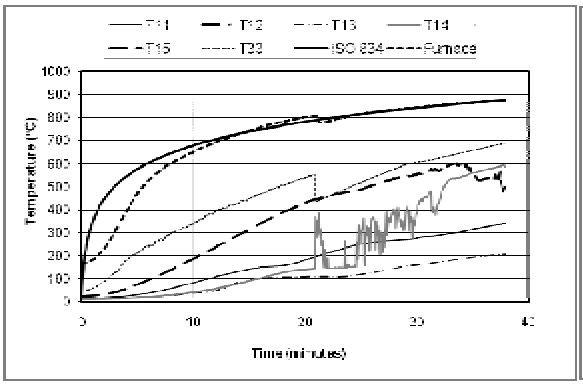

Figure 6 – Temperatures – FCTUC4 - Section S3

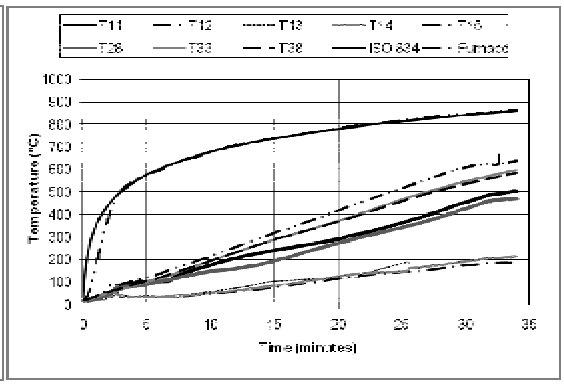

Figure 7 – Temperatures – BAM3-Section S3

4.2. Evolution of restraining forces

Figures 8 and 9 present the evolution of the restraining forces related to the initial load in function of the test duration.

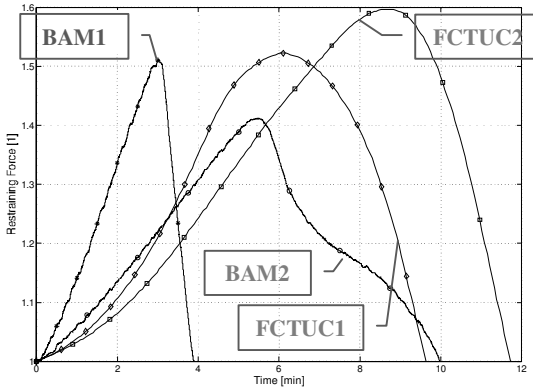

Figure 8 – Restraining forces – steel columns

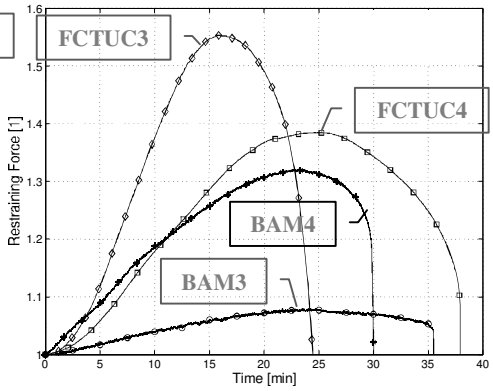

Figure 9 – Restraining forces – composite columns

In figure 8, for the steel columns, comparing the FCTUC tests between them, the HEA200 (*FCTUC2*) registered higher restraining forces and fire resistance than the HEA160 (*FCTUC1*). The comparison of the HEB180 (*BAM2*) with HEA200 (*FCTUC2*) and the HEA140 (*BAM2*) with the HEA160 (*FCTUC 1*) that have nearly the same slenderness, show some differences on the pattern of the curves and in the values of the restraining forces and the fire resistance. This is maybe explained by the different distribution of mass around the inertia axis of the section.

In figure 9, for composite columns, comparing the FCTUC tests, the HEA200 (*FCTUC4*) showed higher fire resistance then the HEA160 (*FCTUC3*). The *BAM 4* and the *FCTUC4* that were tested with identical conditions, presented curves for the restraining forces of the same pattern and the values of the fire resistance and the restraining forces were very close. Comparing the BAM tests, *BAM4*, tested with higher stiffness, presented higher restraining forces and shorter fire resistance than *BAM3*.

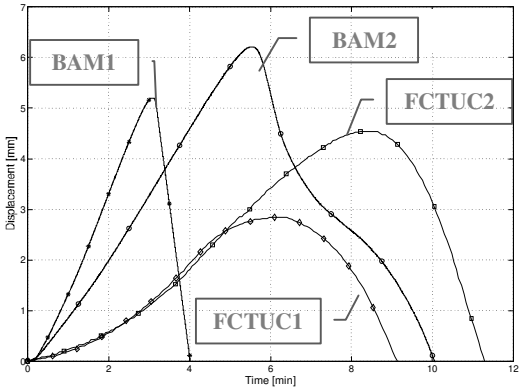

Figure 10 – Axial displacements – steel columns

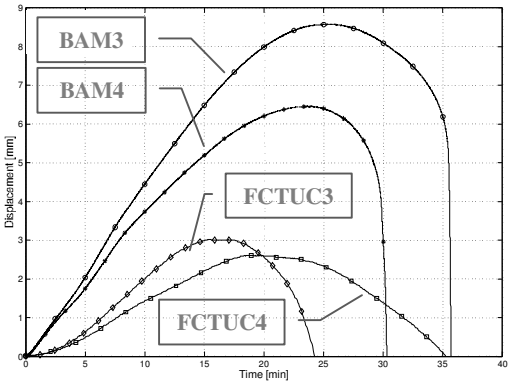

Figure 11 – Axial displacements – composite columns

Figures 10 and 11 present the development of the axial displacements in function of the test duration. The main finding in these graphs is that the axial displacements experienced by the BAM specimens were in general higher than the ones of FCTUC specimens.

5. FINAL REMARKS

These fire resistance tests allowed us to understand not only the real behaviour of steel and composite steel concrete columns in fire, but also find specific problems of the performance of both systems. As a main conclusion of this work it can be pointed out that the higher stiffness of the surrounding structure induces higher restraining forces and lesser fire resistance for steel and composite columns. Moreover, the less slender columns presented higher fire resistance.

REFERENCES

[1] Rodrigues, J.P.C.; I. Cabrita Neves; J. C. Valente – "Experimental research on the critical temperature of compressed steel elements with restrained thermal elongation", Fire Safety Journal, Vol. 35 No. 2, 2000, pp. 77-98.

[2] Korzen, M.; G. Magonette; Ph.Buchet – "Mechanical Loading of Columns in Fire Tests by Means of the Substructuring Method" - Zeitschrift für Angewandte Mathematik und Mechanik, Vol. 79, 1999, pp. S617-S618.

FIRE RESISTANCE OF BAR-REINFORCED CONCRETE-FILLED STEEL TUBE COLUMNS

Su-Hee Park [a] Kyung-Chul Song [a] Kyung-Soo Chung [b] Byung-Yeol Min [c] Sung-Mo Choi [a]

[a] Department of Architectural Engineering, University of Seoul 130-743, Seoul, Korea
[b] Research Institute of Industrial Science & Technology Steel Structure Research Laboratory, Kyungkido, Korea
[c] Korea Institute of Construction Technology, Kyungkido, Korea

INTRODUCTION

thanks to the thermal storage effect created inside the steel tube, the CFT structure has better fire resistance than that of conventional steel structures. In this regard, In this study, we conducted an experimental evaluation and analytical study on the fire resistance of a non-coated square tubular steel as well as a circular tubular column (Chung K.S., et al, 2008, Park S.H., et al, 2007), and identified that it sufficiently resisted fire for two hours or less under high axial force. We also proposed a simple design formula with a range limitation.

However, in the Ministry of Land, Transport and Maritime Affairs Notice No. 2005-1225, the standard of fire resistance structure under the regulation 'Fire Resistance Accreditation and Management Standards' states that every column used in the construction of high-rise buildings with more than 12 floors is required to secure a three-hour fire resistance. Accordingly, in order to apply a non-coated CFT column to a high-rise building, additional repairs and reinforcement for fire resistance should be suggested. To secure fire resistance, a steel-reinforced non-coated steel square CFT column was set.

In a related foreign research study, Kodur (V.K.R. Kodur 1999) conducted an experiment and analytical study on a concrete-filled steel square column or circular column specimens that were unreinforced, fiber-reinforced and steel-reinforced. With major parameters such as the presence or not of concrete reinforcement, external diameter, working axial force, effective length and concrete strength, a parameter analysis was conducted. Through this, a simple design formula with range limitation was proposed, which identified that steel-reinforced concrete-filled steel square column offers improved fire resistance.

In this study, we designed specimens of a steel-reinforced non-coated steel square CFT column based on existing researches, and projected the fire resistance of each specimen. A fire resistance test under load was conducted on the steel-reinforced non-coated square CFT columns. Through this, the study attempted to evaluate the effect of steel reinforcement in applying cross-section diameter and axial force ratio and high-strength concrete, along with determining the effect of applying steel reinforcement.

1 EXPERIMENT DESIGN

1.1 Specimen Design

Fig. 1 shows the details of specimens used in the experiment, which are the following: square steel tubular column with 280mm and 360mm in cross-section diameter: 2902 ㎜ of member length, sectional members and sizes. The thickness of the steel column was set to be 6 ㎜ and 9 ㎜ whereas width thickness ratio was set to be 46.6~40, sufficient deformation capacity being expected at room temperature. The end-plate of a steel column was set to be 50 ㎜. In the case of steel reinforcing concrete cover, the concrete cover was set to be 50mm in order to perform full fire resistance. In order to emit internal steam of a CFT column heated at the height of 340 ㎜, 1311 ㎜ and 1011 ㎜ at the lower end-plate of an upper column, a paired hole was made (Fig. 1). A SS400-grade steel column was used. Table. 1 shows the result of a coupon tensile test in accordance with KS B 0810. The design

strength of in-filled concrete used normal strength and high strength of 35Mpa and 55MPa, whereas slump was measured at 21.5 ㎝ and 25 ㎝, respectively. The column was filled with concrete by inserting a tremie pipe into the top of a steel column. After concrete pouring, the top of the column was covered, followed by curing. Fire resistance cover at the steel column was done. Table 2 shows the parameters of specimens, which are the following.

Table 1. Material Characteristics of Steel and Concrete

Concrete		Steel			
Age (day)	compressive strength (MPa)	thickness (㎜)	grade	Yield Strength (Mpa)	Tensile strength
28	36.1	6	SS400	240	422
28	56.8	9	SS400	237	410

Table 2. Specimen Parameter

Name	size (㎜)	Concrete strength f_{ck} (Mpa)	Steel strength F_y (Mpa)	Axial force ratio N_a/N_c	Effective length KL (mm)	Reinforcement ratio (%)	Fire resistance time FR (min) Test time
APL1	□-360×9	36.1	240	0.4	2902	-	99
ARL1		36.1	237	0.4		2%	171
BRL1	□-280×6	36.1	237	0.4			158
BRL2		36.1	237	0.6			80
BRH1		56.8	237	0.4			146

D×t (㎜)		Reinforcement (concrete)		f_{ck} (MPa)	
A	B	P	R	H	L
360×9	280×6	Plain	Bar-reinforced	High	Low

D: cross-section diameter, t: steel thickness, f_{ck}: concrete strength,

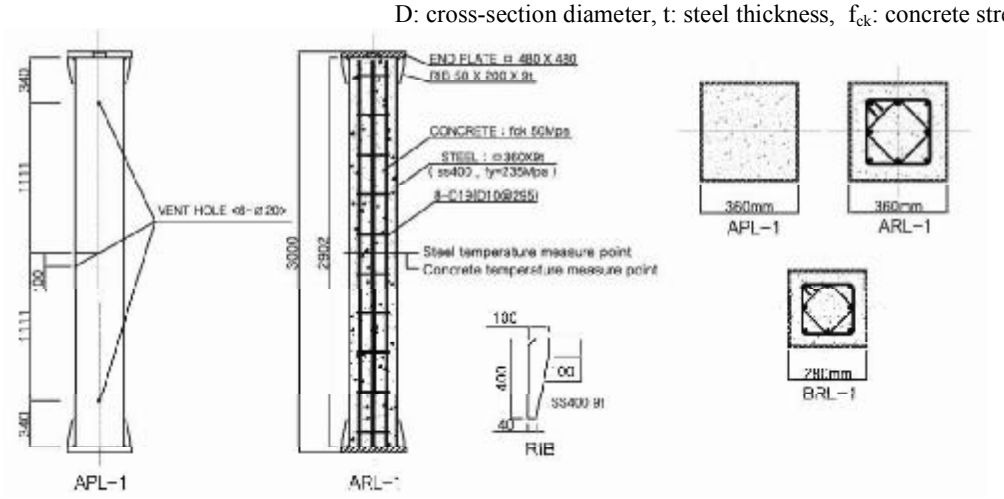

Fig. 1. Section and Size of Column Specimens

1.2 Experiment Method

The outline of the experimental equipment is shown in Fig. 2. A loading equipment that can exert axial force with a column-used reheating furnace from top to bottom, in other words, a compression tester with a loading capacity of 3000kN, was installed. Specimens were vertically installed in the center of a reheating furnace. Oriented amounts by heat expansion and shrinkage were measured by the linear variable differential transformer (LVDT) attached to a hydraulic cylinder. Items for temperature measurement were Fig. 4. The experiment proceeded as follows:

(1) A CFT square column in the reheating furnace is vertically set up after fitting in the center of a hydraulic jack.

(2) 15 minutes prior to heating, compressive force is introduced in the column center.

(3) The surface temperature of a steel column before the experiment is set to be approximately 5℃, whereas the reheating furnace's temperature is set according to the heating curve of ISO 834 during the experiment.

(4) If shrinkage reaches L/100 or more of the total shrinkage, or targeted fire resistance time is met, the experiment ends.

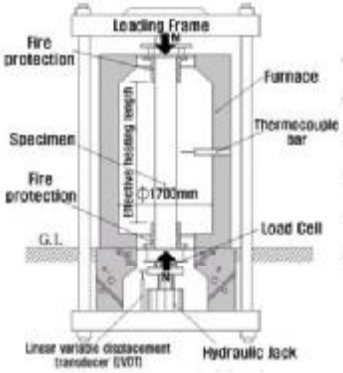

Fig. 2. The Loading device

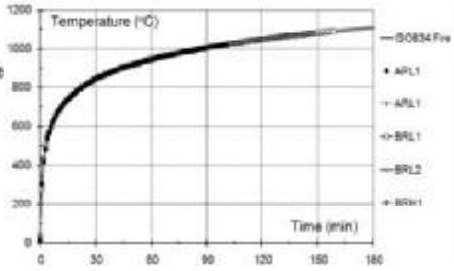

Fig. 3. Comparison of ISO Standard Fire Curve and test Curve

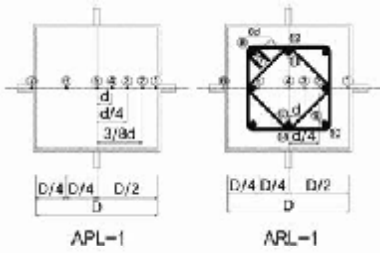

Fig.4. Temperature Measurement Position

2 EXPERIMENT RESULT OF FIRE RESISTANCE TEST UNDER LOAD

2.1 Temperature Distribution

As for temperature distribution by heating, specimens were compared at the surface of the steel column, 1/4 of the concrete cross-section center and surface, and internal and external point of steel. In looking into the temperature distribution, data regarding the steel surface in Fig. 5-(a) and concrete surface in Fig. 5-(b) show that the distribution of average temperature is located at the position lower than that of the standard fire curve. However, it shows a pattern similar to the standard fire curve after the middle section. This is attributable to having little influence of the initial parameters. The spot, 1/4 of concrete cross-section in Fig. 5-(c), shows that the temperature distribution of the BRH1 specimen drastically increases after 80 minutes of heating due to the spalling effect. The concrete cross-section center in Fig. 5-(d) shows that the temperature distribution of a steel-reinforced CFT column is higher than that of a non-reinforced CFT column after 40 minutes. Steel has a higher thermal conductivity than concrete. This is because steel-reinforced CFT column has smaller concrete-only area than that of the non-reinforced one.

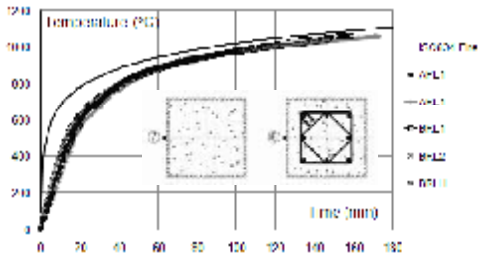

(a)Temperature Distribution of a Steel Surface

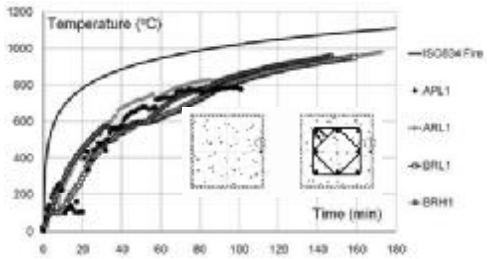

(b) Concrete Surface

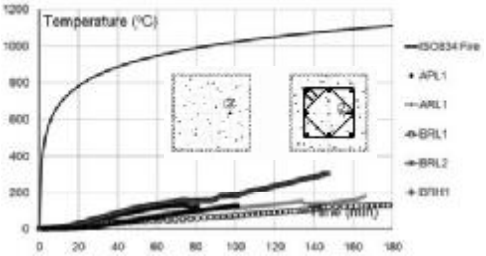

(c)1/4 spot of Concrete Cross-section

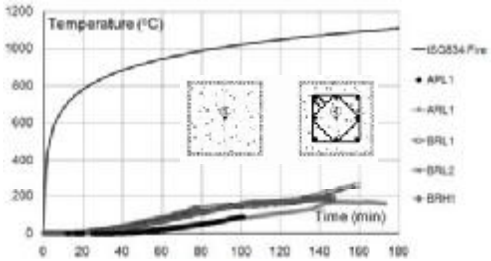

(d) 1/2 spot of Concrete Cross-section

Fig. 5. Temperature Distribution of Steel and Concrete

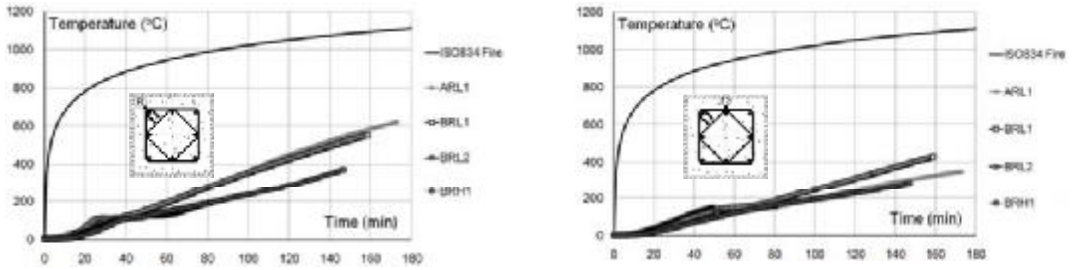

(a) The Concrete Diagonal Direction Boundary (b) The Concrete Central Direction Boundary

Fig. 6. The Temperature Distribution of Internal and External Boundary of Steel

In Fig. 6-(a) of the concrete diagonal direction boundary, the BRH1 specimen shows a reduction in the rate of temperature change in comparison with other specimens. This is attributable to a reduction of heat transfer by high-strength concrete, which has high density but minimal moisture content. With the ARL1 specimen, it is considered that the thermocouple location has changed due to the effect of concrete pouring after the installment of the thermocouple. In Fig. 6-(b) of the external concrete central direction boundary, there was the same distribution of temperature before 80 minutes, whereas other specimens show a higher increase rate of temperature except for ARL1 after 80 minutes. This is because of the thermal storage effect of the internal concrete area in which specimens with a smaller cross-section diameter than the others tend to have a higher temperature distribution.

2.2 Axial Deformation

To classify time–axial displacement relations, there are four stages: the section for steel resistance; load dislocation section; concrete resistance section; failure section. The section with the largest resistance against loading is the concrete resistance section. Fig. 8 shows the concrete resistance section collected from the Time–Curve Graph with the rate of each specimen. The 360mm cross-section steel-reinforced ARL1 specimen had a high resistance of 89%, demonstrating longer resistance as compared with the 77% of a non-reinforced APL1 specimen. This is because concrete-coated steel has the effect of thermal storage, thereby creating a long resistance to loading, as shown in the temperature distribution. Moreover, the BRL1 specimen is 79% resistance, showing a short section in comparison with the ARL1 specimen. This is because the steel area decreased by 65%. In the case of the BRL2 specimen, the loading rate against the strength of specimens is 0.6, which is the case of overloading, showing a significantly low fire resistance. The BRH1 specimen is a steel-reinforced CFT column with the application of high-strength concrete. High-strength concrete has low fire resistance due to its lower moisture content than that of normal-strength concrete. However, with steel reinforcement, fire resistance can be improved, thanks to the confining effect of steel. The BRH1 specimen has approximately 89% of concrete resistance section.

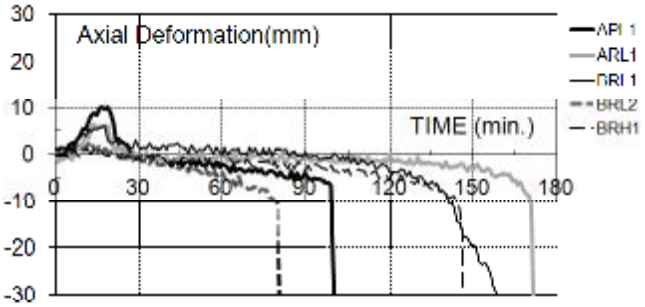

Fig. 7. The Axial Displacement by CFT column in fire resistance under load

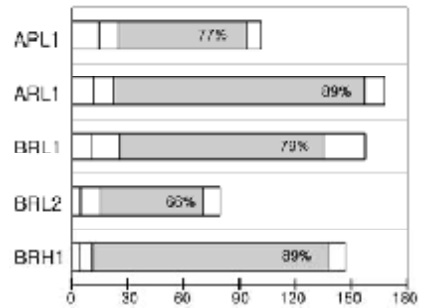

Fig. 8. The Sectional Ratio of Concrete Load resistance by each Specimen

2.3 Failure Mode

The APL1, ARL1, BRL1 specimens were set to have an axial force rate of 0.4 for fire resistance test under load, and 1/3 spot from the upper had local buckling. In the case of BRH1, which had steel-reinforcement and high-strength concrete, steel column fractured at the 1/3 spot where local buckling took place. The BRL2 specimen with an axial force rate of 0.6 had a total buckling of a column. Except for BRL2 specimen with 90 minutes or less in terms of fire resistance time, all other four specimens had separation on the surface of steel columns.

(a) A CFT column before the Experiment (b) BRH1Specimen after the Experiment (c) BRL2 Specimen after the Experiment (d) Separation and column Fracture of BRH1 Specimen

Fig. 9. A CFT Column Before and After the Experiment

3 ANALYSIS OF FIRE RESISTANCE INFLUENCING FACTORS

3.1 The Effect of Steel Reinforcement

Fig. 10 compares a non-reinforced CFT square column (APL1) and steel-reinforced CFT square column (ARL1). Both specimens were set to have an axial force rate of 0.4. In the case of the ARL1 specimen, working axial force increased approximately by 14% due to the 2% increase in steel reinforcement. As for the fire resistance, it was identified to have an approximately 70% increase, from 99 minutes to 171 minutes. This is because the steel is coated in concrete as in Fig. 6 of the Temperature Distribution of Boundary of Steel with up to 160 minutes of thermal storage effect, and concrete and steel create a composite effect, securing the target three-hour fire resistance until local buckling occurs.

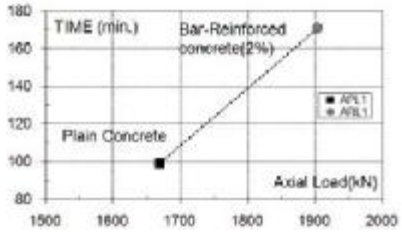

Fig. 10. The Effect of Concrete Reinforcement

3.2 The Effect by Parameters in Steel Reinforcement

Fig. 11 summarizes the comparison of a steel-reinforced CFT square column according to each major influencing factor, such as cross-section diameter, axial force ratio and concrete strength. As the cross-section diameter increases from 280 ㎜ to 360 ㎜, the area of a CFT column increased approximately by 65%, whereas fire resistance increased approximately by 8%, from 158 minutes to 171 minutes. As axial force ratio was set to be 0.6 from 0.4, the working axial force increased by 607kN, whereas fire resistance decreased approximately by 50%. Moreover, as concrete strength from 36.09Mpa to

56.81Mpa increased from normal strength to high strength, fire resistance decreased by approximately 6%, from 158 minutes to 147 minutes. The result of the analysis shows that the axial force ratio appeared to have the largest portion in determining the fire resistance of specimens. Moreover, as in Fig. 9 of failure mode, when the axial force ratio was 0.4 of low axial force, local buckling occurred at the end of fire resistance. However, when the axial force ratio was 0.6 of high axial force, total buckling on a column occurred.

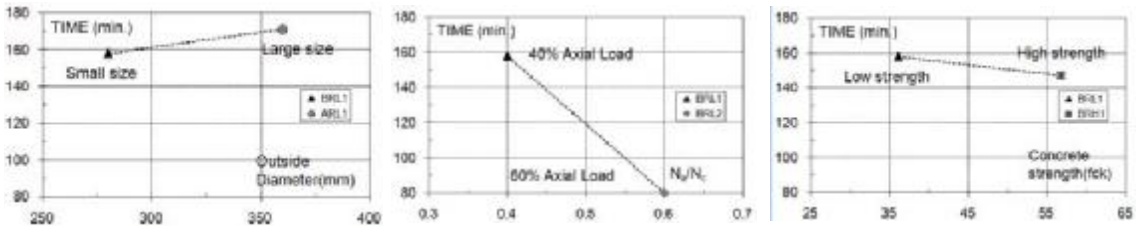

(a) Cross-section Diameter Change (b) Axial Force Ratio Change (C) Concrete Strength Change

Fig. 11. The Effect of Influencing Factors in Steel Reinforcement

4 CONCLUSION

The study was conducted to evaluate the fire resistance of a steel-reinforced CFT square column under a certain degree of axial force. In order to meet the required three-hour fire resistance, non-reinforced CFT square column and a steel-reinforced CFT square column were compared. The effects of the major influencing factors in steel reinforcement on the fire resistance of the inside column, such as cross-section diameter, axial force ratio and concrete strength change, were compared and analyzed.

The result of the fire resistance comparison between a non-reinforced CFT square column and a steel-reinforced CFT square column shows that in the case of a CFT column with a 2% steel reinforcement, working axial force increased approximately by 14%, whereas fire resistance increased approximately by 70%, from 99 minutes to 171 minutes when the axial force ratio was set at 0.4. Accordingly, it was determined that the target three-hour fire resistance was achieved.

Following the comparison of the major influencing factors with a steel-reinforced CFT square column, it was found that 8% of fire resistance increased when increasing the area by 65%, and the cross-section diameter from 280 ㎜ to 360 ㎜. When increasing the axial force ratio from 0.4 to 0.6, fire resistance decreased by 50%. Moreover, when increasing concrete strength from 36.09MPa to 56.81MPa, there was a strength decrease of approximately 6%. Accordingly, in the case of fire resistance experiment designed in the study, the effect of cross-section diameter and concrete strength appeared to be minimal, whereas the axial force ratio appeared to play a significant role as the major parameter.

REFERENCES

[1] Park S.H., Ryoo J.Y., Chung K. S., Choi S.M., An Evaluation for the Fire Resistance of Concrete-fillde Steel Square Tube Columns under Constant Axial Loads, *KOREAN SOCIETY OF STEEL CONSTRUCTION, 2007*

[2] Park S.H., Chung K. S., Choi S.M., A Study on Failure Prediction and Design Equation of Concrete Filled Square steel Tube Columns under fire Condition, *International Journal of STEEL STRUCTURES, 2007*

[3] Chung K. S., Park S.H., Choi S.M., Material effect for predicting the fire resistance of concrete-filled square steel tube colum under constant axial load, *Journal of Constructional Steel Research, 2008*

[4] V.K.R Kudur., Design Equations for Evaluating Fire Resistance of SERC-filled HSS Columns, *Journal of Structural Engineering, 1998*

[5] Y.C Wang., Steel and Composite Structures-Behaviour and Design for Fire Safety, *Spon press-Taylor & Francis Group, 2002*

[6] ISO, Fire Resistance Test-Elements of Building Construction, *ISO 834, 1975*

CALCULATION OF TEMPERATURE DISTRIBUTION IN COMPOSITE COLUMNS

Yuan Weifeng, Tan Kang Hai

School of Civil & Environmental Engineering, Nanyang Technological University, Singapore 639798

INTRODUCTION

An accurate prediction of temperature distribution across a section for a given fire condition plays a key role in the simulation of thermal effect in structural analyses [1, 2]. In numerical modeling, fiber model is frequently applied to column members since it offers a good balance between simplicity and accuracy [3, 4]. According to this model, the cross-section of a column member is divided into a matrix of fibers; each of these fibers can have different material, thermal and mechanical properties. Normally, to simplify the simulation, the temperature in a fiber is assumed to be uniform along the longitudinal direction of members. Currently, several existing methods can be used to predict the temperature distribution on column members in numerical analysis that is based on fiber model, such as finite element analysis (FEA) [5], boundary element method (BEM), analytical approach [6] and engineering assumption [7]. Among these methods, FEA is the most popular tool used by engineers to conduct heat transfer analysis. However, due to the meshing of the cross-section, it is tedious to incorporate FEA of heat transfer into fiber model formulations. Compared with FEA, BEM seems more convenient to be used since it only requires discretization on the boundaries of the cross-sections of beams and columns. But, BEM will become inefficient if the fibers have many different types of material properties. Although analytical approach is the basis of numerical validations for FEA and BEM, its use is rather limited. Engineers resorting to analytical approach will encounter great difficulties when dealing with a cross-section of complex shape consisting of anisotropic material. The fourth approach — engineering assumption supposes that the temperature distribution on a cross-section follows a linear or quadratic function in spatial domain. This method is easy to use but lacks rigor. To overcome the difficulties mentioned above, the authors propose a mesh-free method based on cellular automaton (CA). The history of CA can be traced back to 1940s when Von Neumann et al. studied biological reproduction and crystal growth [8]. Since then, CA has been used to model complex phenomena in various areas such as fluid dynamics [9], biology [10] and emergency evacuation [11, 12]. Basically, CA is a discrete model which consists of a regular grid of cells, each cell in one of a finite number of states. In a CA model, time is also discretized into finite number of steps, and the current state of a specific cell is influenced and determined by the states of its neighboring cells at the last time step. When CA is applied to heat conduction problems, the rules which dominate the simulation are deduced directly from physical phenomenon instead of solving differential equations. To implement the CA approach, random nodes are generated within a domain and along its boundary as well. Since meshing is not required, this approach can be used to model domains with arbitrary boundaries. Moreover, it can also be used to calculate the temperature distribution in non-homogeneous materials. Therefore, the proposed approach provides a useful and practical numerical tool to simulate heat conduction in composite structural members, such as composite concrete columns with embedded I-section steel.

1 FORMULATION

Generally, a CA model requires the spatial domain to be discretized into regular cells. Besides, the time domain is divided into a series of intervals. As a main feature, a CA model is established based on several local rules which relate the current state of a particular cell to the states of its neighbouring cells at the last time step. To analyze heat conduction in solids, this basic concept of CA is extended in the present study. Firstly, irregular grid of random nodes in spatial domain is used to replace regular cells in traditional CA. Secondly, a virtual time domain is generated and divided into constant intervals to match the features of CA. In this paper, only steady-state heat conduction is discussed, although with some modifications, the method may also be extended to transient-state heat conduction.

Consider an arbitrary 3-dimensional solid domain Ω as shown in Figure 1. The term T_i is the temperature at an arbitrary point P_i within Ω. The point P_i is located at the centre of its neighbouring area which is illustrated by a sphere with a radius r_0. Within the sphere, P_j is a typical node among N_i monitoring points. Similar to P_i, the temperature at point P_j is denoted by T_j. To construct a CA model, the relationship between point P_i and other points within its neighbouring sphere is defined by Eq. (1).

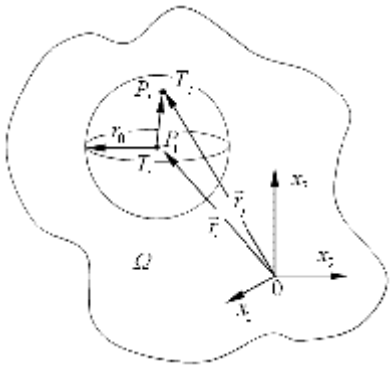

Figure 1. Illustration of an arbitrary three-dimensional domain

$$T_i = \sum_{j=1}^{N_i} \omega_{ij} T_j \tag{1}$$

where ω_{ij} is weighting factor where subscript i denotes point P_i and j relates the congregate effects of temperatures at neighbouring points P_j. Thus, clearly, from Eq. (1), the temperature at point P_i is determined by temperatures at its neighbouring points. This rule is based on the assumption that the variable T_i will not vary too much within a very small sphere. It is assumed that there is continuous variation of temperature over distance within the sphere. Eq. (1) also indicates that the influence of point P_j to T_i is dependant on the value of weighting factor ω_{ij}. Assuming that the material in the domain is non-homogeneous, ω_{ij} is given by Eq. (2):

$$\omega_{ij} = (k_i + k_j) \Big/ \sum_{l=1}^{N_i} (k_i + k_l) \tag{2}$$

where k_i, k_j and k_l are thermal conductivities at points P_i, P_j and P_l, respectively. One observes that $\sum_{j=1}^{N_i} \omega_{ij} = 1$.

From Eqs. (1) and (2), one finds that the temperature of each point within the neighbouring area of P_i affects the value of T_i. The definition given in Eq. (2) accords with physical law in that, , the larger the average thermal conductivity between points P_i and P_j, the closer are the temperatures at these two points.

To complete the construction of the CA model, Eq. (1) is extended to Eq. (3) by incorporating virtual time steps t:

$$T_i(t_m) = \sum_{j=1}^{N_i} \omega_{ij} T_j(t_{m-1}) \tag{3}$$

The interpretation for Eq. (3) is that the temperature at P_i at t_m is determined by the temperatures at neighbouring points of P_j at previous time step t_{m-1}.

To implement the CA model described above, similarly to points P_i and P_j, one can define randomly many points within Ω and on its boundary. During an analysis, the temperature at each point is updated according to Eq. (3) until it converges to a stable value. The final values of the temperature at each point form a state which represents the solution of the particular domain. One may realize that Eqs. (1) ~ (3) are entirely based on physical intuition of the heat conduction phenomenon. Differential equations are not involved in the derivation. Like traditional CA model, the procedure to calculate the distribution of temperature forms a loop which contains the following steps:

(1) Generate random nodes in the modelled domain and on its boundary.

(2) Assign an initial value to each node where temperature is unknown.

(3) Based on the state at time t_{m-1}, calculate the temperature at each node at t_m using Eq. (3).

(4) Repeat step (3) till the final time step t_M. At t_M, temperature at each node cannot be updated compared with previous time t_{M-1}.

2 NUMERICAL EXAMPLES

Example 1: As shown in Figure 2, a rectangular two-dimentional domain a-b-d-c is subjected to thermal conditions. In the domain, the varying thermal conductivity of the material is described by the function $k(x,y) = e^{x^2-y^2}$ where x and y represent the physical domain. On the boundaries, it is assumed that the temperatures are known as $T_{ab} = 0$, $T_{ac} = 0$, $T_{bd} = 2y$ and $T_{cd} = x$.

For comparison purpose, the analytical solution is derived for this example. From the heat transfer theory, one knows that Eq. (4) is the governing partial differential equation for example 1.

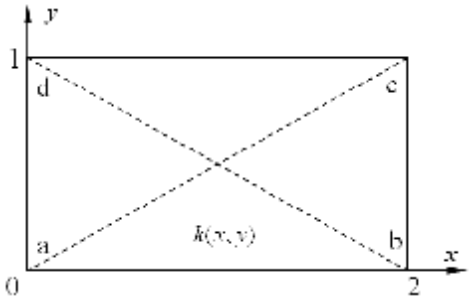

Figure 2: A rectangular domain under thermal conditions

$$\partial\left(k\,\partial T/\partial x\right)/\partial x + \partial\left(k\,\partial T/\partial y\right)/\partial y = 0 \tag{4}$$

The solution of Eq. (4) can be obtained without difficulty. Its expression is:

$$T = xy \tag{5}$$

The diagonals a-c and d-b can be respectively described by $y = x/2$ and $y = 1 - x/2$. Hence, the temperature distributions on the diagonals of rectangle a-b-d-c can be derived:

$$T = \begin{cases} x^2/2, & (y = x/2) \\ x - x^2/2, & (y = 1 - x/2) \end{cases} \tag{6}$$

On the other hand, to evaluate the temperature distribution using CA method, 1200 points inside the domain and 120 points along the four edges are generated randomly, as shown in Figure 3. In the figure, there are 21 points (in red dots) distributed along the two diagonals of rectangle a-b-d-c. Temperatures at these points are used for comparison with analytical answers given by Eq.(6). The value of spatial distance of the sphere r_0 is set to 0.1 in the calculation.

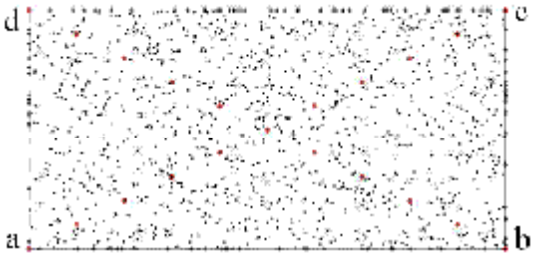

Figure 3 Distribution of points generated randomly in example 1

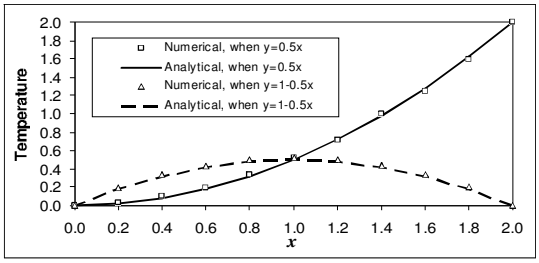

Figure 4: Numerical and analytical temperatures on diagonal lines

Both numerical and analytical results are depicted in Figure 4. It can be seen from the figure that the CA predictions agree very well with the analytical results. In fact, to minimize numerical errors, one can conduct several trial runs based on different distribution of random points. The average values of all trial run results will be more accurate.
During the study, it has also been found that the accuracy of simulation is affected by the number of nodes and the value of r_0. In general, more nodes will result in more accurate results. This feature of CA model is no different from FEA or BEM. However, large amount of random nodes will require longer CPU time.

Example 2: Figure 5 shows the cross-section of a rectangular composite concrete column modelling using fiber model. It can be seen that an I-section steel is embedded in the concrete interior. The dimensions and the thermal boundary conditions are illustrated in the figure. In the analysis, it is assumed that the temperatures on the top and bottom boundaries are $T_1 = 100^0 C$ and $T_2 = 500^0 C$, respectively. It is also defined that $k_C / k_S = 1/50$ where k_C and k_S denote the thermal conductivities of concrete and steel, respectively.

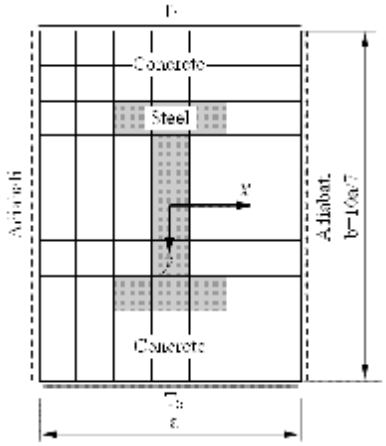

Figure 5. The cross-section of a composite concrete column

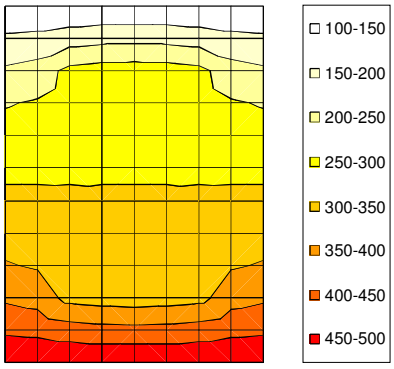

Figure 6. Temperature distribution on the cross-section of a composite concrete column

It should be mentioned that the segments on the cross-section are generated for fiber model. However, if heat conduction is required, these segments can be used to calculate the temperature distribution based on the proposed CA model. In this problem, the central points of all segments coincide to form a grid of CA cells, as shown in Figure 5. Thus, the present CA approach can be directly applied.
As shown by the temperature contour in Figure 6, the temperature distribution on the cross-section is symmetric about the column centroid $x = 0$. Along y direction, between $y = b/2$

and $y = -b/2$, the temperature increases gradually from T_1 to T_2. More details can be seen in Figures 7 and 8. However, it is noteworthy that the temperature on the column cross-section is not linearly distributed.

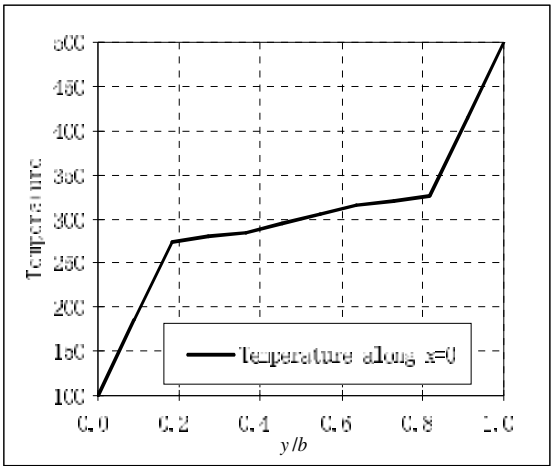

Figure 7. Temperatures along $x = 0$

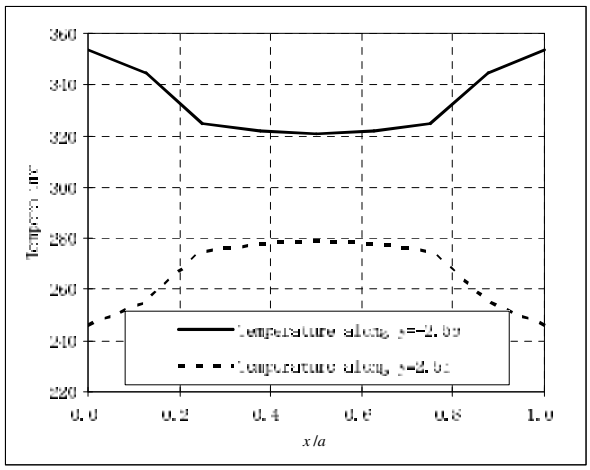

Figure 8. Temperatures along $y = \pm 2.5b$

3 THE RELATIONSHIP BETWEEN DIFFERENTIAL EQUATION AND CA

The two examples illustrate that the proposed CA model can be used as a numerical tool to analyze steady-state heat conduction, although the local rules incorporated into the CA model are deduced without the consideration of differential equation. However, it should be realized that differential equation is an analytical tool applied to the same problem. Hence, it is believed that there exists a relationship between the present CA model and classical differential equation since they both describe the problem correctly. It is well-known that one-dimensional heat conduction is governed by:

$$d\left(k\,dT/dx\right)/dx = 0 \tag{7}$$

Based on this, one infers that $k\,dT/dx = C_1$ where C_1 is a constant. Applying classical limit theorem to Eq. (7), one obtains:

$$\lim_{x_j \to x_i} \left(k_j T_j - k_i T_i\right)/(x_j - x_i) = C_1 \tag{8}$$

Let spatial distance $\Delta_{ji} = x_j - x_i$ and thermal conductivity $k_j = k_i = (k_j + k_i)/2 = \eta_{ji}$ arbitrarily. By applying Eq. (8) to all points within the neighbouring domain of point P_i, one obtains Eq. (9).

$$\sum_{j=1}^{N_i} \eta_{ji}\left(T_j - T_i\right) = C_1 \sum_{j=1}^{N_i} \Delta_{ji} \tag{9}$$

Thus,

$$\sum_{j=1}^{N_i} \left(\eta_{ji} T_j\right) - \left(\sum_{j=1}^{N_i} \eta_{ji}\right) T_i = C_1 \sum_{j=1}^{N_i} \Delta_{ji} \tag{10}$$

It should be noted that P_j is a random point in the neighbourhood of P_i. Therefore, according to statistics, the term $C_1 \sum_{j=1}^{N_i} \Delta_{ji} \to 0$ when N_i is large enough. For this situation, one obtains:

$$T_i = \sum_{j=1}^{N_i} \left(\eta_{ji} T_j\right) \Big/ \sum_{l=1}^{N_i} \eta_{li} = \sum_{j=1}^{N_i} \omega_{ij} T_j \tag{11}$$

4 CONCLUSION

Based on the concept of cellular automata, a new numerical approach is developed without the consideration of differential equation for analyses of heat conduction in anisotropic domain. Numerical examples show that this approach can be applied to steady-state heat conduction. Since CA is a mesh-free method, the proposed approach is convenient to use when it is incorporated into the fiber model in structural analyses for composite concrete beams or columns. Additionally, no complicated mathematical derivation is required during the development of the proposed approach. The numerical implementation of this model is simple because it is based on one local rule (Eq. (1)). After necessary improvement, such a methodology can be used in other fields, for instance, columns subjected to torsion since this kind of problems is governed by Poisson equation. In this study, only steady-state heat conduction is discussed. So it would be more meaningful to develop a new CA model for transient problems in the future.

REFERENCES

[1] Tan KH, Yuan WF, Buckling of Elastically Restrained Steel Columns under Longitudinal Non-Uniform Temperature Distribution, *Journal of Constructional Steel Research*, (2008) 64: 51-61.

[2] Tan KH, Yuan WF, Inelastic Buckling of Pin-ended Steel Columns under Longitudinal Non-uniform Temperature Distribution, *Journal of Constructional Steel Research*, (2009) 65 (1): 132-141.

[3] Spacone E, Filippou FC, Taucer FF, Fibre Beam-column Model for Non-linear Analysis of R/C Frames: Part I. Formulation, *Earthquake Engineering and Structural Dynamics*, (1996) 25: 711-725.

[4] Spacone E, Filippou FC, Taucer FF, Fibre Beam-column Model for Non-linear Analysis of R/C Frames: Part II. Applications, *Earthquake Engineering and Structural Dynamics*, (1996) 25: 727-742.

[5] Huang ZF, Tan KH, Phng GH, Axial Restraint Effects on the Fire Resistance of Composite Columns Encasing I-section Steel, *Journal of Constructional Steel Research*, (2007) 63 (4): 437-447.

[6] Wang ZH, Tan KH, Radiative Heat Transfer for Structural Members Exposed to Fire: An Analytical Approach, *Journal of Fire Sciences*, (2008) 26 (2): 133-152.

[7] Tan KH, Ting SK, Huang ZF, Visco-elasto-plastic Analysis of Steel Frames in Fire, *Journal of Structural Engineering-ASCE*, (2002) 128 (1): 105-114.

[8] Von NJ, Burks AW, *Theory of Self-reproduction Automata*, University of Illinois Press, Urbana, (1966).

[9] Wolfram S, Cellular Automaton Fluids 1: Basic Theory, *Journal of Statistical Physics*, (1986) 45 (3/4): 471-526.

[10] G. Bard Ermentrout and Leah Edlestein-Keshet. *Journal of Theoretical Biology*, 160, January (1993) 97-133

[11] Yuan WF, Tan KH. An Evacuation Model using Cellular Automata, *Physica A*, (2007) 384 (2): 549-566.

[12] Yuan WF, Tan KH. A Novel Algorithm of Simulating Multi-velocity Evacuation Based on Cellular Automata Modeling and Tenability Condition, *Physica A*, (2007) 379 (1): 250-262.

PARAMETRIC NUMERICAL ANALYSIS OF STEEL AND CONCRETE COMPOSITE FLOORS EXPOSED TO ISO FIRE

Mohsen Roosefid and Bin Zhao

CTICM - Centre Technique de la Construction Méttalique, Paris, France

INTRODUCTION

In recent years, increasing interest has been observed throughout Europe in developing steel and concrete composite construction, i.e. the floors are constructed using composite slabs with profiled steel decking attached through shear connectors like headed studs to downstand beams. Indeed, the full-scale natural fire tests in the steel framed buildings have shown the beneficial effects of membrane forces in improving the load-carrying capacity of composite floor system, compared to estimates of capacity based on only flexural behaviour. From observation and analysis of these full scale natural fire tests, a new fire design concept (design method and corresponding design guide) was developed in UK concerning modern multi-storey steel-framed buildings using composite floor systems [1]. This design method is aimed at fire resistance assessment of partially protected composite floors not only under natural fire condition but also in a standard ISO fire situation. In order to extend this design concept to other European countries, the dissemination project FRACOF [2] has been launched in 2007 and within the scope of this project, a demonstration full scale fire test was carried out to show the fire behaviour of steel and concrete composite floors exposed to the ISO fire. The steel and concrete composite floor used in this test was supported by four columns, occupying an area of 7.35 m by 9.53 m, so around 70 m². All steel structural members were designed in accordance with the requirement related to simple design rules of EN1994 [3, 4].

The mechanical loading of the floor is applied using fifteen sand bags uniformly distributed over the floor, each of which weighs exactly 15.0 kN leading therefore to an equivalent uniformly distributed load of 3.87 kN/m² (see *Fig. 1*).

In compliance with the existing simple engineering design method of such type of floor, the two secondary beams and the composite slab are unprotected. However, all the boundary beams of the floor (all beams in direct connection with columns) are fire protected to ensure a global structural stability under fire situation.

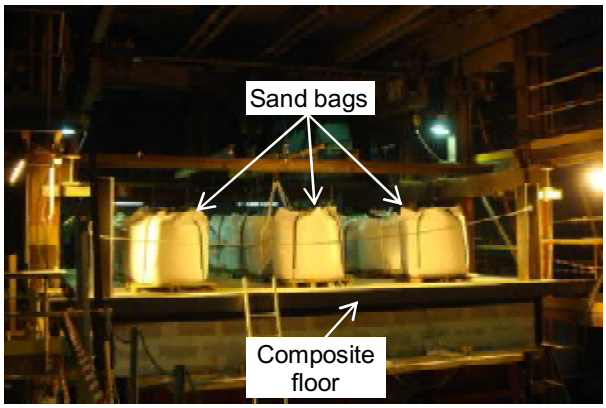

Fig. 1. Loading of the floor with sand bags

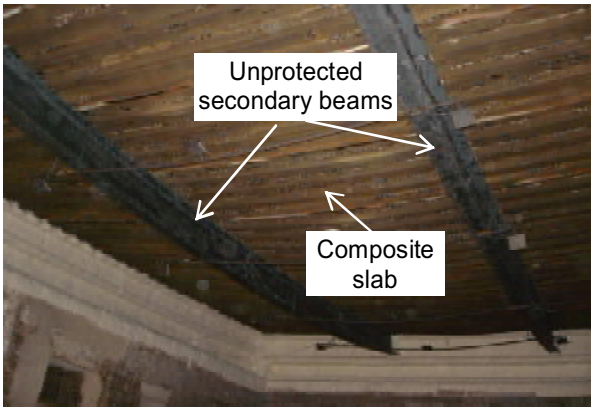

Fig. 2. View below the floor inside fire furnace after the test

The states of the floor before and after the fire are shown in *Fig. 2*. The experimental results illustrated clearly the excellent fire performance of partially protected composite floors with adequate reinforcing steel mesh under membrane action for a long ISO fire duration exposure. Further to above fire test, based on a 3D numerical modelling validated against the experimental results within this research project, a numerical parametric investigation is performed in order to enlarge the verification field of the design method.

1 VALIDITY OF DEVELOPED NUMERICAL MODELLING

Before the presentation of the parametric study, it is important to get an idea about the validity of adopted numerical model from the computer code ANSYS. In fact, the developed numerical model is composed of two different parts, one for heat transfer analysis and another one for structural analysis.

1.1 Heat transfer analysis

The heating of all structural members is predicted with help of 2D models using their typical cross sections. As the validation of the numerical model concerns mainly the structural behaviour of the floor, the thermal properties of insulation material is adjusted so that the prediction of a heating of protected steel members is as close as possible to reality. However, as far as steel and concrete are concerned, their thermal properties are those given in EN1994-1-2 [4].

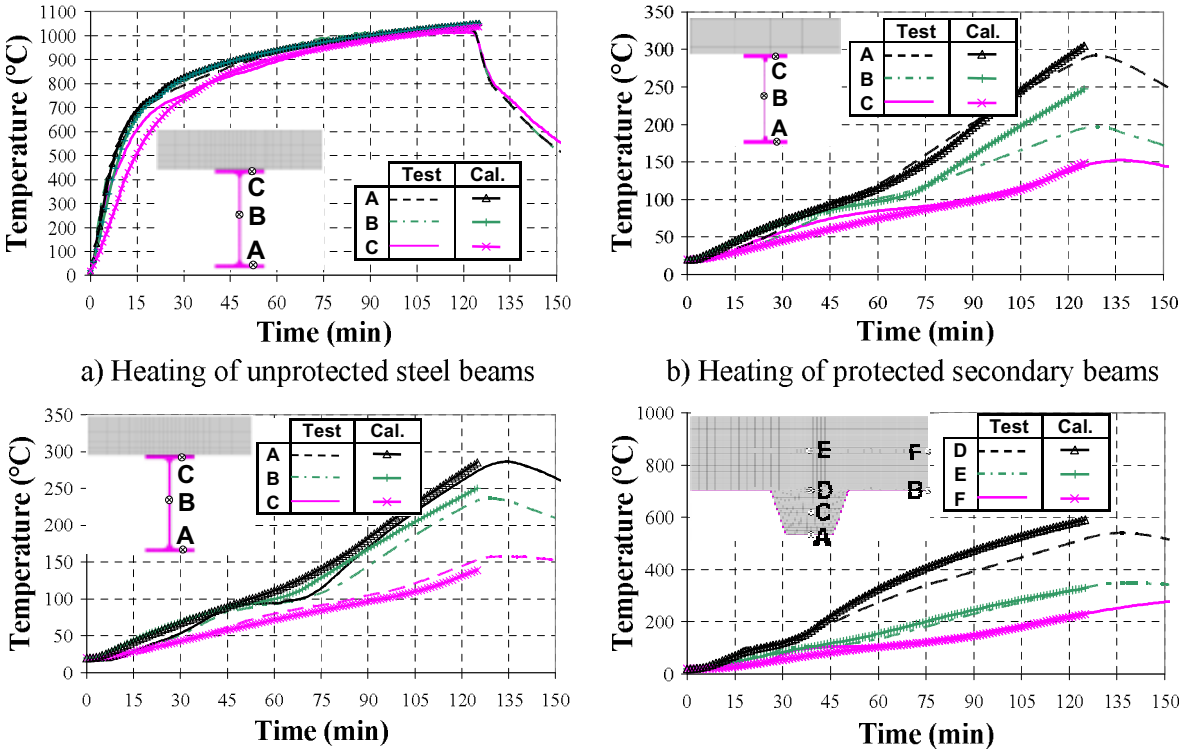

a) Heating of unprotected steel beams

b) Heating of protected secondary beams

c) Heating of protected main beams

d) Heating of composite slab

Fig. 3. Temperature comparison between test and numerical calculation

A comparison of calculated temperatures with measured ones during the test for different structural members is illustrated in *Fig. 3.* From this comparison, can be found an excellent agreement between test and numerical modelling which constitutes also a good basis for mechanical analysis.

1.2 Mechanical behaviour of structural members

The analysis is based on a hybrid structural model which takes account of steel beams, steel sheet, concrete rib, concrete slab and reinforcing steel mesh (see *Fig. 4*).

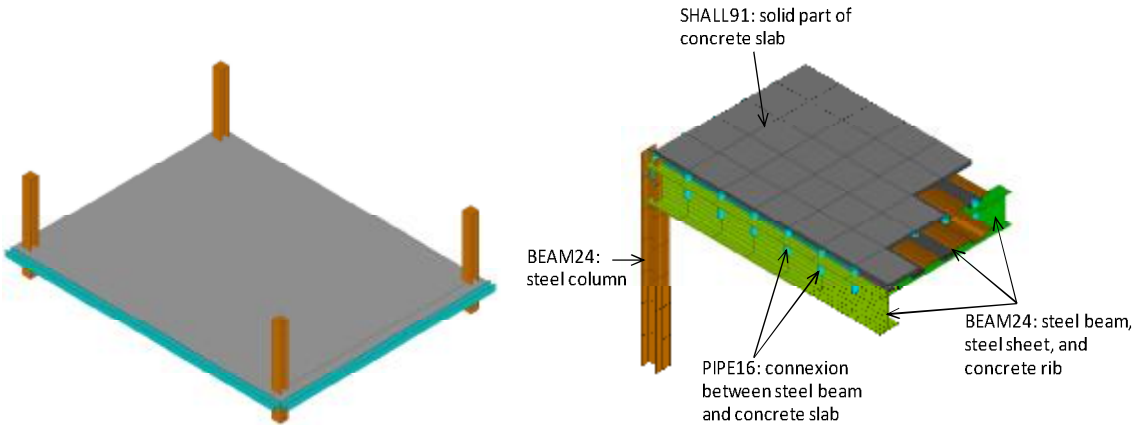

a) Modelled structure of full scale test b) Detail of the structural modelling

Fig. 4. Numerical modelling for structural analysis of full scale ISO fire test

In this structural modelling, the steel structural members are represented by 3D non-linear line element of BEAM24. As for concrete part over the steel sheet, a layered orthotropic shell element SHELL91 was used. The connection between steel beam and concrete slab was modelled using 3D linear line element PIPE16.

The structural behaviour of the floor is then analysed on the basis of previously calculated temperatures and a global structural model. The simulated structural behaviour of the floor is shown in *Fig. 5* which illustrates the deformed shape predicted by the numerical model at 120 minutes of ISO fire.

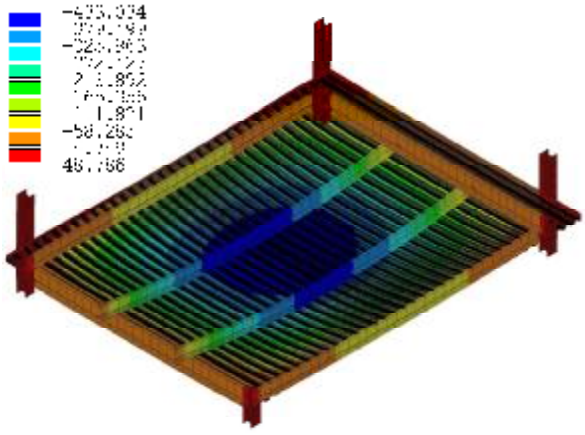

Fig. 5 Simulated deformed shape of the floor

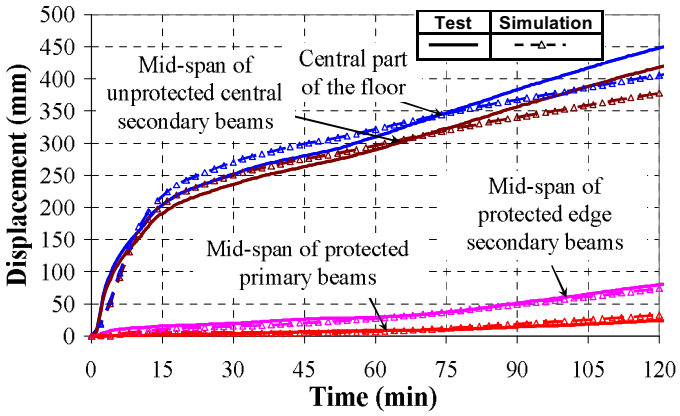

Fig. 6 Comparison of the predicted deflection and the floor recoded during the heating period of test

A comparison of floor vertical displacements between numerical calculation and test is shown in *Fig. 6.* It can be observed that globally the numerical modelling follows very closely the test results. However, a very slight discrepancy seems to occur after 75 minutes of fire for unprotected steel beams due to the fact that at about 50 minutes of fire test one of welded joints between two steel reinforcing meshes started to break which induces a small change in

the floor behaviour. Despite this small difference, the validity of the numerical model as well as its capacity of predicting in good way the fire behaviour of the composite floor is proved without any doubt. In consequence, the adopted numerical model can be applied more widely for global parametric investigation for a deeper check of the simple design method.

2 PARAMETRIC NUMERICAL STUDY

In order to take advantage of the tensile membrane action with composite floor systems subjected to fire, a new simple design method was proposed [1]. This simple design method gives designers access to whole floor behaviour and allows them to determine which members can remain unprotected while maintaining the safety level at least equivalent to that obtained with traditional design methods. This method is based on the yield-line approach of slab panels, which takes account of the enhancement due to membrane action of the slab and the beam systems. The details of the formulation are given in [6].
In order to extend the verification of this assessment method to its full application domain, a numerical parametric study on the basis of above advanced calculation model is performed, in which several specific features, such as deflection limit of the floor and maximum elongation of reinforcing steel are systematically checked.

2.1 Input data for parametric study

With the parametric study, the investigation of the simple design method may be extended to its full application domain. However, a full parametric study means at least several hundreds even more than thousand of numerical simulations, which necessitate a huge computation cost. Considering this situation is carried out only a reduced parametric study in which the following parameters are considered as the most representative or sensitive, resulting thus in a total of 112 numerical simulations.

2.1.1 Grid size of the floor

With respect to grid size of floor investigated in the parametric study, were adopted seven values, which are respectively (in m) 6x6, 6x9, 6x12, 9x9, 9x12, 9x15 and 7.5x15 (*Fig. 7*). All boundary beams are assumed protected but all central secondary beams are supposed unprotected.

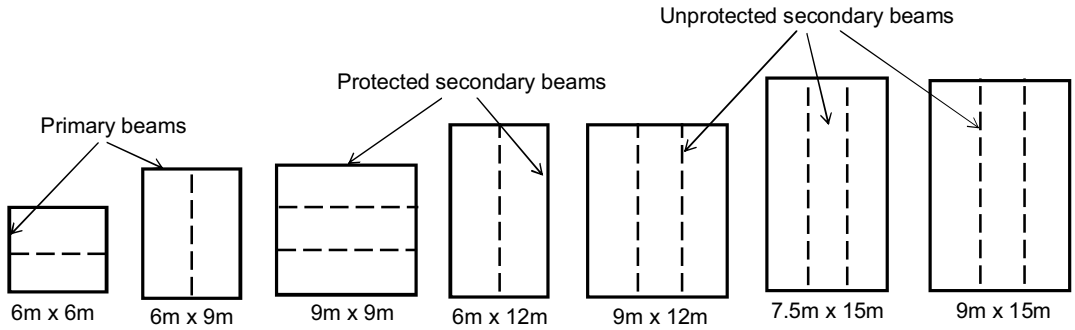

Fig. 7 Floors considered in the Parametric numerical study

2.1.2 Load levels

Two load combinations corresponding to load values commonly used in room temperature design over French market, are considered in this study which are given in *Table 1.*

Table 1. Load combinations considered in this parametric study

Case	Permanent load G	Live load Q
1	Self weight + 1.25 kN/m²	2.5 kN/m²
2	Self weight + 1.25 kN/m²	5.0 kN/m²

2.1.3 Link condition between floor and steel columns

The numerical analysis is conducted with two link assumptions, one of which considers that the composite slab is mechanically linked to steel columns with help of additional reinforcing bars and another one assumes that this link does not exist at all.

2.1.4 Fire duration

Four standard fire durations, that is 30, 60, 90 and 120 minutes, are investigated. As the necessary total depth of the composite slab depends directly on these fire durations, the minimum values according to the simple design method are adopted which are respectively 120, 130, 140 and 150 mm in case of open trapezoidal steel decking. Also, the size of all reinforcing steel mesh is derived directly from this simple design method. In addition, their axis distance is always taken as 45 mm. It has to be pointed out here that this parametric study considers only the steel decking of COFRAPLUS60. The reason of using such steel decking is due to the fact that it is not only, for the time being, the most commonly used one over French market but also the most open trapezoidal steel decking for composite slabs. One can understand easily that the composite slab using such steel decking will be the most critical from the point of view of mechanical resistance under fire situation. Therefore, if the simple design method is checked with this steel decking, the conclusion will be equally valid for any other types of steel decking.

2.1.5 Heating of boundary beams

In this parametric study, all peripheral beams are supposed to be heated up to 550 °C which corresponds to the critical temperature proposed for French market using such design concept.

2.2 Results of parametric study

For each numerical analysis, two special points of corresponding numerical results have been systematically checked, which are related to:

- maximum deflection of floor
- maximum mechanical strain of reinforcing steel

Concerning the deflection of floor, the first step of current investigation is to check whether the maximum allowable deflection is reached or not. In consequence, the maximum deflection obtained by numerical analysis in two cases, that is with and without link condition between floor and steel columns is compared to the maximum allowable deflections according to simple design method (SDM limit) and the results are illustrated in *Fig. 8.* It can be found that in any case, the maximum allowable deflection used as the validity limit of the simple design method is beyond the maximum deflection according to numerical analysis by assuming that the composite slab is mechanically linked to steel columns. Even if this link condition does not exist, the simple design method remains still valid as its deflection limit is exceeded only in very few cases.
In addition to the deflection of the floor, the elongation of reinforcing steel is the second feature which is investigated in detail in this parametric study. In reality, as the reinforcing

steel mesh is put over the whole area of the floor, it is certainly continuous across all beams including protected boundary beams. In this case, as the central part of the floor deflects largely under fire situation and meanwhile the protected boundary beams bows much less with their reduced heating, the reinforcing steel will then subject to important stretching in particular at the supports of protected boundary beams and around columns. If the elongation becomes too important, the failure could occur which may lead to following consequences: firstly the loss of integrity and insulation performance of the floor and secondly the reduced load bearing capacity as the continuous condition of the slab disappears. However, the question arises about the criterion to be applied to elongation capacity of reinforcing steel. According to EN1992-1-2 [5], the minimum elongation capacity among all types of reinforcing steel is at least 5%. Therefore, this value is taken as the maximum elongation that one can accept in this parametric study for reinforcing steel mesh.

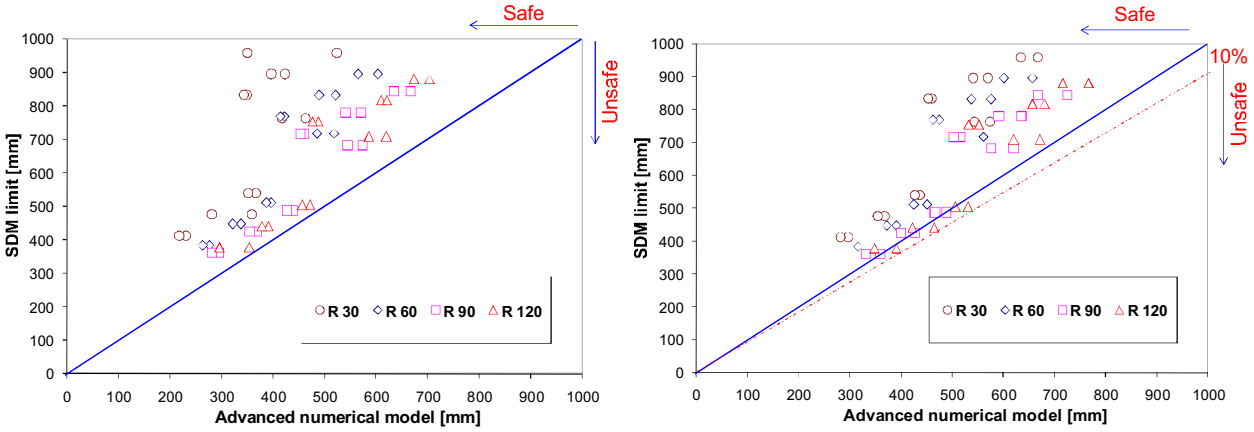

a) with link condition b) without link condition

Fig. 8. Comparison of the deflection predicted by ANSYS with SDM limit

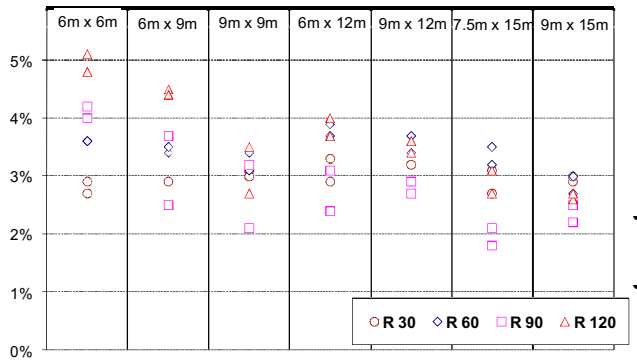

Fig. 9. Predicted maximum mechanical strain of reinforcing steel assuming no link condition

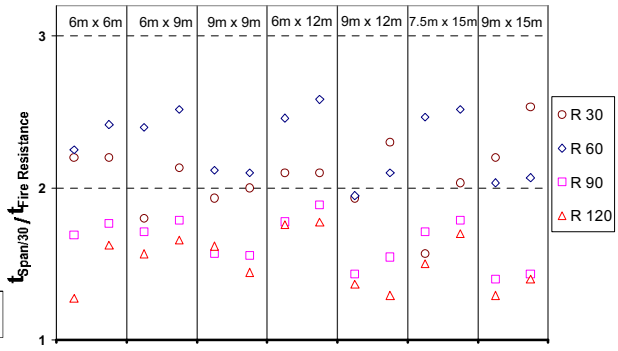

Fig. 10. Comparison between predicted fire ratings according to deflection criterion of span/30

Fig. 9 shows the predicted maximum mechanical strain of reinforcing steel according to numerical analysis by assuming no link condition, considering the most critical case. It can be found that the predicted maximum deflection of the floor varies in general between 2% and 5% which once again is satisfactory.

In addition, the fire resistance of a beam can be also expressed by fire ratings based on a total deflection limit not exceeding span/30 of all assembled structural members (primary beams, secondary beams, slabs). A special investigation is made in the numerical analysis to check

the necessary duration to reach this deflection criterion. If these durations are compared to corresponding standard fire ratings to be looked for (see *Fig. 10*), one can find that the ratio between them is always beyond one and in certain cases even more than two. Such results are very meaningful to show the validity of the simple design method which apparently provides the conservative fire ratings in comparison with advanced calculation tools.

Conclusion

The objective of the parametric study is to make a detailed investigation of simple design method with help of advanced calculation models validated against ISO fire test. This investigation should lead to the improvement of simple design method if necessary. From obtained results, it can be concluded that:

- with respect to deflection criterion, the simple calculation method gives conservative results compared to advanced calculation models;
- concerning the elongation of reinforcing steel mesh, it remains generally below 5%, the minimum allowable elongation capacity recommended by EN1992-1-2 for all types of reinforcing steel.

The results derived from this parametric study show clearly that the simple design method is capable of predicting in a safe way the structural behaviour of composite steel and concrete floor subjected to ISO fire condition and there is no need to include additional limitation to this simple design method in its application to assess the fire performance of composite floor.

Acknowledgements

The authors would like to give their acknowledgement to ArcelorMittal of which the financial support is highly appreciated.

References

[1] Fire Safe design: A new approach to multi-storey steel-framed buildings, Steel Construction Institute Publication no 288.

[2] Zhao B., Roosefid M. and Vassart O., Full scale test of a steel and concrete composite floor exposed to ISO fire, SIF Conference proceeding, 2008

[3] CEN, EN 1994-1-1, Eurocode 4: Design of composite steel and concrete structures" – Part 1-1: General rules and rules for buildings, *European Committee for Standardisation* , 2004

[4] CEN, EN 1994-1-2, Eurocode 4: Design of composite steel and concrete structures, Part 1-2: General rules - Structural fire design, *European Committee for Standardisation*, 2005

[5] CEN, EN 1992-1-2, Eurocode 2 "Design of concrete structures" – Part 1-2: Structural fire design, *European Committee for Standardisation,* 2003

[6] Bailey C.G. and Moore D.B., The structural behaviour of steel frames with composite floor slabs subject to fire, Part 1: Theory, Part 2: Design, *The Structural Engineer*, 2000

CELLULAR COMPOSITE BEAMS AT ELEVATED TEMPERATURES
Experimental investigation

Gisèle BIHINA [a], Bin ZHAO [a] and Olivier VASSART [b]

[a] CTICM, Saint-Aubin, France
[b] Arcelor Mittal, Luxembourg

INTRODUCTION

Cellular beams offer long uninterrupted clear spans, which are ideal for offices. However, increasingly, questions are being asked about the performance of cellular beams in fire situation.
In order to overcome the present lack of knowledge, a research project, FIre resistance of long span CEllular Beams (FICEB), has been carried out for more than one year [1]. In this project, four full-scale fire-tests of composite steel and concrete cellular beams were conducted over a fire furnace at the test facilities of Efectis France, the subsidiary of CTICM which is one of the partners of the project. These experiments aimed at investigating the fire behaviour of cellular beams under different configurations.
All these beams were made of a steel profile with circular and/or elongated web openings, connected by shear studs to a composite slab composed of a reinforced concrete part and a trapezoidal re-entrant deck spanning perpendicularly to the profile. The steel profile consisted of two "tees" from standard I-sections, which were welded together.
The first part of this paper describes the experimental set-up, whereas the results of the tests are given and discussed in the second part.

1 EXPERIMENTATION SET-UP

1.1 Beam geometric and material properties

An overall view of the four beams is shown in *Fig. 1.* As parts of composite floors, beams 1, 3 and 4 were considered to be secondary beams, and beam 2 was considered as a primary beam. They were fire designed according to [2].

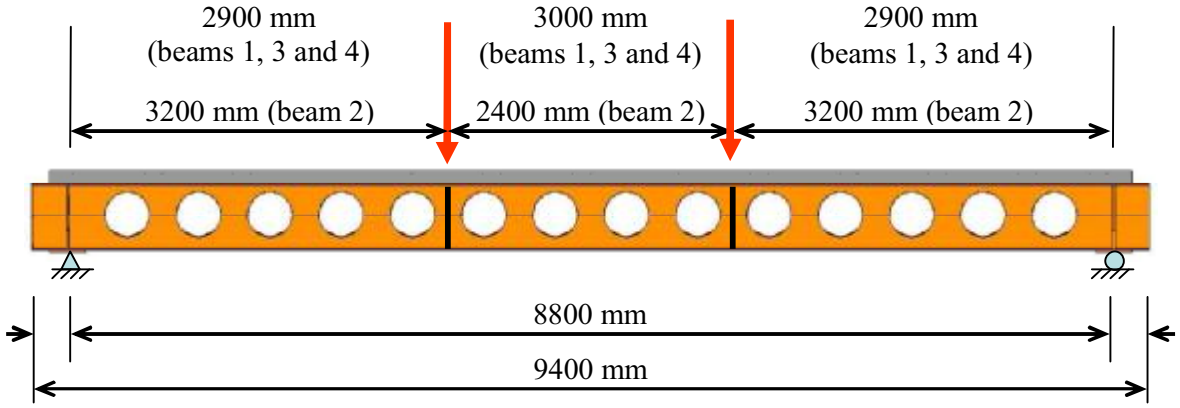

Fig. 1. Elevation view of the composite beams

The main geometric and material properties of the beams are shown in *Table 1* [1, 2, and 3]. In addition to the web stiffeners at load points and at its end supports, For beam 4, there was a one-side stiffener at each web-post. The upper steel flange was fully connected to the 120 mm deep composite slab, which comprised a COFRASTRA 40 ® re-entrant deck, via Nelson headed studs. The slab width was 2.20 m which equals to the effective width b_{eff} according to Eurocode 4 part 1.1 [4], i.e. $2 \times L/8$. As for the reinforcement steel, a mesh of 252 mm²/m was used.

	Beam 1	Beam 2	Beam 3	Beam 4
Top tee section	IPE 360	IPE 450	IPE 360	IPE 360
Top tee depth h_{top} (mm)	255	275	255	255
Bottom tee section	IPE 450	IPE 450	HEB 450	IPE 450
Bottom tee depth h_{bot} (mm)	300	275	300	300
Stiffener thickness (mm)	20	20	20	20 / 15
Span : L (mm)	8800			
Overall slab length: L_t (mm)	9100			
Slab width : b_{eff} (mm)	2200			
Number of openings	13	13	13	14
Number of circular openings	12	11	12	14
Number of elongated openings	1	2	1	0
Number of semi-infilled openings	0	2	0	0
Cell diameter (mm)	375	335	375	375
Reinforcement mesh	A252			
Number of shear studs	59			
Shear stud diameter (mm)	19			
Shear stud length (mm)	100			
Shear stud spacing (mm)	150			
Mechanical load (kN)	140	160	160	140
Steel grade	S355			
NWC compressive strength (MPa)	31.0	33.0	33.5	29.5

Table 1. Geometric and material properties of the fire-tested beams

1.2 Mechanical load

A mechanical load was applied through a hydraulic pump, and then distributed via a steel beam to 2 horizontal steel cylinders, providing two loading lines corresponding to the stiffeners' location. The hydraulic jack had a 400 mm stroke.

1.3 Thermal load

The thermal load was applied from beneath: hence, the steel profile was fire-exposed on 3 sides, while only the lower side of the slab was fire-exposed (see *Fig. 2*).
None of the four beams was fire-protected. For beams 1, 3 and 4, a 30-min exposure to the standard fire was assumed, whereas a specific bi-linear fire curve was used for beam 2, in order to simulate the heating regime of a fire protected beam.
For beams tested under ISO fire condition, despite their failure criterion occurred prior to 30 minutes, the thermal load was maintained until 30 minutes (see *Table 2*) in order to investigating the heating of the beams to the lowest standard fire rating commonly defined by the fire regulations. The average furnace temperatures are given in *Fig. 3*.

	Beam 1	Beam 2	Beam 3	Beam 4
Heating phase (min)	30	80	30	30
Collapse time (min)	~18	~73	~26	~19

Table 2. Test duration

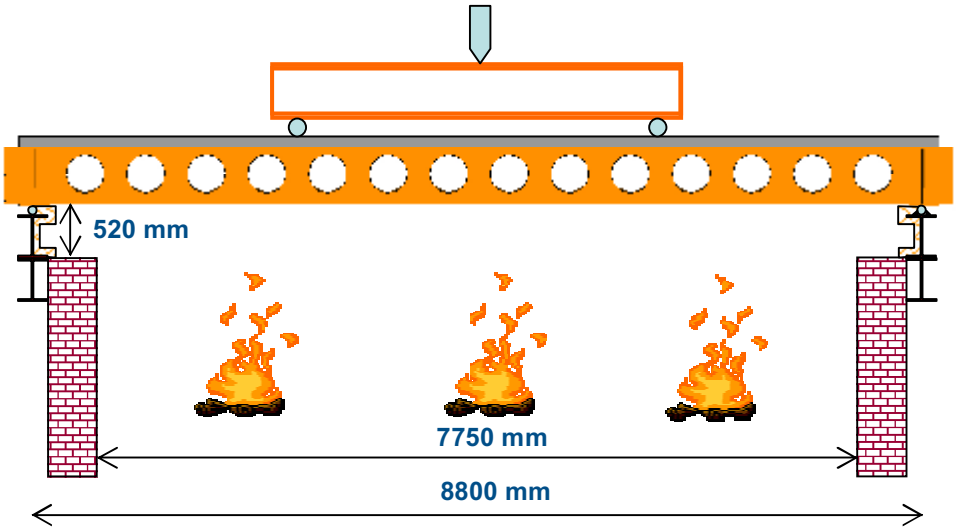

Fig. 2. Schematic view of the furnace

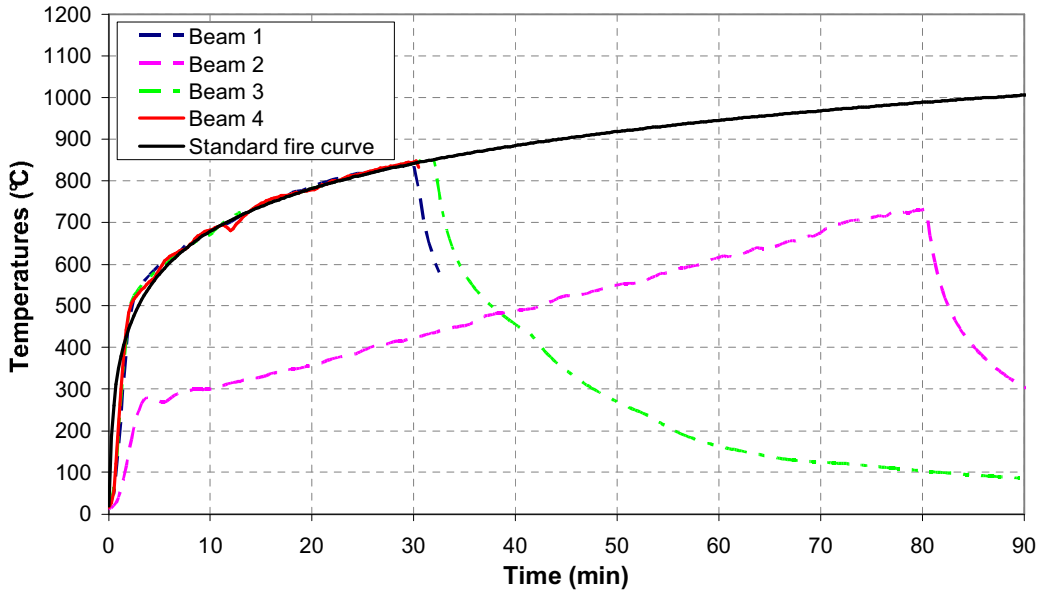

Fig. 3. Furnace average temperature vs. time

1.3 Measurement of experimental results

For each test, about 100 thermocouples were disposed in the furnace and at various locations along the beams in both the steel profile and the composite slabs, though most of them were located in the steel profile. Transducers were also used to check the rotations near the supports, the bond-slip between the steel profile and the slabs, and the vertical displacements in the central part of the slab.

2 RESULTS AND DISCUSSION

2.1 Temperatures

Fig. 4. shows the temperatures of a steel cross-section around mid-span of all tested beams [3] (cross-section without cell in the central zone of webs), which was the hottest one due to the shadow effect. In each graph, the failure time is given by the vertical line.

It is observed that there was always a significant thermal gradient, i.e. about 150 °C, between the top flange, which was the "coolest" steel part, and the remained parts of the cross-section, especially for beam 1 and 4, which underwent very close temperature rises. Moreover, the maximum temperature values were recorded in the web, reaching up to 820 °C in the secondary beams after 30 minutes of ISO fire and up to 690 °C in the primary beam after 80 minutes of fire (fire temperature: 735 °C).

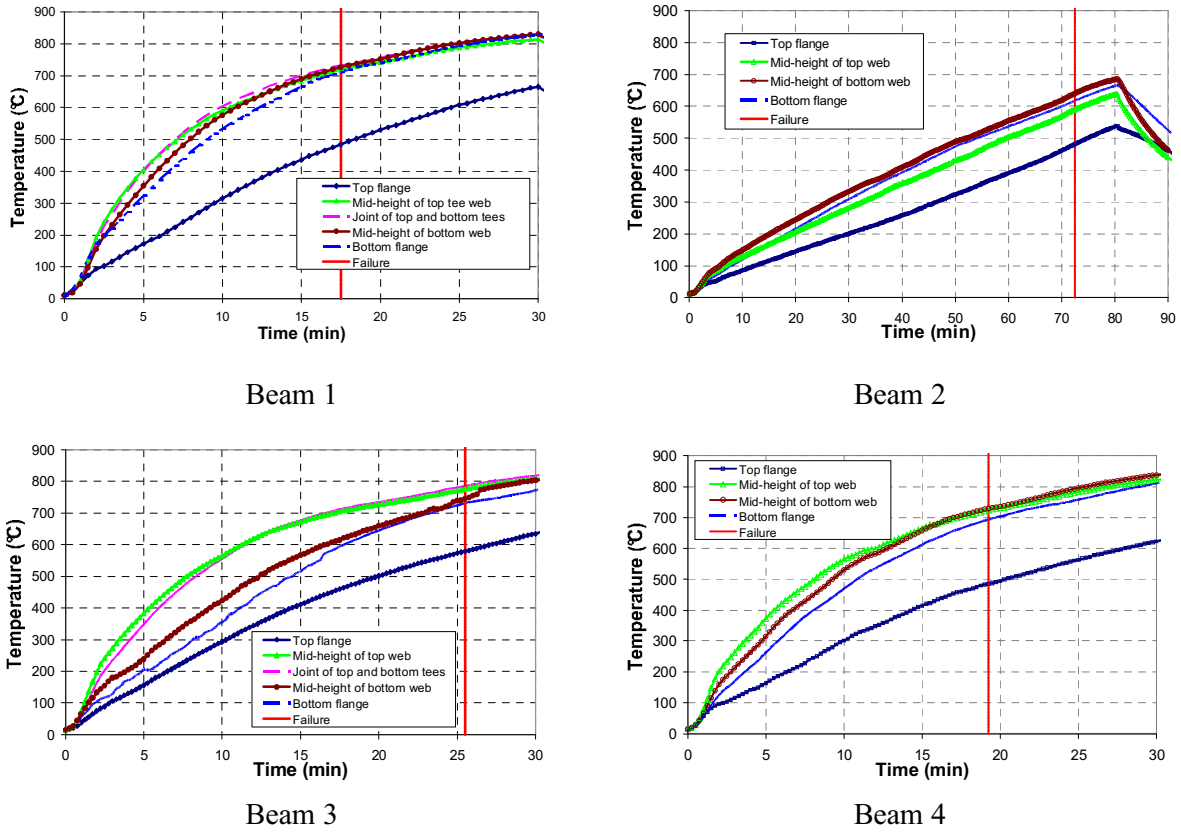

Fig. 4. Temperatures in a central cross-section

2.2 Deflections

The deflections recorded at a *L*/4 distance from the supports and at mi-span are shown in *Fig. 5* [3]. As long as a mechanical load was applied, the beams underwent vertical displacements increasing progressively and linearly until a heating around 700 °C for beams exposed to ISO fire and 550 °C for beam subject to protected situation. Afterward, their deflections increased very quickly with the temperature rising until the collapse.
A slight deflection decrease was observed once the hydraulic jack reached its stroke limit and was taken away. However, after this decrease, some beams continue bending downwards under their self-weight without any additional mechanical load until maximum thermal load.

It must be reminded that all the beams exposed to ISO fire had the same top tee section and in particular the beams 1 and 4 had exactly the same cross-section. Nevertheless, in spite of its one-side additional stiffeners, beam 4 underwent approximately the same deflections as beam 1. In fact, the behaviour of these two beams is very close if it is related to the their heating instead of the time. Besides, beam 3 behaved stiffer than both beam 1 and beam 4, as its bottom tee section was more resistant.

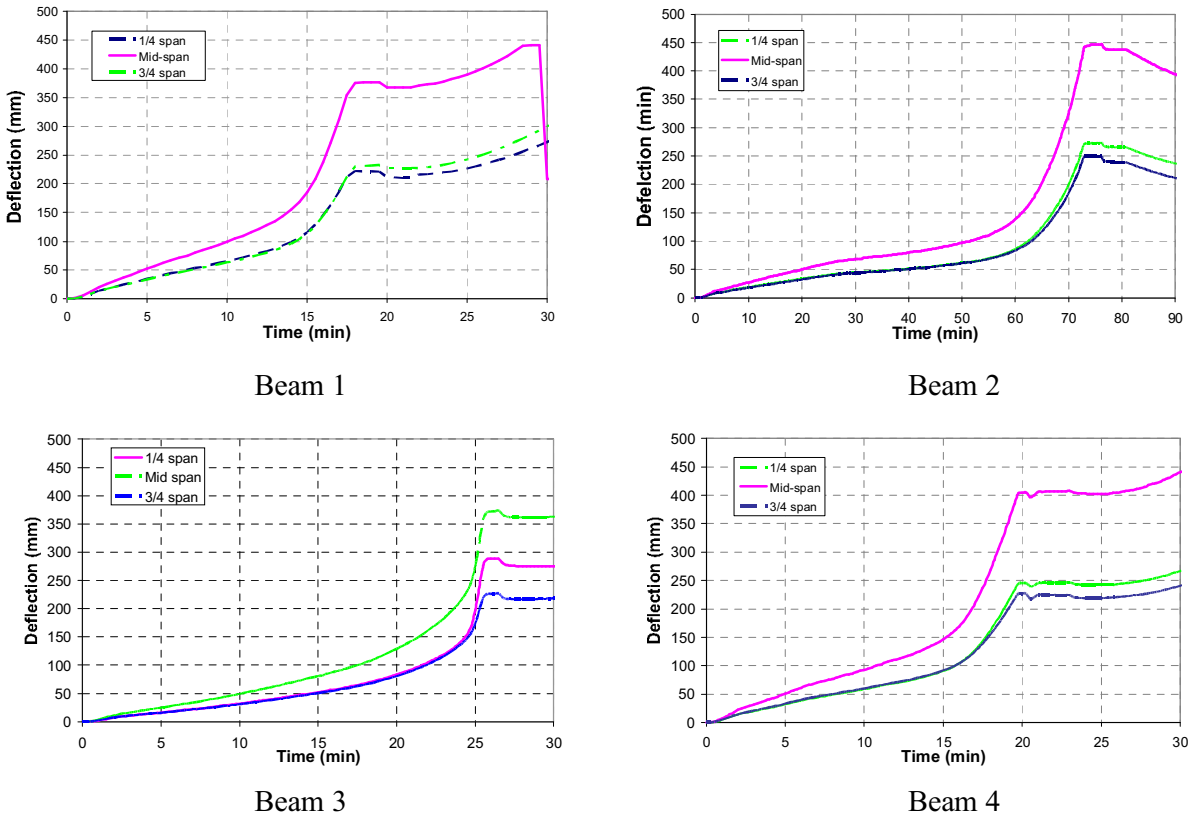

Fig. 5. Deflection vs. time

2.3 Failure mode

For both beam 1 and beam 3, the failure was due to web-post buckling near the beam supports (see *Fig. 6*), which is one of the usual modes of failure observed for such beams in fire situation. This web-post buckling could even generate a tee welding breakage.

Besides, because of its web-post stiffeners, beam 4 could only have a flexural bending failure, as it behaved like an "ordinary" beam. Hence, as beam 1 and beam 4 had the same cross-section, and as their deflection vs. time graphs are very close, beam 1's collapse might have been caused by combined web-post buckling and flexural bending.

As for the primary beam, i.e. beam 2, no web-post buckling was observed, which leads to the conclusion that this beam also failed by flexural bending.

Beam 1

Beam 2

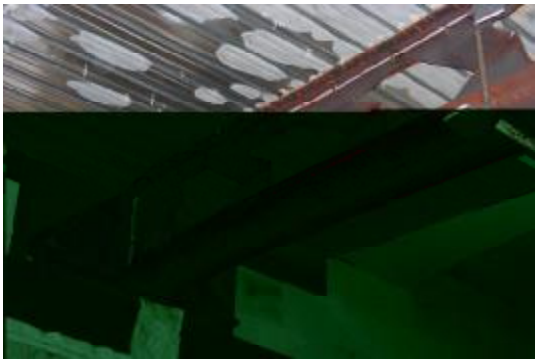

Beam 3

Beam 4

Fig. 6. Deformed beams

CONCLUSION

The tests carried out on cellular composite steel and concrete beams at elevated temperatures have highlighted two modes of failure:

- a web-post buckling near beam supports, when the web stiffeners were located only in the loading zone (and at the beam ends);
- a flexural bending, when the beam's web was thicker, or when its web-post was stiffened, making the beam behave like an "ordinary" beam without cells.

It should be noticed that no particular damage, such as concrete crushing, occurred in the composite slabs.

The next step of actual investigation is to use these results for validating finite element models such as *ANSYS*, *Cast3M* and *Safir* to predict the fire resistance of this type of structural members. Afterwards, these models will be used to conduct parametric studies for the development of corresponding simple fire design rules.

REFERENCES

[1] Technical annex of RFCS project FICEB (FIRE RESISTANCE OF LONG SPAN CELLULAR BEAM MADE OF ROLLED PROFILES), ArcelorMittal, WESTOK, SCI, CTICM, ULG, Ulster University, 2006

[2] Westok Limited, Input data – design summary, 2008

[3] Rapports d'essais 08-G-399, 08-G-431, 08-G-407, 08-G-419, Efectis France, 2009

[4] CEN, Eurocode 4 - Design of composite steel and concrete structures – Part 1-1: General rules and rules for buildings, 2005

CONCRETE AND COMPOSITE SLABS IN FIRE
Discussion of the Load Bearing Characteristics

Martin Mensinger, Martin Stadler

Technische Universität München, Faculty of Civil Engineering and Geodesy,
Chair of Metal Structures, Munich, Germany

INTRODUCTION

In the last years several research results have been published which discuss the load bearing characteristics of composite floor systems in case of fire. Diverse design methods were presented to calculate the load bearing capacity using assumptions that the slabs behave like a membrane due to large deflections (e. g. [1]-[3]). However, results of fire tests performed on such structures in the last years show some discrepancies between the available design methods and the real behaviour (e. g. [4]). Therefore, this paper presents some new approaches which may describe the influence factors on the load bearing characteristics.

1 STRESSES DUE TO TEMPERATURE CHANGES OVER THE CROSS-SECTION

The temperature distribution in concrete and composite slabs which are exposed to fire at one side is highly nonlinear. In addition, the thermal strains of concrete are not straight proportional to the temperature of the material. Therefore, also the strains in a concrete slab are distributed nonlinearly. Fig. 1 shows such a temperature and strain curve of a 100 mm thick unprotected concrete slab which is exposed to the standard fire curve (ISO 834). The temperatures and temperature-strain relations can be found in Eurocode 4 [5].

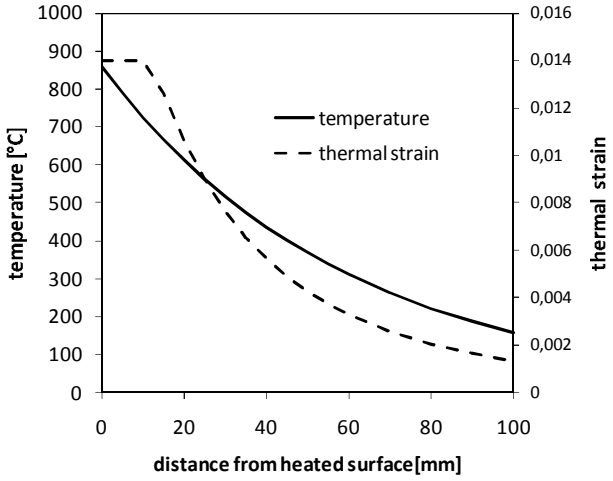

Fig. 1. Temperature and resulting strain distribution in a concrete slab

If these curves are used to analyse larger structures, a very high effort of calculation is necessary. A calculation by hand is virtually impossible. It is more practical to use linear strain distributions but not easy to find an appropriate approach. Furthermore, it is necessary to take into account that the nonlinear strain distribution leads to additional stresses. Related effects occur in hot-rolled steel sections during its production where non-uniform cooling generates self-equilibrating stresses. In contrast to steel sections a concrete slab cannot yield in such a way that these stresses can be neglected at design.

2 INTERNAL FORCES AND LOAD TRANSFER

Some of the following thoughts are mentioned in [3] and described in more detail in [6]. Here some new aspects shall be discussed. The temperature distribution over the depth of a cross-section is simplified considered as linear and the thermal expansion factor α_T as constant. This leads to linear thermal strains which can be divided into a constant part $\Delta\varepsilon_{unif}$ and a linear strain gradient $\Delta\kappa$.

$$\Delta\varepsilon_{unif} = \alpha_T \cdot \frac{\Delta\theta_{top} + \Delta\theta_{bottom}}{2}$$

$$\Delta\kappa = \alpha_T \cdot \frac{\Delta\theta_{top} + \Delta\theta_{bottom}}{h}$$

In a simple beam which is horizontally unrestrained the constant part causes a longitudinal extension u_{unif} and the gradient causes a uniform curvature and bowing of the beam.

$$u_{unif} = \Delta\varepsilon_{unif} \cdot L$$

For fast heating like the standard fire curve, large curvatures result and geometrical nonlinear approaches are necessary to calculate deformations. Second order theory assumes small deformations and is not sufficient. An unrestrained beam with uniform curvature deforms to a circular arc.

$$w_m = \frac{1}{\Delta\kappa}\left[1 - \cos\left(\Delta\kappa \cdot \frac{L}{2}\right)\right]$$

The arc length is the original length of the beam and the ends must move together (u_{grad}). In Fig. 2 these relations are illustrated.

$$u_{grad} = L - \frac{2}{\Delta\kappa} \cdot \sin\left(\Delta\kappa \cdot \frac{L}{2}\right)$$

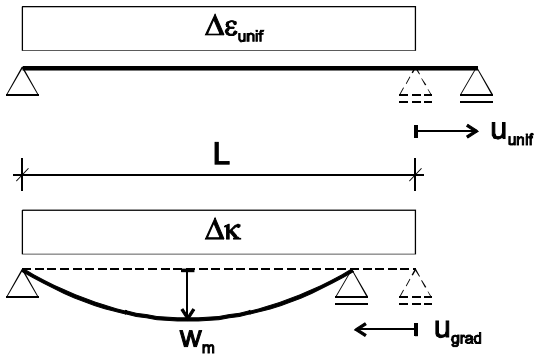

Fig. 2. Horizontal displacement of an unrestrained beam under uniform extension and curvature

If the beam is horizontally fixed on both ends, constraining forces occur. This can be visualized as an unrestrained beam which deforms under thermal loading and afterwards the support is shifted back to its initial position. Depending on whether the total horizontal extension u_{tot} is positive or negative the constraining forces are either an almost uniform compressive normal force with a positive bending moment in curved shape or a tensile force with a negative bending moment. In the special case when both extensions are the same size there will be no constraining forces (see Fig. 3).

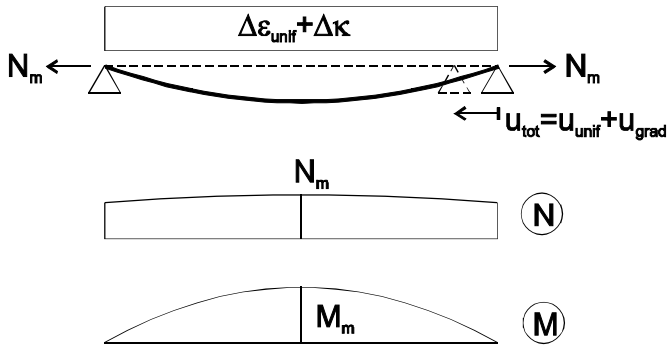

Fig. 3. Resulting constraining forces in a horizontally fixed beam

Slabs which are subjected to the fast heating of the standard fire curve will get a high curvature and in relation a small uniform extension. The curvature changes in both directions of the slab but even at unrestrained slabs the edges cannot move together. The deformations are restrained due to the development of a compression ring around the perimeter of the slab. In this case the thermal loading leads to a tensile force and a negative bending moment in the slab. The height of these forces depends on the bending stiffness of the slab but the tensile force easily reaches the tensile strength of the reinforcement. The negative bending moment generates cracks on the top surface of the slab unless mechanical loads generate contrary moments. On the basis of these facts, it is imaginable that working loads can have positive effects on the structural integrity of slabs or even that slabs fail without any working load only due to the exposure to thermal loading. The influence of the height of the load has not been sufficiently investigated by fire tests until now. If the reinforcement already yields under thermal loading, the contribution to the transfer of mechanical loads becomes very small. It seems that mechanical loads like the dead load of the slab or working loads are mainly transferred by reduction of the bending moment. This kind of load transfer can be compared with the behaviour of prestressed concrete structures.
If the slab is heated slower like it probably is in real fire conditions, the uniform expansion becomes more important and the slab will get under compression. In this case the additional loads can be transferred by reducing the compression force and after that, generating membrane tensile forces.

3 TENSION STIFFENING

In most engineering models only the reinforcement makes contribution to the load transfer because the concrete cracks at tension. Thus, the deflection of the slab only depends on thermal and mechanical strains of the reinforcement. But actually the concrete does not completely crack. Between the cracks stresses occur in the concrete and in the cracks the strains of the reinforcement increase. The slab becomes stiffer and the reinforcement is not stretched constantly. This so-called tension stiffening, which is well-known at ambient temperatures, also appears at elevated temperatures. For the design of beams and plates in bending, this effect does not influence the load bearing capacity but only the deflection. But in the engineering models using membrane action the load bearing capacity depends decisively on the deflection. Therefore tension stiffening must be included when the slabs are designed. In [7] approaches are published how these effects can be handled at ambient temperatures and for high reinforcement ratios $\rho = A_s / A_c$. Here it is discussed what happens at low reinforcement ratios.
Fig. 4 shows the stresses in a rebar related to its strain. Line a) is for a simple rebar without concrete. The curve is linear until it reaches the yield stress f_y with the related yield strain ε_y. Then it begins to yield, the stresses only rise slowly until the bar cracks at the ultimate stress f_u and strain ε_u. It is the well-known simplified stress-strain curve of steel with a linear elastic part and a hardening slope.

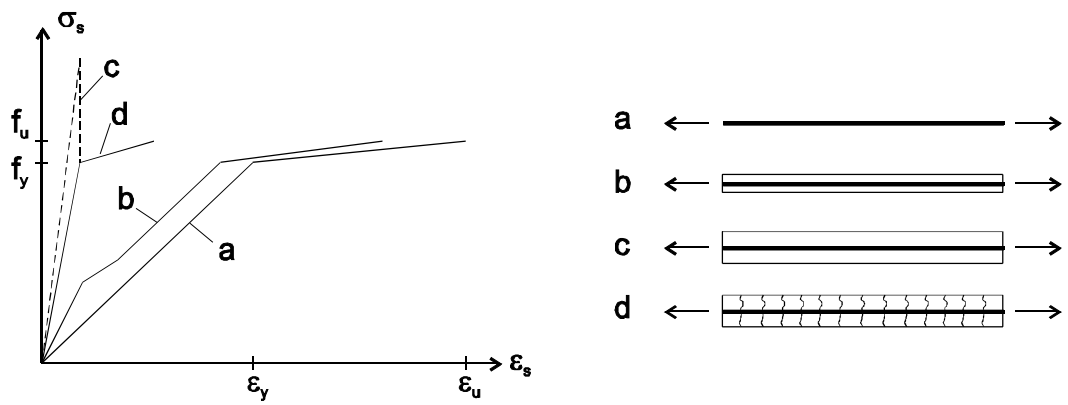

Fig. 4. Tension stiffening

If the rebar is embedded in a small concrete section, the reinforcement ratio is high and the stress-strain curve of the rebar looks like line b) in Fig. 4. In the first part the concrete is not cracked, it acts together with the rebar and the beam is very stiff. At the first bend of the curve the tensile strength of the concrete is reached and the first cracks appear. The stress in the rebar at this point can be calculated as follows:

$$\sigma_{s,cr} = f_{ct}\left(\frac{1}{\rho} + \frac{E_s}{E_{ct}}\right)$$

After the second bend the cracking is finished and the curve runs parallel to line a). The yield and ultimate stresses are the same as for line a) but the related strains are smaller. The reason is that the strains are concentrated in the cracks and in Fig. 4 an average strain over the length of the beam is shown.

Line c) shows the behaviour of a slightly reinforced beam. With rising strains the stress in the rebar theoretically rises higher than the yield stress. The reason is that the force which is necessary to reach the tensile strength of the concrete cross-section is higher than the force which the rebar can absorb. If the beam is stretched further, a first crack appears in the concrete and the force falls down to the tensile strength of the rebar. After a short hardening the beam fails with a small elongation. This curve can only be generated in a displacement-controlled test and is rather theoretical.

More realistic is line d). There the concrete beam is pre-cracked like it is the case at composite slabs in fire. The stiffness of the beam is higher than the stiffness of a simple rebar but lower than the stiffness of a reinforced concrete beam without cracks. Like for line c) the total possible deformation is much smaller than for a simple rebar.

Transferred to slabs in fire the tension stiffening effects can explain why some specimen in tests failed before the estimated deflection was reached. Reaching the yield stress of the reinforcement cannot be the only failure criterion. The ductility of the whole slab must also be taken into account. This ductility is influenced by the reinforcement ratio and the ductility of the reinforcement itself. The load bearing capacity of concrete and composite slabs in fire can be increased on the one hand by increasing the reinforcement ratio. It not only increases the bearable load of the reinforcement but also the tension stiffening effects decrease and the slab becomes softer. On the other hand, reinforcement with higher ductility enables larger displacements and hence higher load bearing capacities without need of additional reinforcement. Unfortunately most fire tests were not run until the slabs failed. The estimated deflections and load bearing capacities are therefore difficult to prove.

REFERENCES

[1] Bailey, C. G.: Membrane action of slab / beam composite floor systems in fire. *Engineering Structures 26 (2004), 1691-1703*

[2] Li, G.-Q., Guo, S.-X., Zhou, H.-S.: Modeling of membrane action in floor slabs subjected to fire. *Engineering Structures 29 (2007), 880-887*

[3] Cameron, N. J. K, Usami, A. S.: New design method to determine the membrane capacity of laterally restrained composite floor slabs in fire, Part 1: Theory and method. *The Structural Engineer 83 (2005), 28-33*

[4] Bailey, C. G., Toh, W. S.: Small-scale concrete slab tests at ambient and elevated temperatures. *Engineering Structures 29 (2007), 2775-2791*

[5] EN 1994-1-2 August 2005: Eurocode 4: Design of composite steel and concrete structures – Part 1-2: General rules – Structural fire design

[6] Lamont, S.: The Behaviour of Multi-storey Composite Steel Framed Structures in Response to Compartment Fires. *PhD Thesis, University of Edinburgh, 2001*

[7] CEB-FIP Model Code 1990. *Comité Euro-International du Béton, 1993*